UNIVERSITY OF MESSINA
DEPARTMENT OF MATHEMATICAL AND COMPUTER SCIENCES,
PHYSICAL SCIENCES AND EARTH SCIENCES

Doctoral Programme in Physics (Cycle XXXIV)

Myoelectric control and functional Near-Infrared spectroscopy in cognitive neurosciences: applications to neuro-motor control and neurological disorders

Doctoral Dissertation of:
Sergio Gurgone

SUPERVISOR:
Prof. **Valentina Venuti**

CO-SUPERVISORS:
Prof. **Giuseppe Acri**
Prof. **Andrea d'Avella**

COORDINATOR:
Prof. **Vincenza Crupi**

Academic Year 2020/2021

Contents

Abstract

The high dimensionality of the human motor system is at the core of the long-standing debate on how the central nervous system controls and learns new movements. Such high dimensionality implies redundancy, i.e., the fact that many combinations of muscle activations can generate the same movement. These muscular patterns lie in the muscular null space, whose exploration plays an important role in the learning of new movements. However, null space activations could be modulated independently from movement-generating activations and used to control external devices for augmentation. Monitoring the changes in neural activations related to such control, for which techniques such as functional near-infrared spectroscopy (fNIRS) can be particularly suited due to their easy applications in complex motor tasks, could lead to new insights on the processes underlying motor learning and motor recovery after neurological lesions.

This thesis aims at investigating the effects of exploration and modulation of muscular null space activations. In addition, it tests fNIRS efficacy in the monitoring of brain activations during the execution of a motor task during multiple sessions.

Three studies are presented: the adaptation to novel perturbations, that can be compatible or incompatible with the existing muscle synergies of an individual, in a virtual environment across multiple experimental sessions; the simultaneous control of natural motion degrees of freedom and an additional degree of freedom controlled by modulating activations in the muscular null space; and finally, the monitoring of cerebral activity in patients affected by Parkinson's disease while performing a finger tapping session before and after a thalamotomy performed through magnetic resonance guided focalised ultrasound surgery (MRgFUS).

In the first study, participants could not compensate the incompatible perturbations (which requires learning of new synergies and exploration of null space) in the first experimental session, but they were able to reach high level of performance in the last session. These results indicate that, with enough practice, it is possible to learn new null space patterns.

The findings of the second study demonstrated that participants were able to modulate null space patterns to successfully control one additional degree of freedom simultaneously with natural ones, although high variability in performance was present among them.
Finally, the results of the third study showed that patients' conditions improved after the MRgFUS treatment, with a consequent change in brain activations highlighted through fNIRS, in agreement with the results obtained in literature using other techniques.
The findings of this thesis advance our knowledge on human motor learning mechanisms, and may lead to novel applications, such as personalized neuro-rehabilitation procedures and efficient augmenting devices.

1. Introduction

1.1 Human neuro-motor control

The problem of **human neuro-motor control**, i.e., how the **central nervous system** (CNS), which is composed by the brain and the spinal cord, **controls and learns new movements**, has been a long-term source of debate in the neuroscience field, and it is still unsolved. As it was stated by Bernstein in 1967 [1], such problem rises because the **human body is a high-dimensional system** composed by a **large number of degrees of freedom** (DoFs), i.e., the possible independent variables the body can activate, with **many combinations** of them (such as neuronal and muscular activations, as well as and joint torques at a higher kinematic level) that **can lead to the same set of movements**. The comprehension of the mechanisms underlying such process not only would fill a gap in the knowledge of how our body works, but also would have important consequences in both **engineering applications** (such as prostheses for amputees) and **medical treatments** (such as rehabilitation from neurological diseases in which a reorganization of motor functions occur).

Many models to describe the neuro-motor control have been developed, with one of them whose popularity is growing in the scientific community: the **synergy model** [2, 3]. It suggests that **the CNS recruits muscles synchronously in fixed arrays**, the **synergies**, with each muscle having a specific weight for each synergy. Therefore, instead of controlling a much larger number of single units (the muscles) independently, the CNS controls a reduced number of "modules" (the synergies), lowering the amount of information to be processed for each movement. A schematization of a synergy is reported in Fig. 1.1.

An advantage of this model is the independence from a minimization function (such as for model based on optimal control), the form of which cannot be defined with complete certainty, but can only fitted to experimental data. On the other hand, synergies can be directly extracted from the electromyographic (EMG) patterns through dimensionality-reduction methods as the principal component analysis (PCA) or the

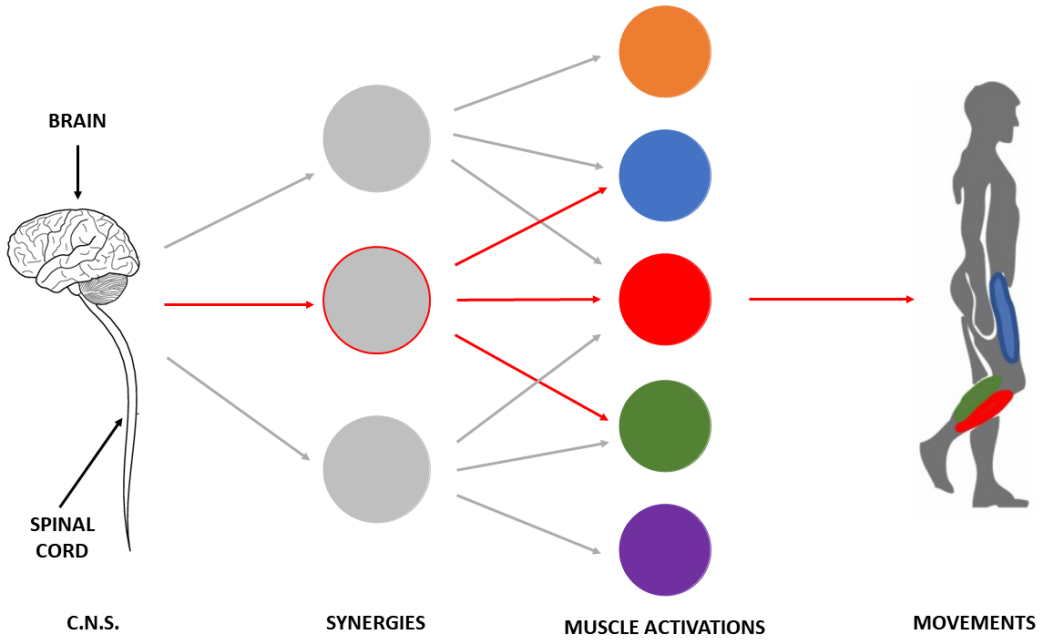

Figure 1.1: Schematic representation of a synergy, highlighted in red, whose activation generated a specific muscle activation pattern with consequent generation of movement.

non-negative matrix factorization (NNMF) [4]. Evidence for modularity has been found in many studies on vertebrate animals [2, 5, 6]. However, a definitive proof of their validity has not been found yet. A recent work [7] showed differences in the adaptation rates, in human participants, relative to the exposure to perturbations of synergies applied through EMG control in a virtual environment. While participants were able to compensate perturbations that allowed to explore all the task space (compatible perturbations), the same did not happen with the ones that did not allow to do that (incompatible perturbations), which in theory required **learning new synergies**, and therefore **exploring the muscular** (or EMG) **null space**. This includes those activation patterns that do not generate movement, but are used, for example, to control joint impedance, such as when keeping a limb in a fixed position. Up to date, there are no studies on the learning of such patterns to compensate incompatible perturbations with prolonged exposure, leading to the learning of new muscle synergies from the exploration of the muscular null space.

1.2 Augmentation: exploiting motor redundancy to surpass human limits

While **muscular null space**, as it has been said before, plays an important role in the learning of incompatible synergy perturbations because its exploration could in principle allow the learning of new synergies, it is less clear whether it can be independently modulated to **control additional movement DoFs** external to the human body, but related to an augmenting device. Humans has always been attracted by the possibility of surpassing their body limitations through technology, and the beginning of the development of sophisticated human-computer interfaces made finally doable what some decades ago was a simple utopia. EMG exoskeletons able to increase human capabilities exist [8]. Devices such as additional fingers controlled through other body parts [9, 10] have been successfully tested (see Fig. 1.2), as well as additional arms controlled through brain-machine interface [11].

Figure 1.2: Examples of augmenting devices: the "Third Thumb" by the London Plasticity Lab (on the left) [9], and the "Sixth Finger" by the Siena Robotics Systems Lab (on the right) [10].

A recent study demonstrated that cocontraction of two antagonistic muscles can be used to control one movement direction of a 2D cursor [12]. Nonetheless, the possibility of controlling extra DoFs by using muscular null space extrated from many muscles

directly involved in the principal task has not been tested yet. If this could be possible, myoelectric control could also be used to increase movement DoFs, by controlling devices that can help humans to perform complex tasks that otherwise cannot be performed alone, without the help of another person. In fact, EMGs, apart from taking the direct signal of muscle activations, can be used to measure null space activations in real time, constituting an alternative to control external augmenting devices.

1.3 Motor impairments and neurological disorders: when the body does not move the way it should

EMG signals, being directly related to the motor commands that originate muscle activations, are indeed useful to understand mechanisms underlying brain functionalities relative to motion generation and learning. However, to investigate **how brain structures changes** as a consequence of such processes, it is necessary to directly observe brain activations. Diagnostic techniques such as computed tomography (CT), positron emission tomography (PET), functional ultrasound imaging (fUS) and functional magnetic resonance imaging (fMRI) are widely used in neuroscience to study brain properties in both healthy individuals and patients affected by neuromotor disorders such as Alzheimer's disease, Parkinson's disease (PD), epilepsy or essential tremor (ET). In neuroimaging, fMRI has covered a predominant role in the last decades, establishing itself as the most used technique in this field because of its high spatial resolution and accuracy [13]. However, fMRI, as well the other previously mentioned techniques, present a lot of challenges when aiming to measure cerebral activations during complex motor tasks, as limited motion freedom and motion artifacts could make difficult to perform such measuresements. Moreover, not many devices can be introduced inside magnetic fields without compromising their functions. For this reason, other techniques such as the **functional near-infrared spectroscopy** (fNIRS) are employed in those researches for which other metodologies are unsuitable, especially when dealing with movement tasks [14] (see Fig. 1.3).
Such technique allows measuring the changes in concentration of chromophores such as the oxygenated and deoxygenated hemoglobin, through the absorption of near-infrared radiation. Although it presents lower spatial resolution with respect to fMRI, it has better temporal resolution and is less sensible to movement artefacts. Moreover, light sources and detectors can be easily put on the head of an individual, and many wireless

Figure 1.3: Examples of fNIRS measurement performed during a pursuit rotor task from [15].

systems are nowadays present on the market, allowing high motion freedom. All these factors, plus the low costs of implementation, helped fNIRS to become a popular technique for neuro-motor research. Its suitability for medical applications is also being highly tested, as it could become a tool for monitoring cerebral activations during the recover from brain surgical interventions in patients affected by neurological disorders, such as essential tremor or Parkinson's disease.

1.4 Outline of the thesis

The aim of this thesis is that of investigating motor learning and properties through myoelectric control, with the study of the exploration (synergy perturbation) and modulation (muscular null space control) of motor patterns do not used for the generation of movements. Furthermore, fNIRS has been tested as a monitoring tool for brain activation changes related to corrupted motor patterns due to pathological conditions and after a treatment aimed at the recovery of the original activation profiles. The structure of the following chapters will be as follows:

- In the **second chapter**, **myoelectric control** and **functional near-infrared spectroscopy** will be described in detail, with particular focus on their historical

evolution, scientific basis and the most common applications. Furthermore, the setups used in the researches presented in the following chapters and involving these techniques will be described.

- The **third chapter** will present a study about **learning of virtual perturbations**, compatible or incompatible with synergies, **in multi-day experimental sessions**, with the aim to further investigate learning of new synergies in longer exposure periods.
- The **fourth chapter** will describe a novel method to **control an additional degree of freedom** through **EMG null space control** while simultaneously performing an isometric force control task.
- In the **fifth chapter**, a novel combined approach employing **magnetic resonance-guided focused ultrasounds** and **fNIRS** for treatment and monitoring of patients affected by essential tremor or Parkinson's disease will be described.
- The **sixth chapter** will be dedicated to **conclusions** and **future perspectives**.

2. Methodologies

2.1 Myoelectric control

2.1.1 Background

Myoelectric control consists in the acquisition, processing and application of EMG signals from many different muscles to command specific devices of different nature, such as prostheses of missing limbs, exoskeletons for rehabilitation or assistance and end-effectors in virtual reality. Myoelectric control is also a powerful instrument to investigate the properties of the human motor system, as learning of new movements or adaptation to motion perturbations.

The first applications of myoelectric control date back after the end of World War II, when the first gripers, whose opening and closing velocities were controlled using EMG signals of residual muscles, were developed [16]. Since then, myoelectric control has been highly refined, and nowadays a wide range of EMG controlled devices, in particular prostheses, is available even for consumers.

Two methods for controlling myoelectric prostheses (and more in general all myoelectric devices) are currently employed: the on-off control and the proportional control. On-off control is the simpler of the two: an output quantity of the prosthesis, which can be its velocity in a fixed direction or around an axis, is turned on when the input signal is higher than a defined threshold [17]. In the proportional control, the output quantity of the prosthesis is instead proportional, linearly or non-linearly, and within a finite, useful and continuous interval, to the input signal, within a corresponding continuous range [18]. An example of proportional control is the one from Morita et al., who developed a direct torque control method for prosthetic hands that uses a neural network based on feedback learning [19]. While on-off control is still popular due to its simplicity of application, proportional control underwent a high success because human neuro-motor system exhibits properties typical of such a control policy, and it has been demonstrated that it is preferable in some situations. In [20] the authors showed that proportional control allows varying with higher precision grip force of a

prosthesis with respect to on-off control. For this reason, many proportional control based prostheses are now available in commerce, such as the ones by Ottobock or Touch Bionics. Furthermore, constant improvements in prosthesis functionalities are still going on, with the most sophisticated allowing for the rotation of the thumb or the individual control of all the fingers while keeping light weights and high grip forces. Myoelectric control of prostheses helped neuroscientists and physicians to improve the quality of life of amputee people, giving them the opportunity to overcome (at least partially) their disability. This was possible thanks to the development of EMG pattern recognition algorithms: these allow associating movement degrees of freedom of joints and limbs to the muscle activation patterns that generate them. Sang-Hui Park and Seok-Pil Lee developed an EMG pattern recognition method based on artificial intelligence [21]. Englehart and Hugkins developed a method that allows continuous identification of signal classes, without the need of segmenting EMG signals [22]. Muceli et al. developed a method which uses sEMG signals to estimate wrist kinematics for proportional and simultaneous control of multiple DoFs, and which is based on one multilayer perceptron neural network for each DoF [23], while Young et al. developed another algorithm based on Bayesian theory [24].

EMG activation signals are also being used for the control of robotic devices such as exoskeletons. The main difference between prostheses and exoskeletons is that the former are designed for non-able-bodied people to substitute a missing body part, while the latter can be used by both able and non-able-bodied people.

The first researches on exoskeletons are dated back to the 1970s, when Vukobratovic and his collaborators started working on biped locomotion to develop constructions for disabled people [25]. Since then, many researchers dedicated their studies to exoskeletons, which indeed have a wider spectrum of applications with respect to prostheses. Exoskeletons can be used to assist able-bodied people, for example increasing their strength, such as in the case of the Berkeley lower extremity exoskeleton (BLEEX), a military exoskeleton designed to help militaries to carry heavy loads [26], or of the Technische Universitat Berlin Powered Lower Extremity Exoskeleton (TUPLEE) developed by Fleisher and Hommel [8]. Another important application of exoskeletons is rehabilitation of people who are affected by neural disorders or have been injured. Colombo et al. developed a lower-limb robotic exoskeleton to be used with treadmills for the rehabilitation of incomplete spinal cord-injured subjects, avoiding the need of a physiotherapist whose variability in experience could affect training [27]. Ambrosini

et al. developed a passive upper-limb exoskeleton for both assistive and rehabilitative purposes, successfully testing it on both healthy subjects and spinal cord-injured subjects [28]. Stein et al. developed and successfully tested an upper-limb exoskeleton for rehabilitation of patients with chronic hemiparesis after stroke [29]. Finally, as said before, myoelectric control can be used to investigate basic principles of human motor system [7, 30, 31]. In fact, EMG signals allow altering the mapping between motor commands and the motion of virtual end-effectors in a way that could not be done with real ones without invasive intervention, to study how the central nervous system adapts to such perturbations. In [7], a linear mapping of EMG signals onto isometric end-point forces applied to a simulated mass was altered ("virtual surgery") such that new muscle synergies are required to compensate the perturbation. In addition to linear mappings, also non-linear mappings [32] and musculoskeletal models [33] have been used.

2.1.2 Experimental setup

The setup we used for our researches is composed by the experimental structure in which participants performed the task, and three computational units devoted to specific roles: the experiment controller, which was used for starting/stopping an experiment, for monitoring its status and performing calculations; the xPC, which was used for the acquisition of the data; and the graphical renderer, which was used to render the graphical scene.

The experimental structure presents a gaming chair that can be regulated in height, rotation and inclination, with belts to keep participants' torso sustained without stiffening of the participant itself. The chair can also be fixed at a specific position using a blocking system mounted on two rails (Figure 2.1). In front of the chair, a participant finds a desktop with an orthosis positioned in order to keep arm and forearm at an angle of 90°, and rigidly connected to a force transducer (Delta F/T Sensor, ATI Industrial Automation, Apex, NC, USA)(Figure 2.1 and 2.2). This one can measure a force up to 500 N in three directions and torques around the respective axes, and was connected to the acquisition board of the xPC. Participants inserted their hand in the orthosis, and the chair was regulated in height in order to have the hand at the level of the solar plexus. Over the orthosis, a mirror was placed to occlude the vision of the real arm, while a monitor, connected to graphical renderer and positioned above the mirror, projected specularly the 3D experimental scene. This presented, apart

Figure 2.1: Photo of the experimental structure of the Modulimb setup, in which it is possible to see the gaming chair where participants seat, the orthosis with the force transducer and the desktop with mirror and monitor.

for the cursor and targets, the dimensions and shapes of which can be regulated to satisfy experimental demands, a texture of the same type of the desktop's one, to better simulate the real environment. Participants were able to visualize stereoscopically this scene through 3D shutter glasses (NVIDIA GeForce 3D Vision), with the lenses operating at a 60 Hz frequency each one, alternating to create a 3D image at 120 Hz. They also communicate with the graphical renderer through wireless IR protocol.
Electromyographic activations were acquired using active wireless bipolar surface electrodes (Trigno System, Delsys Inc., Natick, MA, USA) (Figure 2.2), with a sample rate of 1000 Hz. EMG signals were bandpass filtered (20-450 Hz), amplified (gain: 1000), and sent to the EMG base station connected to the acquisition board of the xPC.
The muscles from we recorded the activity were fifteen, all acting on the shoulder and elbow: brachioradialis (BracRad), biceps brachii long heads (BicLong) and short head (BicShort), pectoralis major (PectMaj), anterior deltoid (DeltA), middle deltoid

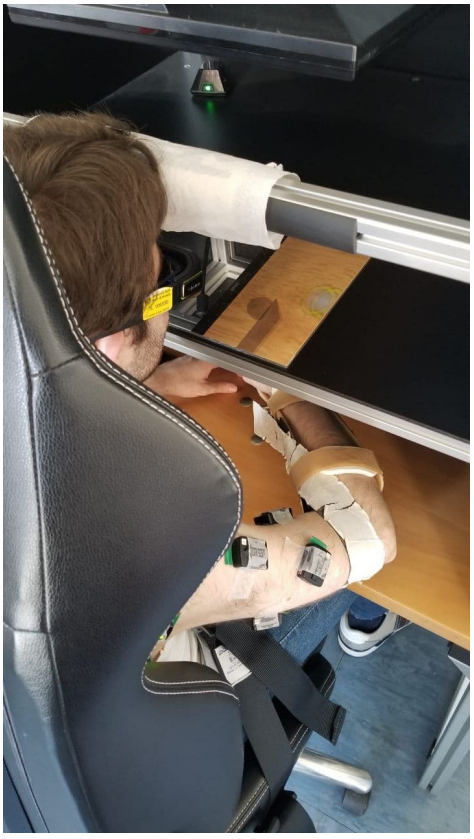

Figure 2.2: Photo of the experimental structure while a participant was performing a 3D isometric task. Electromyographic signals were recorded in real-time through the wireless Delsysi Trigno EMG electrodes, and the 3D force through the force transducer connected to the orthosis.

(DeltM), posterior deltoid (DeltP), triceps brachii lateral head (TriLat) and long head (TriLong), infraspinatus (InfraSp), teres major (TerMaj), latissimus dorsi (LatDorsi), lower trapezius (TrapLow), middle trapezius (TrapMid), and upper trapezius (TrapSup). Both the skin over the muscle position and the electrodes (made in silver) were cleaned with sterile gauze soaked with alcohol.

To place the electrodes on the different muscles, we followed the recommendations from SENIAM [34]: sEMG sensors were put on the muscle belly, following the orientation of the fibres.

During experiments, all the data measured through both force transducer and surface EMGs were transmitted to the xPC, and then saved by the experimental controller in the experiment file. The software used in these two computers was MATLAB, while the graphical renderer used Java and communicated with the other computers through a protocol in the Eclipse development environment.

This setup has been used to perform the studies we will discuss in the next two chapters: the adaptation to virtual surgeries compatible and incompatible with existing synergies during three-day experimental sessions, and the simultaneous control of an extra degree of freedom through EMG null space during an isometric force control reaching task.

2.2 Functional near-infrared Spectroscopy

2.2.1 Background

Functional near-infrared spectroscopy (fNIRS, called also optical tophography or near-infrared imaging), is a non-invasive brain imaging technique that uses low intensity levels of non-ionizing near-infrared (NIR) light to detect changes in cerebral blood flow in the brain, by measuring the absorption of the NIR light through optical sensors placed on the surface of the scalp.
The first application of NIR light in medicine goes back to the 1977 in the form of NIR spectroscopy (NIRS), when Jöbsis proved that NIR light can be used to perform non-invasive cerebral blood flow measurements [35]. After this study, the interest in NIRS started to grow esponentially. In 1985, Ferrari and collaborators started to use NIRS prototype instruments to measure changes in brain oxygenation in human adults [36], while in 1986, Wyatt and collaborators published a study in which they used NIR spectrophotometry to quantify indices of cerebral oxygenation and haemodynamics in sick newborn infants [37]. In the nineties, many companies (such as Somanetics Corporation, Hamamatsu Photonics, Hitachi, Shimadzu and Artinis) developed prototypes of NIRS instrumentations and released on the market their own commercial single-channel devices [38].
The first uses of NIRS for functional neuroimaging on human adults purposes date back to 1992. Hoshi and Tamura observed, using a two single-channel CW-instruments from Shimadzu, bilateral prefrontal cortex oxygenation changes (increase in oxygenated haemoglobin (HbO) and decrease in deoxygenated haemoglobin (HbR)) in fourteen volunteers during a mental task [39], while Okada and collaborators highlighted gender- and handedness-related differences of prefrontal cortex oxygenation in 72 volunteers [40]. Multi-site fNIRS has been successfully tested in 1993 by Hoshi and Tamura [41]. These researchers detected region-specific changes in HbO and HbT (the total

haemoglobin, defined by the formula: $HbT = HbO + HbR$) concentrations, during different mental tasks and as a response to visual and auditory stimulations.
The first clinical study using fNIRS by Okada and collaborators focused on patients affected by schizophrenia and succeeded in finding anomalies in brain oxygenation during a mirror drawing task in such patients with respect to a control group of healthy subjects [42]. One year later, the first study demonstrating that fNIRS can be used for tomographic maps of human brain activity was published [43].
Since then, fNIRS underwent a significant evolution process not only from a technological perspective, with many multichannel, wireless fNIRS systems now available, but also in terms of applications, with fNIRS now often employed in clinical studies even simultaneously with other techniques, such as fMRI and PET, as the combination of different imaging methods allows a description of human brain activity with a combination of spatial and temporal resolutions that cannot be achieved using only a single technique.
fNIRS is based on the property of tissues such as the skin and the skull bones to be not particularly sensitive to NIR light (in the ∼700-900 nm wavelength range), while pigmented compounds, or chromophores, like the HbO and HbR, are strong absorbers of NIR light (see Fig. 2.3). fNIRS measurements are anyway possible because NIR

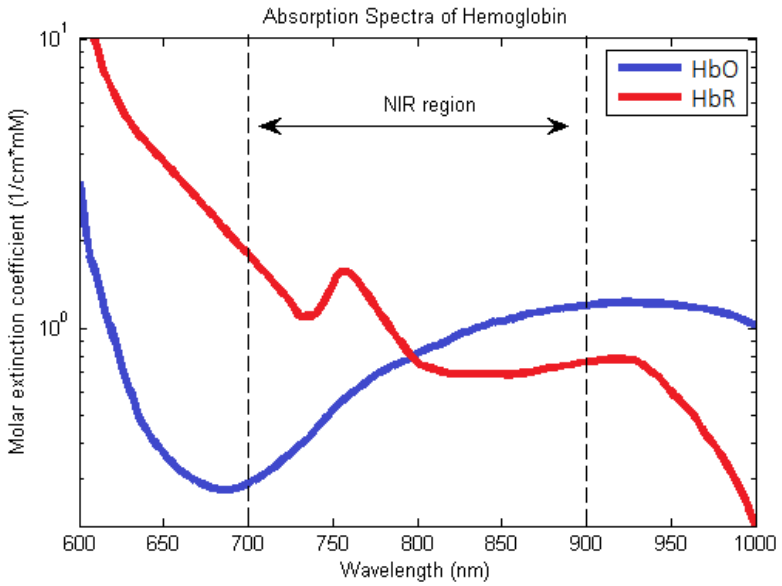

Figure 2.3: Molar extinction coefficient of both HbO and HbR as a function of the wavelength of incident radiation. Both chromophores are strongly absorbers of light in the range ∼700-900 nm

light can penetrate human tissues, as scattering phenomena are the most probable events in this case, 100 times more probable than absorption. This means that the fraction of absorbed light is relatively smaller than the scattered radiation, which can be measured and confronted to the incident one to calculate how much NIR light has been absorbed by chromophores. However, it is worth noting that, from a general point of view, blood vessels with diameter higher than 1 mm completely absord NIR radiation, therefore information about haemoglobin concentrations can be obtained only for small vessels of the microcirculation [38]. Furthermore, only 30% of the blood volume fraction in the human brain is related to arterial blood [44], with the venous blood being the principal subject of fNIRS measurements.
There are three types of NIRS/fNIRS instrumentation currently used, based on different methods of illuminations:

- the **continuous-wave (CW) method**, which is based on constant illumination of tissues and allows measuring light attenuation through the head;
- the **frequency-domain (FD) method**, which is based on intensity-modulated irradation that allows measuring both light attenuation and phase delays;
- the **time-domain (TD) method**, which is based on irradiation with short light pulses, and allows detecting the shape of the pulse after the propagation through the different tissues.

The most common instrumentations are based on the CW method, and as said before, they allow only measures of oxygenation changes of HbO and HbR (expressed in µmolar·cm or mmolar·mm), with respect to an arbitrary initial value. Furthermore, if compared to the others, CW-based systems present lower costs and are easier to transport. However, only the FD and TD methods allow to absolutely characterize optical properties of tissues, such as absorption and reduced scattering coefficients, with the possibility to calculate absolute HbO and HbR concentrations.

2.2.2 Experimental setup

Changes in oxygenated and deoxygenated haemoglobin concentrations in the brain were measured using a Hitachi ETG-4100 NIRS system (Fig. 2.4), with two near-infrared light beams of wavelengths 695 nm and 830 nm, respectively, and a sampling rate of 10 Hz.

Figure 2.4: The Hitachi ETH 4100 NIRS System used for the acquisition of light absorption related to haemoglobyn changes.

The used optodes configuration matrix was composed by 3 x 5 optodes, 8 sources and 7 detectors that allow using 22 acquisition channels, whose schematization can be seen in Fig. 2.5. On average 13 $\pm$ 1 channels were positioned on the right hemisphere and 9 $\pm$ 1 channels on the left hemisphere.
The matrix was positioned above the forehead, to acquire signal changes mostly from the prefrontal, motor and parietal cortices. For this reason, subjects' hair was cut before each session. This reduced the amount of noise generated by hair presence. Nevertheless, other sources of noise still remained, as the scalp depth and the conformation of the head.
To register the positions of the optodes, which were saved in MNI (Montreal Neurological Institute) coordinates, four references were used: the nasion (Nz), the inion (Iz), the left preauricular point (AL), and the right preauricular point (AR).

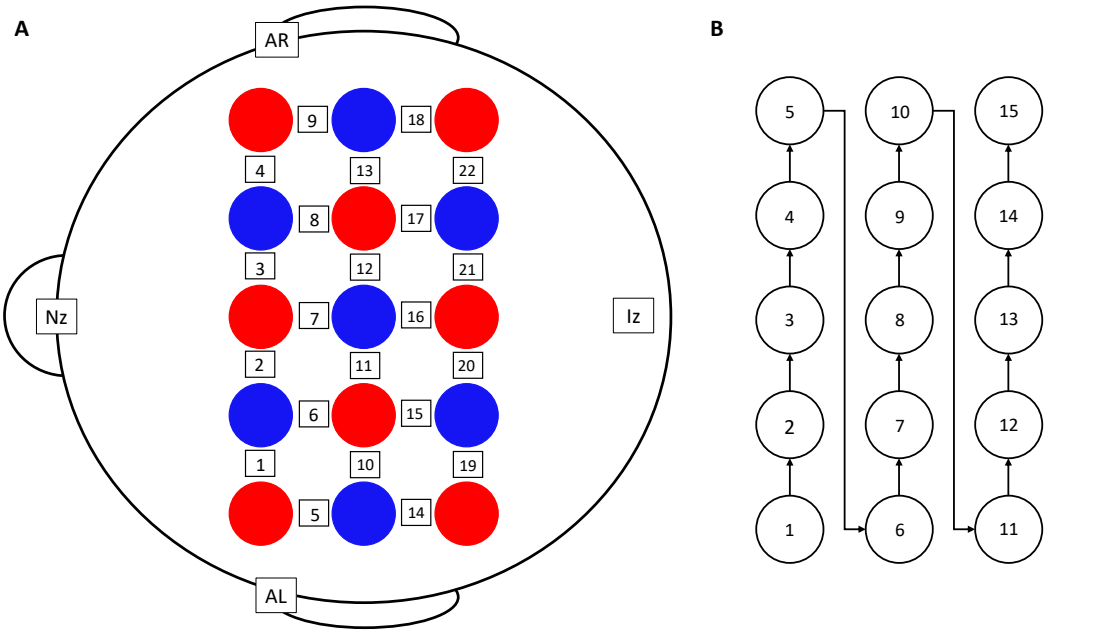

Figure 2.5: Schematization of the configuration matrix of the optodes used, together with the four reference positions (nasion (Nz), inion (Iz), left preauricular point (AL), and right preauricular point (AR)). In panel (A), the red circles indicates the light sources, the blue circles the light detectors, and the squares the channels. Panel (B) shows the order in which optodes positions are registered by the 3D digitalizer included in the dedicated software "NIRS-SPM".

3. Adaptation to compatible and incompatible virtual surgeries across multiple experimental sessions

3.1 Background

The problem of how the central nervous system (CNS) controls body movements and acquires new motor skills is one of the most challenging in the field of motor neuroscience. Such problem arises for one key reason: the human musculoskeletal system is composed by a large number of degrees of freedom (DoFs), i.e., joint angles. Therefore, many combination of control signals (muscle activations, neural activations, joint torques) can generate the same set of movements [1]. As an example, just moving the hand in three-dimensional space involves the activation of more than 20 muscles between arm and shoulder. Even considering two single levels of activation (an "on-off" situation), which is a high simplification of the problem, the possible solutions to the system of three equations in 20-3 variables are $2^{20-3} = 2^{17} = 131072$. While human brain possess a high computational capability, it is unreasonable that for executing such simple movements it calculates all the possible solutions every time and just selects one of it randomly. For these reasons, many models have been developed and tested to understand how motor control is performed. Such models can be divided in two general classes: descriptive models and complete models [45, 46]. To the first belong all those models that try to predict spatial and/or velocity trajectories without considering the underlying neurobiological aspects. The second in turn is divided in dynamic models, which include body dynamics and biophysical properties in their formulation, as for example joints kinematics and muscle activations, and stochastic models, which, besides using dynamic quantities of the body, relay on the assumption that noise in CNS plays an important role in motion control [46]. Many models from both categories are based on the concept of **optimal control**, in which a cost function is chosen to estimate the motor plan (and eventual corrections due to feedback) rela-

tive to a specific task goal [45]. Generally, the cost function is defined as the integral of an instantaneous cost in the time interval of interest, with the aim of minimizing the function itself: this means that, among all the possible solutions/movements, only the one with the lowest cost is chosen. One of the most important and consistent optimal control models, belonging to the category of descriptive models, is the bell shaped velocity profile (or minimum jerk) model [47]. Assuming that the main objective in motor control is the smoothness of movement, the authors developed a cost function based on the derivative of the acceleration (the jerk J), which for planar movements have a magnitude equal to:

$$J = \sqrt{\left(\frac{d^3x}{dt^3}\right)^2 + \left(\frac{d^3y}{dt^3}\right)^2}.$$

The cost function C is just the integral of the square of this quantity over time:

$$C = 1/2 \int_0^{t'} J^2 dt.$$

Its simplicity and its capacity to predict general features of reaching movement and correct velocity profiles made this model quite prominent. Many revisions of such model have been proposed to be applied in different contexts, such as the constrained minimum jerk model proposed to be applied only to velocity profiles [48].
When considering dynamic models, the minimum torque change model is one of the first and most popular [49]. Criticizing kinematic models (as the minimum jerk one) for their lack of consideration for dynamical aspects of the human body, the authors chose a cost function based on torque τ, which gave the best fit with the observed data in their work:

$$C = 1/2 \int_0^{t'} \sum_i \left(\frac{d\tau_i}{dt}\right)^2 dt,$$

where the sum is performed on all the considered joints. The cost function was minimized under the constraints of a two-joint robot dynamics representing musculoskeletal dynamics. However, models as the minimum torque change failed to predict adaptation to visual or force field perturbations (contrary to kinematic models), because trajectories depend only on initial and final positions.
This is why models integrating both kinematics and dynamics of the arm were proposed, as the TOPS (Task Optimization in the Presence of Signal-Dependent Noise)

model by [50], which can be considered the first stochastic model and had the relevant contribution of introducing the concept of noise in motor control. This model takes the endpoint (i.e., the final point of the trajectory) variance as the quantity to be minimized, because experimental observation showed that different repetitions of the same task are never the same, being motor control corrupted by noise that causes this variation. Furthermore, noise is assumed to be linearly proportional to the input signal magnitude, which means that dynamical aspects must be taken into account.
Optimal control is widely considered one of the best strategies to mimic the biological processes underlying human motor control. In fact, optimization could reproduce important biological processes, such as motor learning, that enhance behaviour similarly as an optimization process could do [46, 51]. However, there are two limitations of optimal control that must be taken into account: the first is that the cost function does not have a clearly defined dependence on physiological quantities, which is why many different models with different cost functions have been proposed. The second is that some studies demonstrated that motor control is not strictly optimal, but rather sub-optimal, with motor coordination patterns being particularly robust to alterations of limb biomechanics, such that activation patterns that are consistent with the habitual ones and "good enough" to accomplish a task are used [31].
To overcome such issue, other approaches to solve motor redundancy were proposed, such as the **muscle synergy** theory. A synergy (from the Greek $\sigma\upsilon\nu\varepsilon\rho\gamma\acute{\iota}\alpha$, which means "working together") is defined as a group of muscles that are recruited in a coordinated pattern, in which each muscle has its own invariant weighting of a common time-varying activation (spatial synergies), or all muscles share the same invariant activation waveform (temporal synergies), or each muscle has its specific invariant activation waveform (spatiotemporal or time-varying synergy). Different synergies can be combined to generate a variety of movements. Recalling the example of the wrist movement in three-dimensional space with two-level muscle activations, if we divide 20 muscles in 6 spatial synergies, we obtain $2^{6-3} = 2^3 = 8$, which is a drastic reduction in the number of possible solutions.
From an historical point of view, Babinski (1857-1932) was the first to introduce the concept of "asynergia", which he defined as an atypical pattern of activation of muscle groups in pathological conditions. Similarly, Brunnstrom (1898-1988) observed abnormal, stereotypical movements after corticospinal system damage. The definition of synergy as it is known nowadays was first formulated by Bernstein (1896-1966), who

referred to synergies as muscle groups working together in a coordinated, task-specific manner [1]. Evidence for a modular organization of spinal cord circuitry was found in many studies on vertebrate animals, as frogs [5], rats [2] and cats [6]. Using microstimulation on the spinal cord, it was possible to generate different force fields at the limb endpoints of the animals depending on the stimulated spinal module. The simultaneous stimulation of two spinal modules resulted in the generation of force fields that were the linear combination of the force fields corresponding to each module. These results were in support of the hypothesis that force patterns are generated by groups of muscles acting as individual units, i.e., muscle synergies [3].

In addition to microstimulation, decomposition of EMG signals recorded in different motor tasks and in a variety of conditions have supported synergy existence. The estimation of muscle synergies from EMG signals can be considered a blind source separation problem [52]. For this reason, many matrix factorization algorithms have been applied for the extraction of synergies from activations recorded from multiple muscles [53, 54]. The most common factorization approaches are principal component analysis (PCA) [55], independent component analysis (ICA) [56], maximum likelihood factor analysis (FA) [57], and non-negative matrix factorization (NNMF) [4]. Using these factorization approaches, muscle patterns have been successfully reconstructed starting from few muscle synergies not only in animals, such as in the case of frog kicking [58], but also in humans, e.g., in postural and balance control [59, 60], in locomotion [61, 62], and in point-to-point reaching tasks using upper limbs [63].

However, despite all the previous cited results, no definitive proof of the validity of the synergy theory has been found. While microstimulation allows to directly probe the neural pathways involved in the organization of muscle synergies, the evoked neural activation patterns may deviate from those observed in physiological conditions. Moreover, evidence from decomposition is based on the description of regularities in the motor output, which is compatible with a neural organization of muscle synergies but it provides only indirect evidence, as a low dimensional motor output might also arise because of task and biomechanical constraints [64, 65]. A recent study has introduced a novel approach to provide direct evidence for muscle synergies by considering the synergy model as causal rather than only descriptive, i.e., testing a prediction of the effect of a manipulation of the mapping between muscle activity and its effect in the task space. Such study introduced the concept of "virtual surgery" [7].

From a mathematical perspective, in isometric conditions, approximating the gener-

ated force as a linear function of muscle activations:

$$\mathbf{f} = \mathbf{H}\mathbf{m},$$

where $\mathbf{f}$ is the tridimensional force vector, $\mathbf{m}$ is the muscle activation vector, and $\mathbf{H}$ is the EMG-to-force matrix that maps muscles activations onto force (see Figure 3.1A), it is possible to define the muscle activations themselves as a function of the synergy activations:

$$\mathbf{m} = \mathbf{W}\mathbf{c} + \boldsymbol{\epsilon},$$

where $\mathbf{W}$ is the synergy matrix, each column of which identifies a time-invariant synergy (i.e., a vector specifying the relative muscle activation levels), $\mathbf{c}$ is the synergy activation coefficient, which describes the activation of each synergy in time, and $\boldsymbol{\epsilon}$ is the residual due to physiological noise (see Figure 3.1B and C). Thus, the $\mathbf{W}$ matrix has a number of rows equal to the number of muscles and a number of columns equal to number of synergies.

Starting from the previous relation, if a modular control scheme is actually employed by the CNS, alteration of the linear mapping between force and EMG signals through a rotation of synergy vectors (the virtual surgeries) which allow to span all the force space (see Figure 3.1D and E) does not require learning of new synergies and should be compensated with a fast learning rate [7] (see Section 3.2.5 for more details). On the contrary, rotations that reduce the dimensionality of the force space (see Figure 3.1F and G) require the learning of new synergies and therefore are characterized by a slow learning rate [7]. The first rotations are called compatible virtual surgeries, while the seconds are called incompatible virtual surgeries. In [7] was found that, while compatible perturbations were compensated in a one-day experimental session, incompatible perturbations were not, as predicted by a synergistic organization of the controller. However, as learning of new motor skill may require new muscle synergies through a slow adaptive process, we wondered whether incompatible perturbations could be compensated with more practice.

In this chapter, we will present work in which we used the virtual surgery approach developed in [7] to test whether, with enough practice, it is also possible to learn new muscle synergies. We tested the performance of individuals during a three-days exposure to compatible or incompatible perturbations in a 3D isometric reaching task, highlighting the differences between the two groups in terms of learning rates. We

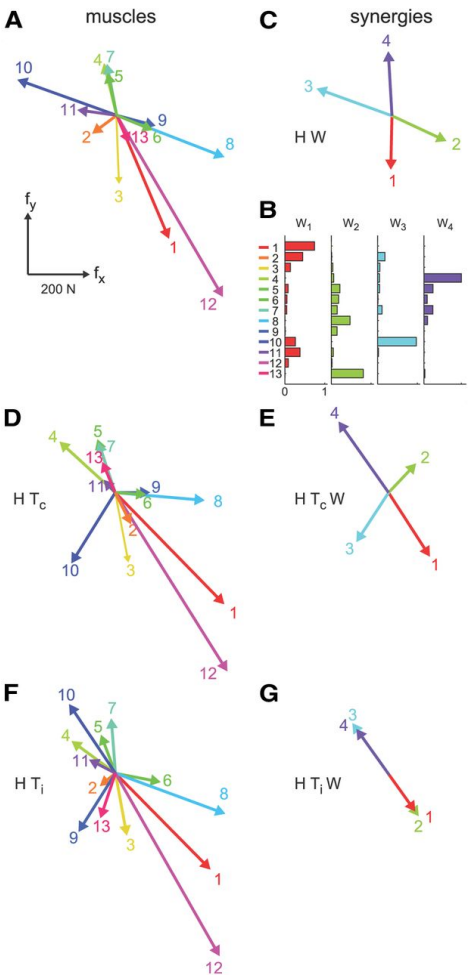

Figure 3.1: Examples of **H** matrix, synergies, and virtual surgeries adapted from [7]. (A) **H** matrix estimated during the generation of planar isometric forces. Each column of **H** represents the force vector generated by one of 13 muscles. (B) Muscle synergies (**W** matrix) identified by NNMF from the EMG data. Each column of **W** represents a vector whose coefficients determine a pattern of relative muscle activation levels, illustrated by color-coded horizontal bars. (C) Forces associated with each muscle synergy (i.e., columns of the $\mathbf{H} \cdot \mathbf{W}$ matrix), which span the entire force space. (D) Forces generated by muscles after the application of a compatible virtual surgery, a recombination of the original force vectors after a virtual rearrangement of the muscle tendons. (E) Synergy forces after the compatible surgery still span all the force space. (F) Muscle forces after an incompatible surgery applied through a rotation matrix mapping a vector in the column space of **W** into a vector in the null space of **H**. (G) Such rotation aligns the force vectors associated with all synergies in the same direction; therefore, synergy forces after the incompatible surgery do not span all the force space.

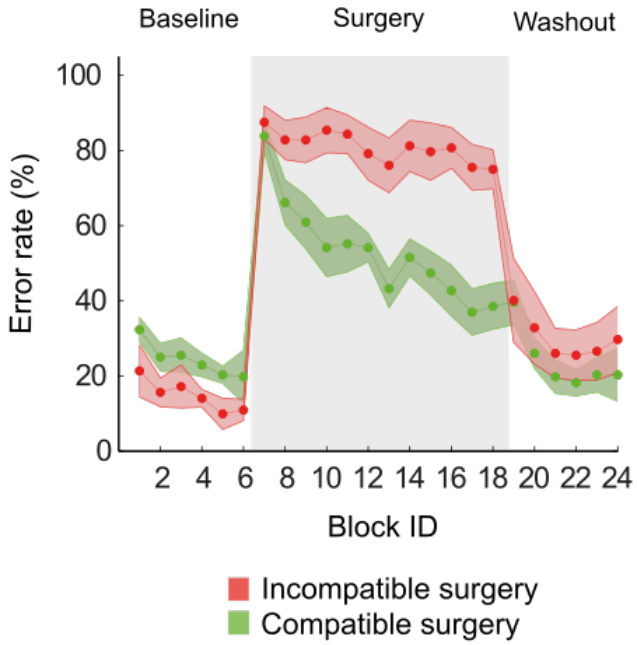

Figure 3.2: The error rate (fraction of unsuccessful trials in which the cursor did not reach and hold on the target), main index of performance in [7]. Significant differences between performance of participants exposed to compatible and incompatible were found at the end of the exposure phase (Surgery Block 12).

hypothesized that, after an incompatible perturbation that requires mapping a target onto a muscle pattern originally in the null space, with longer practice and exploration, participants would be able to improve their performance and achieve an error rate comparable with that observed after a compatible perturbation.

3.2 Methods

3.2.1 Subjects

Eighteen right-handed subjects (mean ± SD age: 27.2 ± 6.5 years, age range: 19–43, 5 females) participated in the experiments after giving written informed consent. All participants had normal or corrected to normal vision and had no known neural diseases or right upper limb injuries. All procedures were conducted in conformance with the Declaration of Helsinki and were approved by the ethics committee IRCCS Sicilia - Sezione Neurolesi "Bonino-Pulejo" (Prot. n. 02/18).

3.2.2 Experimental protocol

The experiment was composed of 3 sessions, performed in 3 consecutive days (see Fig. 3.3A for the protocol schematization). After an initial familiarization, performed at the beginning of the first session, participants performed two blocks of trials in which they received feedback about the force recorded by the transducer as the displacement of a cursor (force control). Then, for the rest of the experiment (i.e., the rest of the first session and the whole second and third sessions), the cursor displacement was proportional to the force estimated from the recorded EMG signal (EMG control).

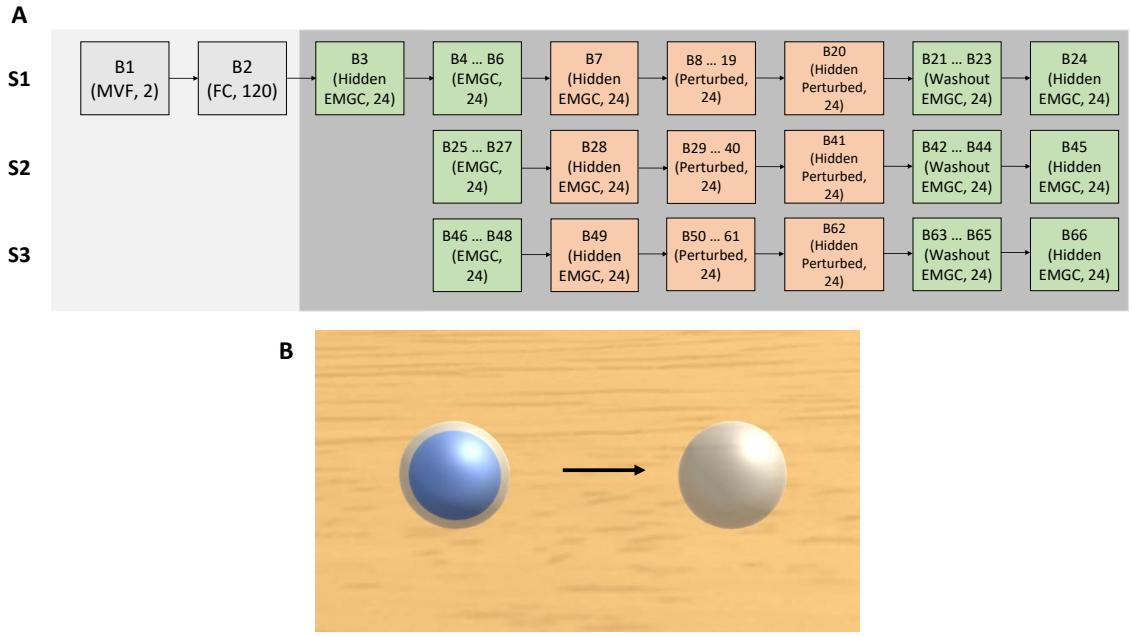

Figure 3.3: A) Experimental protocol. 66 blocks were performed during three sessions in consecutive days. After two initial blocks, in which the cursor displacement was proportional to the force collected by the force sensor (Force control blocks, lighter gray background), for the rest of the experiment the cursor displacement was proportional to the force estimated as the product of an EMG-to-force matrix (unperturbed or perturbed) and the recorded EMG signal vector (EMG control blocks, darker gray background). Blocks with visual feedback were interspersed with blocks in which no feedback was given to the subject (Hidden). EMG control blocks could be either perturbed (the estimated EMG-to-force matrix was multiplied by a perturbation matrix, see Methods) or unperturbed (EMG baseline, performed before the perturbation, and washout, performed after the perturbation). B) Scene displayed during a trial (the blue cursor moves from the home position towards the target in the direction of the arrow).

In the first force control block, participants were asked to generate maximum voluntary

force (MVF) along one direction on the horizontal plane (-y, towards their chest). With an analysis performed on data previously collected with a similar protocol [66], it has been checked that such estimation of the MVF was highly positively correlated to the average maximum force across multiple directions on the x-y plane. During this block, participants were encouraged to exert the maximum force with verbal reinforcements like 'go', or 'more' [67].

Participants were then asked to accurately and quickly move the cursor from a rest position to a target, displaced in one of twenty spatial directions, by applying isometric forces on the orthosis (Force Baseline Block, FC). At the beginning of each trial (rest phase), participants had to relax their right arm muscles to maintain the cursor inside a transparent sphere at the center of the scene for 1 s. Successively, a transparent sphere appeared in one of the twenty target positions (target go event), placed on the vertices of a dodecahedron inscribed into a sphere, centered in the rest position, with a radius corresponding to 15% or 25% of the MVF. Participants were instructed to reach the target and stay within the target sphere, whose radius was 2% of the MVF, for 0.2 s (static phase). A representation of the experimental scene can be observed in Fig. 3.3B. Each target appeared 3 times in random order, for a total of 20 targets x 2 radius x 3 repetitions = 120 trials. EMG and force data collected during the dynamic phase (i.e. the phase from the target go event until the first time the cursor get inside the target) were elaborated to estimate the matrix that maps the EMG activation onto the isometric force generated by the participant (EMG-to-force matrix), the synergy matrix, and the perturbation matrix (see below). The maximum of each EMG signal collected during the execution phase (i.e., the phase from the target go event to the end of the static phase), or during the dynamic phase if the static phase was not defined, was used to normalize that EMG signal during the rest of the experiment. After this Force Baseline Block, there was a 5 min pause to process the recorded data and to construct the myoelectric controller and the virtual surgeries. All subsequent EMG control blocks consisted of 24 trials with targets at 20% MVF in random order within cycles of eight directions equally spaced along the horizontal plane (45° steps).

During the first EMG control block no feedback of the cursor position was provided to participants (EMG Hidden block, block 3). Since without visual feedback participants could not correct for any inaccuracy in the EMG-to-force matrix, hidden blocks allowed to assess the quality of the reconstruction of the end-point force from the recorded EMG signals.

The following series of 21 blocks was repeated in the same order during all the three sessions. Each series consisted of: 3 baseline blocks (EMG baseline), 1 baseline block without feedback (EMG Hidden), 12 virtual surgery blocks (Perturbation), 1 virtual surgery block without feedback (Perturbation Hidden), 3 washout blocks (Washout), and 1 washout block without feedback (Washout Hidden).
At the end of the first and second sessions, the positions of the electrodes were marked with a dermographic pen. Electrode positioning at the beginning of the second and third sessions was conducted based on their relative position with respect to Repere's marker points and skin markers, recorded at the beginning of the first session, on the pictures taken at the beginning of the first session, and on the markers made with the dermographic pen during the previous session. The correct electrodes placement of the second and third sessions was even tested checking the cursor movement during the first EMG control block of the session (i.e., blocks 25 and 46).

3.2.3 EMG-to-force mapping

As it has been specified in Section 3.1, isometric generation of submaximal force allowed to use a linear approximation of the relation between the shoulder and elbow muscles activations and the force exterted at the hand:

$$\mathbf{f} = \mathbf{H}\mathbf{m},$$

where $\mathbf{f}$ is the tridimensional force column vector, $\mathbf{m}$ is the M-dimesional muscle activation column vector (in this case $M = 15$), and $\mathbf{H}$ is the EMG-to-force matrix (of dimensions $3 \times M$) that maps muscles activations onto force. The matrix $\mathbf{H}$ was estimated using multiple linear regressions of each force component, low-pass filtered (second-order Butterworth; 1 Hz cutoff), with EMG signals recorded during the dynamic phase of the first force control block, low-pass filtered (as the force) and normalized to the maximum EMG activity recorded during the force control block targets at 25% of the MVF distance.
The $\mathbf{H}$ matrix extracted during the force baseline block of the first day was used during all three experimental sessions, as it was demonstrated in a previous study that the accuracy of this matrix is preserved across multiple days [66].

3.2.4 Muscle synergies

Muscle synergies were identified by non-negative matrix factorization [4] from the EMG patterns recorded during the dynamic phase of the force baseline block, starting from the expression introduced in Section 3.1:

$$\mathbf{m} = \mathbf{W}\mathbf{c} + \boldsymbol{\epsilon},$$

where $\mathbf{m}$ is the column vector of EMG signals at a given time, $\mathbf{W}$ is the synergy matrix (of dimension $M \times N$, with N number of identified synergies), $\mathbf{c}$ is the N-dimensional synergy activation coefficient column vector at the same time, and $\boldsymbol{\epsilon}$ is the residual due to physiological noise.

The non-negative matrix factorization algorithm was applied to the EMG signals after mean value subtraction, rectification, low-pass filtering (second-order Butterworth filter; 1 Hz cutoff frequency), baseline noise level subtraction, and normalization to the maximum EMG activity of each muscle recorded during the generation of 25% the MVF during the force baseline blocks. The baseline noise was estimated during the rest phase at the beginning of the experiment and periodically throughout the experiment.

The algorithm for the synergy extraction was repeated 10 times for a number of synergies ranging from 1 to 15 (i.e., the number of recorded muscles) and, for each number, the repetition with the best reconstruction (i.e., the one with the highest R^2) was retained. The minimum number of synergies that explained at least 90% of the data variation was selected as the number of synergies used for the calculation of the virtual surgeries.

The synergy matrix extracted during the force baseline block, performed during the first day, was used during all the three sessions of the experiment [66].

3.2.5 Virtual surgeries

Virtual surgeries simulated a rearrangement of the tendons of the shoulder-elbow system, providing the participant with the visual feedback of the effect that such a surgery would have had on the force generated at the hand. Virtual surgeries were performed by altering the EMG-to-force mapping as a rotation in the muscle space ($\mathbf{H}' = \mathbf{H} \cdot \mathbf{T}$, where $\mathbf{T}$ is a rotation matrix). Two types of virtual surgeries (compatible and incom-

patible [7]) were calculated according to the individual EMG-to-force mapping and synergies of each participant.

Participants were randomly assigned to one of the two type of surgeries and practiced it for the whole three sessions. Ten subjects practiced the incompatible surgery and eight subjects practiced the compatible surgery. Both surgery types allowed the generation of any force along the 3D space with a different muscle pattern, but only the compatible surgeries allowed the generation of force along all directions by recombination of the existing synergies. In fact, incompatible surgeries were constructed such that the muscle activation, obtained by combinations of synergies, could only generate forces along a single direction on the horizontal plane. Therefore, if force generation relies on synergy combinations, participants who practiced the incompatible surgery would be required not only to adapt the synergy coefficients, as for participants who practiced the compatible surgery, but to learn new synergy vectors. Therefore, while participants who practiced the compatible surgery were able to quickly adapt to the surgery, participants who practiced the incompatible surgery adapted more slowly, or even did not adapt at all, to the perturbation [7]. Virtual surgeries were constructed with specific muscle space rotations. Compatible rotations ($\mathbf{T}_c$) were chosen as rotations in the subspace spanned by the synergies and incompatible rotations ($\mathbf{T}_i$) rotated a vector of the same synergy subspace into the null space of $\mathbf{H}$. Differently from Berger and collaborators [7], in which participants had a visual feedback only of the force generated in the horizontal plane, in this study a feedback of the force along the vertical direction was also provided to participants. However, the surgeries were designed such to perturb only the horizontal components of the force generated by the synergies, without affecting their vertical components. The algorithm is briefly described below.

The singular value decomposition of the matrix $\mathbf{W}_o^T \cdot \mathbf{N} = \mathbf{U} \cdot \mathbf{S} \cdot \mathbf{V}^T$, where $\mathbf{W}_o$ is an orthonormal basis of the range of $\mathbf{W}$, with N synergies, $\mathbf{N}$ is an orthonormal basis of the null space of the EMG-to-force matrix of D dimensions (i.e., $D = 2$), identified the S matrix, which has $N - D$ non-zero singular values. Therefore, we can identify two orthonormal bases of the common subspace between synergies and null space: $\mathbf{W}_c = \mathbf{W}_o(u_1, \ldots, u_{(N-D)})$ and $\mathbf{N}_c = \mathbf{N}(v_1, \ldots, v_{(N-D)})$, an orthonormal basis of the subspace of synergy vectors not in the null space $\mathbf{W}_n c = \mathbf{W}_o(u_{(N-D+1)}, \ldots, u_N)$, and an orthonormal basis of null space vectors not generated by synergy combinations $\mathbf{N}_{nc} = \mathbf{N}(u_{(N-D+1)}, \ldots, v_{(M-D)})$, where M is the muscle activation dimensionality

(i.e., the number of recorded muscles). The incompatible surgery $\mathbf{T}_i$ was calculated rotating a vector $\mathbf{w}^i_{nc}$, in the span of $\mathbf{W}_{nc}$, onto a vector $\mathbf{n}^j_{nc}$, in the span of $\mathbf{N}_{nc}$. Therefore, the muscle patterns generated by synergy combinations along $\mathbf{w}^i_{nc}$ do not produce any force after the surgery, and synergy combinations can generate forces only in one dimension. On the contrary, the compatible surgery $\mathbf{T}_c$ was calculated rotating a vector $\mathbf{w}^i_{nc}$, in the span of $\mathbf{W}_{nc}$, onto another vector $\mathbf{w}^j_{nc}$. In this way, the forces associated with the synergies are altered, but all force directions can be generated by recombining the same synergies. The rotation matrices used in both perturbations $\mathbf{T}_i$ and $\mathbf{T}_c$, were identified such to make the changes in the muscle patterns, required to compensate the surgery, similar for each subject. Therefore, the rotation angle was chosen such that a difficulty index, defined as the average change across muscles and force targets in muscle activity required to perform the task after the surgery [7], was similar across all subjects performing both surgeries.

3.2.6 Data analysis

Data collected during all trials performed by all participants were visually inspected and those trials in which EMG artefacts were detected were discarded. Inactive trials, i.e. those trials in which the participant did not even attempt to reach the target, were also excluded to avoid performance drop not due to participant behavior. The discarded trials were 90 (39) (median and inter quartile range over subjects) over the 1657 trials of the whole experiment.
One participant in the incompatible surgery group had a poor force reconstruction ($R^2 < 0.6$) and was excluded from the analysis. Therefore, the analysis was performed on the remaining seventeen subjects (9 who practiced the incompatible surgery and 8 who practiced the compatible surgery).

Task performance. Task performance was quantified by the error rate, i.e., the fraction of trials in which the cursor did not reach the target (unsuccessful trials).

Statistical analysis. We used MATLAB to perform a linear mixed model analysis of the relation between a dependent variable (in this case, the error rate) and independent variables or fixed effects (e.g., the type of surgery, i.e., incompatible or compatible, the session index, i.e. from 1 to 3, the perturbed block index of each session, i.e. from 1 to 12, or the target direction, each investigated as a separate dummy variable) tak-

ing into account the participant as a random effect. Similarly, we used a generalized linear mixed model analysis to investigate the relation of a binary random variable representing success/unsuccess in each trial with the fixed and random (participant) effects.

Models were compared through likelihood ratio test. In particular, presence of an effect in the model was determined by likelihood ratio test statistics. P-values were obtained by likelihood ratio tests comparing the full model with the effect to be tested against the model without the effect. A threshold of 0.05 was selected to determine whether the tested effect was statistically significant to determine the variable ($p < 0.05$) or not ($p \geqslant 0.05$).

Linear mixed models, and generalized linear mixed models were fitted with data collected during each trial.

3.3 Results

All subjects (see Table 3.1) were able to control the cursor and reach the target in 81.4 % ± 11.0 % (mean ± SD over subjects) of the trials during the force control block and in 76.8 % ± 9.9 % of the selected trials during the EMG baseline blocks (i.e., blocks 4 to 6, 25 to 27, and 46 to 48).

The R^2 of the reconstruction of the tri-dimensional force, collected during the force control block, was 0.86 ± 0.04. The reconstruction of the force exerted along the horizontal plane during the EMG baseline blocks was 0.84 ± 0.05. Therefore, we can conclude that the placement of EMG electrodes, at least on those muscles that mostly contributes to the unperturbed movement through the targets, was consistent across sessions [66].

Consistently with previous studies [68], the number of synergies identified during the generation of an isometric submaximal tri-dimensional force with the hand was 6.1 ± 0.8 (mean ± SD over subjects). The R^2 value of the synergy reconstruction of the of the EMG pattern collected during the force control was 0.92 ± 0.01 (see Table 3.1) and 0.81 ± 0.07 during EMG control baseline blocks.

During the unperturbed EMG control blocks at the beginning of each session (EMG baseline blocks), subjects displaced the cursor from a central start location to one of eight targets arranged on a circle along approximately straight paths. Immediately after the virtual surgery was introduced, regardless of its type, cursor movements were

Surgery type	Subject	Force R^2 (FC)	Number of synergies	Synergy R^2 (FC)	Difficulty index
I	1	0.86	6	0.92	1.66
I	2	0.80	8	0.92	1.56
I	3	0.91	6	0.91	1.62
I	4	0.85	6	0.92	1.55
I	5	0.85	6	0.91	1.65
I	6	0.83	6	0.92	1.48
I	7	0.81	6	0.92	1.60
I	8	0.94	6	0.91	1.70
I	9	0.90	7	0.92	1.71
	Mean I	0.86 ± 0.05	6.3 ± 0.7	0.92 ± 0.01	1.61 ± 0.08
C	10	0.80	7	0.91	1.68
C	11	0.92	7	0.92	1.63
C	12	0.88	6	0.91	1.66
C	13	0.81	4	0.92	1.42
C	14	0.82	6	0.93	1.60
C	15	0.87	6	0.91	1.63
C	16	0.88	5	0.91	1.61
C	17	0.86	6	0.93	1.60
	Mean C	0.86 ± 0.04	5.9 ± 1.0	0.92 ± 0.01	1.60 ± 0.08
	Mean All	0.86 ± 0.04	6.1 ± 0.8	0.92 ± 0.01	1.61 ± 0.08

Table 3.1: Force R^2 (Force control): fraction of the end-point force data, collected during the Force control block, explained by the product of the H matrix by the EMG data. Force R^2 (EMG control of each session): fraction of the end-point force data, collected during the EMG baseline blocks, explained by the product of the H matrix by the EMG data. Number of synergies: number of synergies estimated from EMG patterns during the force control block. Synergies R^2 (Force control): fraction of EMG data variation, calculated during the Force control block, explained by synergies. Synergies R^2 (EMG control of each session): fraction of EMG data variation, calculated during the EMG baseline blocks, explained by synergies. Difficulty index, average change across muscles and force targets in muscle activity required to perform the task after the surgery.

poorly controlled and the cursor often moved in the wrong direction (Fig. 3.4, Perturbation 1st movement of Session 1). With practice, some participants were able to change their muscle pattern such to, at least partially, compensate the perturbation (Fig. 3.4, see Perturbation last movement of Session 3), while other participants moved the cursor basically without compensating the perturbation, or with slight modifications.

No significant differences, according to an unpaired t-test (see Table 3.1), were identi-

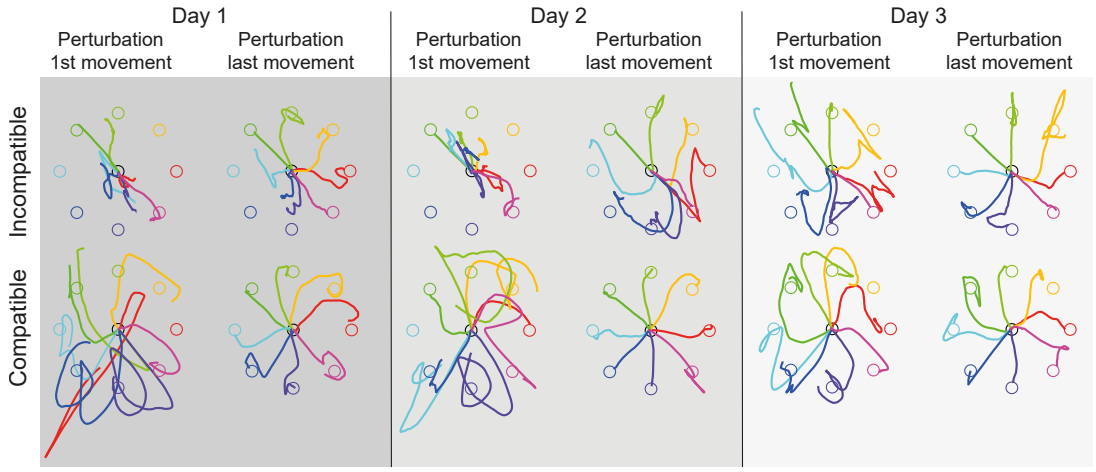

Figure 3.4: Example of the trajectories of the cursor on the horizontal plane during individual trials. (Top) a participant who practiced the incompatible surgery (subject 3). (Bottom) a participant who practiced the compatible surgery (subject 11). Different targets and associated cursor trajectories are color coded.

fied between participants who practiced the compatible and the incompatible surgery in terms of R^2 values for the reconstruction of force by EMG during force control ($p = 0.78$), number of synergies ($p = 0.29$), R^2 values for the reconstruction of EMG by synergies during force control block ($p = 0.81$), and difficulty index ($p = 0.78$).

3.3.1 Error rate

A trial was defined unsuccessful (an "error") if the cursor failed to reach the target at all. As it can be observed in Fig. 3.5, during the first experimental session results comparable to ones obtained in [7] were obtained, with an average error rate visibly lower for participants exposed to compatible perturbations. Such difference in performance is still visible in the second session: here, both groups further decreased their error rates at the end of the exposure. But it is only in the third session that the separation between the mean error rates reaches its smallest gap, with participants exposed to incompatible perturbations showing performance very close to the one of the other group.

Whether differences between the error rates were related to the type of surgery was tested with two generalized linear mixed model (GLMM) analyses (MATLAB function "fitglme") performed on data collected from all subjects during all three sessions.

The two models had the participant as a random effect and block index, calculated during each day (from 1 to 12), session index (from 1 to 3), target (defined by 7 different dummy variables) as fixed effects. Moreover, one of the two models had the perturbation type as fixed effect, while the other did not. An ANOVA compared the two models and the perturbation type was identified as a significant effect ($p = 0.021^*$). Therefore, an overall difference among the behaviors between participants who practiced the incompatible or the compatible perturbation was identified, and, in particular, participants who practiced the compatible perturbation showed a lower error rate.

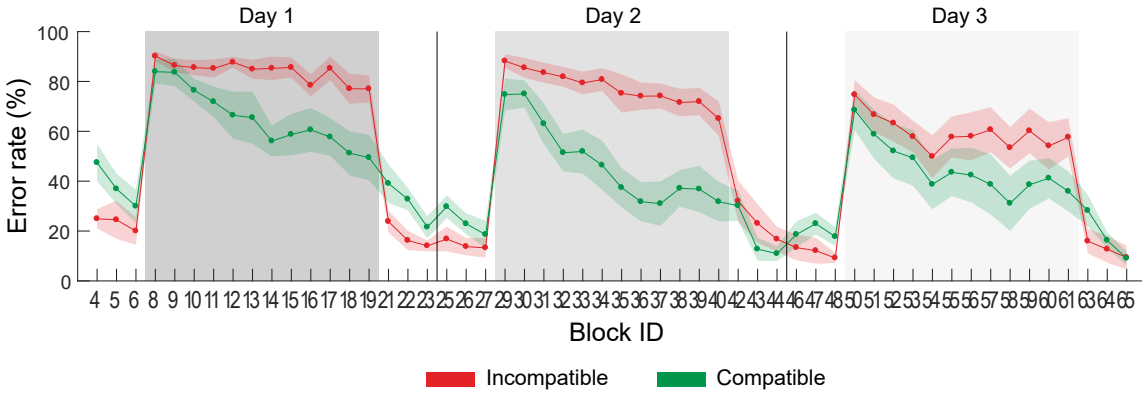

Figure 3.5: Error rate in a single block (hidden blocks were not displayed) of participants who practiced the incompatible surgery (red) or the compatible surgery (green) (mean ± standard error among participans).

However, we also investigated differences of the error rate between participants who practiced different surgeries, investigating data collected during different sessions separately. Two generalized linear mixed model (GLMM) were constructed from data collected during each session separately, using subjects as random effects and the block index and the targets as fixed effects. The two models differed for the perturbation type as fixed effect, considered in one model but not in the other. ANOVA compared the two models and the perturbation type was identified as a significant effect in the first session ($p = 0.013^*$), in line with the study performed by Berger and collaborators [7], and second ($p = 0.002^{**}$) session, but not in the third ($p = 0.19$). So, a long exposure to the incompatible surgery led the error rate to be statistically indistinguishable from the one of the participants who practiced the compatible surgery. In other words, a long exposure led participants to compensate the incompatible surgery as well as

participants who practiced the compatible surgery.

3.3.2 Inter-individual variability

Surprisingly, a considerable variability among participants exposed to both incompatible and compatible perturbations was present in the time-cours of the error rate (Figure 3.6).

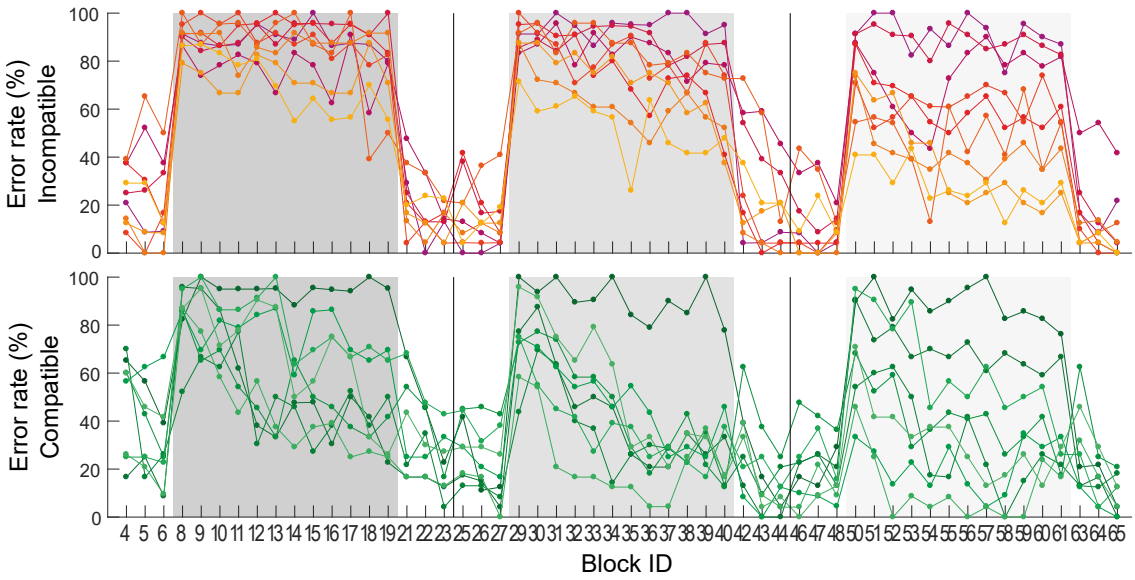

Figure 3.6: Error rate in a single block (hidden blocks were not displayed) of participants who practiced the incompatible surgery (red) or the compatible surgery (green). (Top) Error rate of each participant who practiced the incompatible surgery (color code indicated the drop in the number of unsuccessful trials from yellow, higher drop, to dark red, lower drop). (Bottom) Error rate of each participant who practiced the compatible surgery (color code indicated the drop in the number of unsuccessful trials from light green, higher drop, to dark green, lower drop).

Such variability is a consequence of the fact that, while the difficulty indices were similar, each perturbation was unique for the participant and their ability in finding the right patterns to compensate the rotation could vary due to their baseline abilities in the myoelectric control task. For incompatible perturbations, exploring the muscular null space and finding the direction rotated in the task space requires different amounts of time depending on the regions first explored by participants (for example, co-contracting a pair of muscles with respect to others), which can be arbitrarily chosen, due to the relatively high dimensionality of the null space itself.

3.4 Discussion

To solve the problem of the human neuro-motor control, i.e., how the CNS generates and controls movements [1], many models have been developed based on both kinematic and dynamic properties of the human body. While optimal control models allow to predict movement trajectories in many motor tasks, they rely on assumptions that have not been justified yet, such as the formulation of the cost function on which they are based. For this reason, other possible theoretical approaches have been developed to explain control strategies not based on optimal control, such as the idea that CNS recruits muscles in coordinated groups - muscle synergies. While evidences for synergies have been found in many studies using microstimulation [2, 3, 5, 6] and EMG decomposition [58–63], no definitive proof of the existence of synergies has been found. The study by Berger et al. [7] investigated the adaptation to perturbations of the mapping between muscle activation and force, simulated in a virtual environment using myoelectric control (virtual surgeries) during an isometric reaching task in a one-day experimental session. It was found that, while participants could compensate perturbations that were compatible with the existing synergies, they could not compensate incompatible perturbations, which require learning of new control patterns outside the synergy space. In our study, we used the virtual surget approach to investigate adaptation to compatible and incompatible perturbations across three experimental sessions in three different days. While for the first sessions similar results to [7] were found, with participants able to compensate the compatible perturbations but not the incompatible ones, during the third session participants exposed to incompatible perturbations achieved error rates statistically indistinguishable from the ones of participants exposed to compatible ones Furthermore, a striking inter-individual variability was found both among participants performing the task with the incompatible perturbation and among participants performing the task with the compatible one. While for this last group the different baseline individual motor capabilities, which also affect unperturbed myoelectric control, can be assumed to be the principal reason of such variability, for incompatible perturbation the fact that the exploration of muscular null space cannot lead in the same amount of time to discover the correct null space directions may be due to its high dimensionality.

The learning and retention of new control patterns by the CNS in multiple experimental sessions has been widely discussed in the literature. Shadmehr and Brashers-Krug

[69] investigated the ability of human subjects to learn a reaching task while interacting with one of two conflicting mechanical environments applied through a robotic manipulandum in different sessions. Fu and co-workers [70] investigated learning of new task-specific cortical networks in mice using transcranial two-photon microscopy during the practice of novel forelimb skills in multiple days. More recently, Oby and collaborators [71] conducted a study in which two monkeys performed a reaching task over multiple sessions in which they had to move a computer cursor by voluntary modulation of the activities of about 90 neural units recorded through multielectrode array implanted in the arm region of the primary motor cortex. Each experiment began with a session of natural control achieved with a mapping that relates neural activities to cursor velocities which did not require the animals to learn new neural activity patterns. After this session they were exposed to a perturbation that required the learning of activities outside the natural manifold. They found that monkeys can learn such neural activation patterns that were not used when no perturbation was applied.

With respect to the previous literature, our study represents the first attempt of investigating through myoelectric control the learning of novel synergies in multiple experimental sessions. The hypothesis that two different mechanisms operate in a modular controller, which has been proposed in [7], can also explain the results of this study and it is actually reinforced by them. The first mechanism, which it has been suggested to be implemented in the cerebellum [72–74], presents a fast learning rate, and is responsible for the correction of the synergy activation coefficients to reduce the error between the target force and the real generated force, like in adaptation to visuomotor perturbations [75]. The second process presents a slow learning rate, and is related to the learning of new control patterns (i.e., new synergies, possibly stored in the motor cortex [76]) when it is not possible to compensate the error by simply adjusting the activation coefficients of the existing synergies.

The results of this study raise the possibility of implementing protocols based on myoelectric control for the rehabilitation of individuals after neurological damages or patients affected by neuropathologies, when the existing synergies of the individual have been altered by the pathological condition and could be restored (partially or completely) using such an approach. Possible integration of feedback mechanisms can be elaborated to improve re-learning of the synergies, as the positive role of feedback in learning has been proved in literature [77–79]. Furthermore, understanding of motion

generation and learning in a modular controller could help improving existing robotic interfaces not only for rehabilitation, but also for augmentation, with the possibility of using synergy null space to control additional external devices, in similar ways currently in progress based on kinetic, neural or muscular null space.

4. Simultaneous control of natural and extra degrees of freedom by isometric force and electromyographic activity in the muscular null space

4.1 Background

In the second chapter, we have discussed about the high versality of myoelectric control, which can be employed for applications such as prosthesis replacing missing limbs, exoskeletons for rehabilitation and assistance, and for studies in virtual environment in which a cursor can be controlled through EMG signals, such as the one described in the previous chapter. Indeed, one other interesting application of myoelectric control is **augmentation**: this is the application of robotic technologies, generally resembling human limbs, integrated with the users' physical abilities to enhance them. This enhancement can be referred both to enforce present abilities, such as strength [80, 81], and to the addition of new abilities in term of external movement DoFs controlled simultaneously to the natural ones, such as a hypothetic third arm [11, 82]. In this last case, signals that are not involved in motion generation and that can be voluntary modulated should be used to avoid interference with natural movements.
This could be theoretically achieved using the "**motor task null space**". To perform the same task, due to the redundancy of both the musculoskeletal and neural systems, i.e., the presence of many more active units (muscles and neurons) than the end-effector DoFs involved, an individual could use different combinations of joint angles, muscle patterns and neural signals [83]. If two combinations of signals are equivalent, the variations between the two do not affect task performance, i.e., they do not generate task-relevant movements or forces. The signals corresponding to such variations lie in the null space.
Three different kinds of null space could be applied for augmentation:

- the **kinematic null space**, referred to kinematic variables such as joint angles;
- the **muscular null space**, referred to muscle activation patterns;
- the **neural null space**, referred to neural signals.

While kinematic null space is, among the three, the one with the theoretical lowest dimensionality (and therefore the lowest possible number of additional DoFs that could be controlled), it indeed is barely affected by noise, is non-invasive and requires a lower cost apparatus. Neural null space, due to the theoretical possibility of modulating the activity of a single neural pool or even of one neuron, present the highest dimensionality, but it is invasive when implanted electrode are used, and if non-invasive electroencephalography (EEG) is used, neural signals are also quite noisy and sometimes difficult to decompose in real time from biological signals used to control natural limbs. Muscular null space can be seen as a trade-off between kinematic and neural null spaces: while its dimensionality is not as high as the neural one, it is higher than the kinematic null space and EMG signals are less noisy than neural signals.
Many tests to use null spaces for augmentation have been recently performed. For what concern kinematic null space applications, it has been shown that manipulation of a third hand in a virtual environment is possible using the motion of a foot to control a third hand [82]. Similarly, a third robotic thumb controlled with a toe [9] and a sixth finger controlled through kinematic null space of upper limbs [10, 84] have been developed and successfully tested.
When talking about muscular null space, a recent research showed that facial muscle activations can be used to control a supernumerary robotic finger [85], while another focused on the use of torso muscles to control an extra robotic leg [86].
Finally, neural null space has been used in brain-machine interfaces (BMIs), as in [11] where a third arm has been tested, although difficulties in EEG signal decomposition can bring to low performance.
As it can be noticed from the examples previously showed, especially for what concern kinematic and muscular null spaces, signals used to control the additional DoFs have been recorded from body parts that were not directly involved in the task performed concurrently with the natural DoFs. Such null space signals belong to the "extrinsic" subspace. The main limitation of these approaches is that, while performance could be very good, in many real-life situations the controlled devices could interfere with secondary task, for example walking when using a leg to control an external DoF.

In this context, we propose a new, different approach that makes use of the muscular null space and in particular of its "intrinsic" subspace that, as opposed to the extrinsic one, is formed by those activation patterns belonging to body parts directly involved in the performed task. In the case of muscular null space, such patterns includes the co-contraction of two antagonistic muscles, whose activations counterbalance the respective pulling vectors, during movements of the limb to which they belong (such as when moving an object with an arm and stiffening the arm itself).
Muscular null space has been successfully applied for modulating an end-effector impedance, especially in presence of unstable interactions with the environment [87–89]. It also has been employed for the so-called "tele-impedance", which is the control of a robotic device impendance using the human one [90, 91]. In a recent work, it has been shown that voluntary muscular null space modulation can be used to control the impedance of a virtual end-effector during an isometric force reaching task [92]. Another work tested the possibility of using EMG beta band decomposed in real time from the activation of tibialis anterior muscle to move a cursor in a 2D environment [93]. Moreover, Takagi and collaborators [12] showed that is it feasibile to use co-contraction of two antagonistic muscles to control the vertical displacement of a cursor in a 2D scenario, while controlling its horizontal displacement with the reciprocal activations of the two muscles. Nonetheless, no research to date focused on the feasibility of using intrinsic muscular null space extracted from many muscles to directly control extra DoFs, in a 3D environment, concurrently with natural limb movements for augmenting purposes.
In this chapter, we will focus on our test conducted to assess the validity of task-intrinsic muscular null space control as a possible application for augmentation, with the analysis of a 3D isometric force task in which participants controlled both natural and extra DoFs at the same time.
To quantify participants' performance and to understand how to optimize an eventual device based on such a control method, we performed an analysis based on the Fitts' law for reaching tasks. Fitts' law is widely used to evaluate human performance during a task with or without a device. In its original paper [94], Fitts took the Shannon's theorem 17 as basis to develop his law: such theorem states that the capacity of a noisy, continuous channel is proportional to the difference between the entropy (a measure of "information") of the transmitted signal and the noise. Considering a reaching task as an information transfer process, the movement time MT can be

assumed to be proportional to an index of difficulty ID, which is the logarithm of the target distance D and the target width W. In the Shannon-MacKenzie formulation, Fitts' law is equal to:

$$MT = a \cdot ID + b = a \cdot \left[log \left(\frac{D}{W} \right) + 1 \right] + b, \tag{4.1}$$

where a and b are the slope and the intercept that can be calculated from experimental data.

While Fitts' law general validity has been often questioned [95], recent researches demonstrated that it is possible to derive it through an information-theoretic model that assumes the human motor system to be a noisy channel, and the ID can be derived as the expression of both a source entropy and a zero-error channel capacity with an eventual correction due to erasures [96]. Up to date, many studies in human motor control have used Fitts' approach to quantify performance in tasks of different nature that could be assimilated to reaching tasks [97–99]. However, the application of Fitts' law to "temporal targets", where these targets are time intervals beginning after a specific time lapse from the task start, has been rarely investigated in literature. Here, we will propose a model based on a combined ID, formed by a spatial part and a temporal part, for the performance evaluation of participants during the null space control task.

4.2 Methods

4.2.1 Subjects

Eight naive right-handed participants (mean ± SD age: 27.5 ± 7.8 years, age range: 20-45, 2 females) participated in the experiments after giving written informed consent. All procedures have been conducted in accordance with the principles embodied in the Declaration of Helsinki, comply with national regulations, and have been approved by the ethics committee IRCCS Sicilia - Sezione Neurolesi "Bonino-Pulejo" (Prot. n. 02/18). All participants had normal or corrected to normal vision and did not report any known neurological disorder or upper right limb injuries.

4.2.2 Experimental protocol

First of all, participants performed an initial familiarization phase with the setup and the force control task that will be described below. After this phase, the real experiment started, composed by 18 blocks with different task conditions.
The first block ("maximum voluntary force" (MVF) estimation) was performed by participants to calculate the highest force that they can exert along the -y direction, where y is directed along the anteroposterior axis away from the chest. The norm of this force would be used, in the next blocks, to normalize the distance of target as a fraction of this force.
In the second block ("force control" (FC) block , Fig. 4.1A), participants had to displace a spherical cursor, applying isometric forces on the orthoses, from a central rest position to a target, that could be located in one of twenty spatial positions arranged on the vertices of a dodecahedron inscribed into two spheres with radius 15% or 25% the MVF, respectively. Each trial was divided into different phases: at the beginning (rest phase) participants relaxed their right arm muscles to keep the cursor within a sphere in the centre of the 3D scene (the central rest position) for 1 s. Then, another sphere appeared in one of the twenty target positions (target go event), and the participant had to reach the target, whose radius was 2% the MVF higher than the cursor one, and keep the position for 0.5 s (holding phase). Each target was presented three times, such that each participant performed a total of 120 trials (20 targets $\times$ 2 radii x $\times$ repetitions). EMG and force data collected from the target go event until the first time the cursor entered the target (dynamic phase) were used to estimate a subject-specific matrix that approximates the mapping of EMG activations onto isometric force (see below EMG-to-force matrix) and its null space. The maximum amplitude of each EMG signal (low-pass filtered with second-order Butterworth; 1 Hz cutoff) collected during the same phase was used to normalize EMGs during the rest of the experiment. After this block, there was a 5 min pause to process the data.
In the third block (null space modulation, NSM), participants performed a cursor stabilization task that required using voluntarily co-contraction. The EMG data collected in this condition was used to estimate the null space patterns that each participant generated more naturally. Participants had to maintain the cursor inside a target placed in the rest position, whose radius exceeded that of the cursor by 6% of the MVF, for 1 s while a simulated sinusoidal force perturbed the motion of the cursor

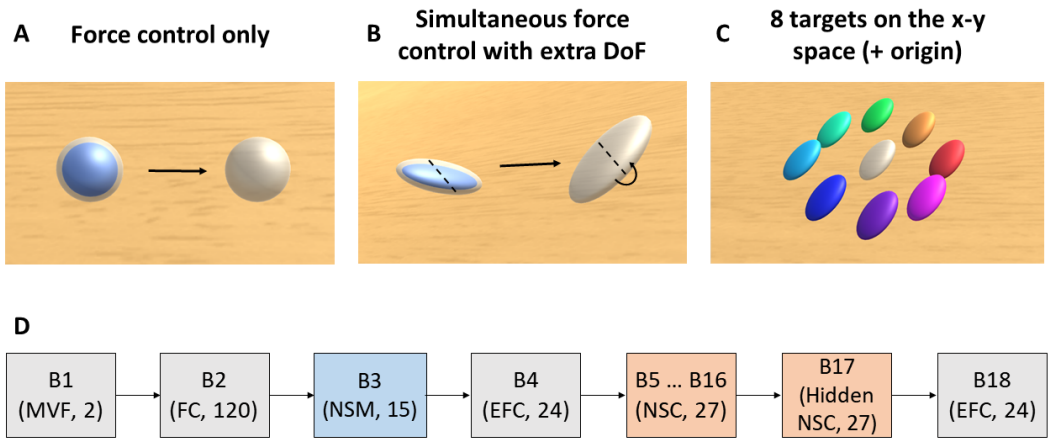

Figure 4.1: (A) Trial scene during force control block (blue cursor moves from home position towards the target in the direction of the arrow). (B) Trial scene during null space control block (the dashed line represent the rotation axis). (C) Target pattern (with home position at the center). (D) Experimental protocol scheme (MVF = maximum voluntary force, FC = force control, NSM = null space modulation, EFC = ellipsoidal force control, NSC = null space control).

[92]. To reduce this oscillation, participants were instructed to co-contract their right arm and shoulder muscles. The time limit for trial completion was 15 s, with 5 s of pause between trials. EMG data collected during the holding phase were used to calculate the null space directions to be used for the control the extra degree of freedom (see "Extra degree of freedom control" section).

In the fourth block (isometric reaching with ellipsoidal force control, EFC), participants performed an isometric reaching task with ellipsoidal cursor and targets. There were eight targets (3 repetitions), placed on the x-y plane at 20% of MVF from the origin, with a tolerance of 2% of MVF, and equally distributed with a 45° angular distance one from the other (0° = +x direction, with x mediolateral axis pointing to the right). Moreover, the cursor and targets were ellipsoidal rather than spherical. This block provided a baseline reference for the following 12 blocks.

In blocks 5th to 16th (null space control, NSC, Fig. 4.1B), participants had to both translate and rotate the ellipsoidal cursor (around the intermediate axis parallel to the forearm axis) to match the position and orientation of the target (see Fig. 4.2 for the schematic of the trial).

Translation was achieved by exerting force and rotation by generating muscle patterns with projections onto the null space directions selected according to the procedure

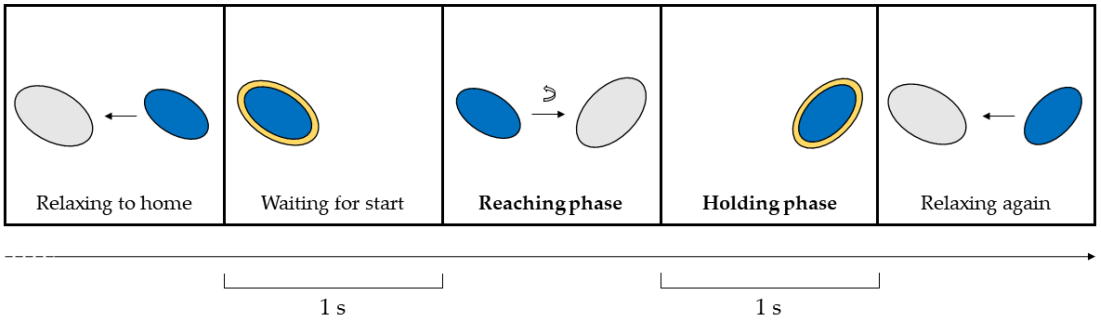

Figure 4.2: Temporal evolution of the different phases in a single trial for the null space control task. Particular focus is given to the two principal movement phases, the reaching phase (i.e., reach the target) and the holding phase (i.e., keep the cursor within the target).

described below (section "Extra Degree of Freedom control") using the data collected in the NSM block. There were nine targets (Fig. 4.1C), in different x-y positions – the same eight as in the EFC block plus one in the rest position – and with the same orientation achieved with a rotation from the rest orientation of 60° (corresponding to 20% of the maximum norm of the null space activation during NSM block, which we call "maximum voluntary co-contraction", MVCC) and a tolerance of 7.2° (4% of 180°). The translation tolerance was also of 4% of MVF. Participants were required to hold the cursor at the target for 1 s. The nine targets were presented in a pseudo-random sequence (cycle). At the end of each cycle, the score for that cycle was visualized. Finally, the 17th block was a null space control block without visual feedback (hidden null space control) and the 18th block an additional EFC block. A schematic of the experimental protocol is presented in Fig. 4.1D.

4.2.3 EMG-to-force mapping

In isometric conditions, i.e., when muscles generate force without reducing or increasing their length, as in our experimental protocol, and when the force exerted is submaximal, the relationship between muscle activation and force exterted at the hand can be approximated by a linear mapping:

$$\mathbf{f} = \mathbf{H}\mathbf{m},$$

where **f** is the tridimensional force vector, **m** is the 15-dimesional muscle activation vector, and **H** is the EMG-to-force matrix that maps muscles activations onto force. The matrix **H** was estimated using multiple linear regressions of each force component, low-pass filtered (second-order Butterworth; 1 Hz cutoff), with EMG signals recorded during the dynamic phase of the first force control block, low-pass filtered (as the force) and normalized to the maximum EMG activity recorded during the force control block targets at 25% of the MVF distance. We verified that the **H** matrix estimated using holding phase data was similar to the one extracted using dynamic phase. In fact, the cosine of the angle between the force vectors of the dynamic phase H matrix and the holding phase **H** matrix for the same muscle was 0.92 $\pm$ 0.26 (median value $\pm$ interquartile range across muscles and participants).
The matrix **H** was also used to compute the null space matrix **N**, i.e., an orthonormal basis spanning the subspace of vectors n that are mapped by the **H** matrix onto the null force vector:

$$0 = \mathbf{Hn}.$$

4.2.4 Selection of the extra degree of freedom control variable

To characterize the subject-specific directions in the EMG null space to be used for the control of the extra DoF, each participant performed a NSM block. This procedure allowed us to identify the directions that each participant could control more naturally and the dimensionality of this subspace. We could then select the directions in the null space with the largest amplitude modulation and use the projection of the instantaneous muscle activity vector onto those directions as the signal(s) to control the extra DoF.
The ideal control variable for null space control should be as small as possible during generation of pure force and have the largest range during voluntary modulation of co-contraction. We investigated three different null space control variables that could be suitable for our task. We tested them on the data previously collected in a task in which participants had to stabilize a cursor by null space activation [92]. Data were collected from eight participants performing five blocks: a force control block (baseline) and four additional blocks. Of these four blocks, the first was a NSM block similar to the one described above, while the other three blocks (force control with null space perturbation, that here we define "perturbation blocks") required the participant to reach targets using force control in addition to reducing the oscillation of the cursor by

null space activation. Furthermore, the intensity of the sinusoidal perturbation (and therefore of the magintude of null space activation required to maintain the cursor within the target) increased from the first to the third block.

We tested the following the null space control variables (labelled f_{DoF}):

- the norm of the projection of the null space activation vector $\mathbf{n} = \mathbf{N}^T\mathbf{m}$, onto the first nc principal components that explain 80% of data variation in the NSM block (after subtraction, due to PCA rotation, of the mean vector of null space activation in that block $\bar{\mathbf{n}}_{cc}$):

  $$f_{DoF} = ||\mathbf{V}_{cc}(:, nc)'[\bar{\mathbf{n}} - \bar{\mathbf{n}}_{cc}]||,$$

  where represents the transposed of the first nc columns of the matrix of the principal components of the null space activation vectors collected in the NSM block;

- the norm of the projection of the null space activation vector n onto the first nc principal components that explain 80% of variance of NSM block (after subtraction, due to PCA rotation, of the mean vector of null space activation in baseline FC block $\bar{\mathbf{n}}_{bl}$, taken as a reference of residual, involuntary null space activation):

  $$f_{DoF} = ||\mathbf{V}_{cc}(:, nc)'[\bar{\mathbf{n}} - \bar{\mathbf{n}}_{bl}]||;$$

- the norm of the projection of the null space activation vector n onto the mean null space activation vector in NSM block:

  $$f_{DoF} = ||\bar{\mathbf{n}}'_{cc}\bar{\mathbf{n}}||.$$

A schermatic illustration of the application of the three different methods to data simulated with a simple toy model is shown in Fig. 4.3.
After calculating all the projection matrices required for computing the three control variables, we assessed the mean value of each variable across the force control block and all the three perturbation blocks for each subject. The different control variables were compared using one-way ANOVA (see "Statistical analysis" for details). Also the difference between the mean value of each variable across all the three perturbation blocks and the force control mean value was performed and the resulting data compared

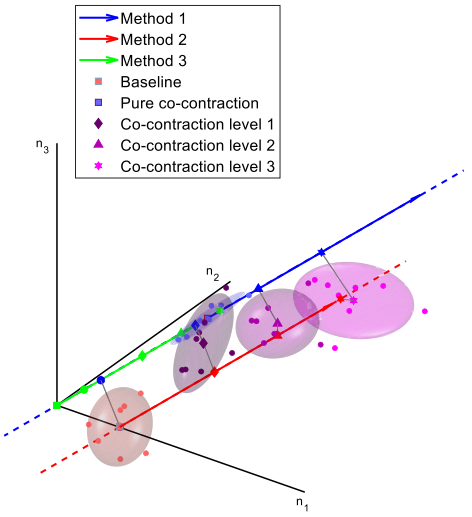

Figure 4.3: Schematic representation of the three methods used for computing a null space control variable. The methods are illustrated using simulated data generated through a toy model of a planar 2-DOF arm with 8 muscles pulling in randomly selected directions. Force and stiffness are a linear function of muscle activation. Baseline data correspond to minimum-norm nonnegative muscle activations generating force in 8 different directions. Pure co-contraction data are muscle activations with zero force and increased stiffness. Cocontraction data are muscle patterns with forces in 8 directions and three different levels of increased stiffness. All muscle patterns are represented as projected onto the direction of first three principal components of the baseline data (n_1, n_2 and n_3). The dashed gray lines represent the projections of the average data from each condiation onto the three vectors used to compute the control variable in each method.

through ANOVA to find the method with the widest significant activation range.
In the NSM block, the perturbation was generated as a sinusoidal force (with different frequencies along different axes) acting on a mass attached to a position (controlled by force) through a spring with an elastic constant that was adjusted in real time according to the norm of the null space activation vector through a logistic function [92]:

$$k(\mathbf{n}) = k_{max}/(e^{(-r_k(||\mathbf{n}||-||\mathbf{n}_0||))} + 1),$$

where $||\mathbf{n}||$ is the norm of the null space activation vector, $k_{max} = 9500\ N/m^2$ is the spring constant, r_k is a variation rate parameter, and $||\mathbf{n}_0||$ is the value of the null space norm such that $k(\mathbf{n}) = k_{max}/2$. The value of $||\mathbf{n}_0||$ was set equal to 2.5 times the

minimum norm ($||\mathbf{n}_{min}||$) of the mean null space activation during the static phases of FC block, while r_k was calculated using the formula:

$$r_k = -log\left(\frac{k_{max}/y_0 - 1}{x_0 - 1}\right)$$

Mean-subtracted holding phase data were used for computing the principal components. We obtained a $\mathbf{V}_{cc}$ matrix of dimensions 12 $\times$ 12 whose columns were the principal components of the data. The null space was 12-dimensional because the muscle space was 15-dimensional and the task space 3-dimensional. Then, we selected the first *nc* components that explain 80% of the total variation of the data (mean value of components $\pm$ SD among participants: 2.1 $\pm$ 0.8, range 1-3).

4.2.5 Null space control law

Once a control variable was selected in the preliminary study (see "Selection of the extra degree of freedom control variable" above) and the data collected in the NSM block were used to identify the null space control directions for each participants, a mapping of the null space control variable onto cursor rotation was used during NSC blocks. To map the null space control variable onto the control signal for the extra DoF we chose a logistic function, as the one used in the null space modulation block, because it is always positive defined, and, to return to the rest position, participants had only to relax their muscles. Moreover, it has a smooth and continue derivative, so that there is no need to put a threshold activation, as it would be for example for a linear relation.
Therefore, the control law that mapped null space activation onto cursor rotation angle was defined as:

$$\theta(f_{DoF}) = \theta_{max}/(e^{(-r_\theta(f_{DoF} - f_{DoF,0})} + 1),$$

where θ is the angle of rotation, θ_{max} is the maximum angle of rotation, set to 145, r is the variation rate, f_{DoF} is the control variable and $f_{(DoF,\theta)}$ is the value of the control value for which $\theta(f_{DoF}) = \theta_{max}/2$.
The value of $f_{DoF,0}$ was computed using $||\mathbf{n}||$ equal to 25% of the MVCC. The r_θ value was calculated using the formula:

$$r_\theta = -log\left(\frac{\theta_{max}/y_0 - 1}{x_0 - 1}\right),$$

where $(x_\theta, y_\theta) = (f_{DoF}(n_{min}), 0.1)$.

4.2.6 Data analysis

Data collected during all trials performed by all participants were visually inspected and trials in which EMG artefacts were detected were discarded. The discarded trials were 13.1 ± 7.6 (mean ± SD over participants) over the 536 trials of the whole experimental session performed by each participant.

Task performance. Task performance was evaluated both as the fraction of trial per block in which participants reached the target (reaching success rate), and as the fraction of trial per block in which participants held the cursor in the target for the required time (holding success rate).
Mean holding time and mean angular error per block were also calculated. In each trial, holding time was defined as the longest time interval in which the cursor remained inside the target (maximum value 1 s, the required holding time). The angular error was defined as the mean difference of the cursor rotation angle and the target rotation angle over the interval in which the cursor positional error in space was under the threshold of 6 % of MVF.

Velocity peaks and movement strategies. Two different velocities of the cursor were calculated: the tangential velocity of the cursor spatial trajectory (therefore related to the force), and the angular velocity of the cursor rotation angle around the axis parallel to the forearm (therefore related to the muscle null space activation).
The two velocities were computed numerically for each trial, after applying a 2nd order Butterworth filter (3 Hz low-pass cutoff frequency) to the cursor position (measured as a fraction of MVF, while the angle in radiants was rescaled to have the same units). The movement onset was defined as the first sample after the end of the rest phase (i.e., when the target appeared on the screen) at which the cursor velocity was higher than a threshold of three times the mean velocity, recorded in the 0.5 s before the 'target go' event. The peak velocity was defined as the first maximum after the movement onset.
Movement onset and velocity peaks were analyzed to assess if different participants used different movement strategies. For example, if a participant displaced the cursor first and then rotated it (using muscle null space activation), or vice versa, or if they

moved and rotated the cursor simultaneously, or if there was no specific correlation between the two movement components.

Performance analysis. In addition to success rates, we used information theory to assess individual control ability. We considered the information about the instructed target that is transmitted by each participants when performing a reaching and holding movement. To generalize the assessment of individual ability beyond the performance achieved by each participant with the specific parameters of the experimental protocol (e.g., the target size or the required holding time) we estimated, through a simulation, the information that would have been transmitted with different target sizes and holding times.
The information transmitted accomplishing a reaching task may be quantified by an index of difficulty, as introduced by Fitts [94]. The Fitts' law states that movement time MT in a reaching task is linearly related to an index of difficulty ID:

$$MT = a \cdot ID + b.$$

The Fitts' ID, for a target of width W and distance D from the origin, in the Shannon-MacKenzie formulation [100], is equal to:

$$ID = log_2(D/W + 1).$$

While Fitts' law validity has been questioned because of its unclear theoretical foundations [95, 101], Gori and collaborators [96] derived this law with a simple model of the human performance, during an aiming task, as a communication process. In this model, the source of the message is the target the individual intends to reach ("aiming is choosing"). In the original formulation of Fitts, aiming at a target of width W at distance D is equivalent to selecting one of n linearly arranged targets of width W such that $D = nW$ (Fig. 4.4A).
If the targets can be selected with the same probability, the entropy of the target distribution, i.e., the entropy of the source, is equal to the ID. The message is then sent through a noisy channel, representing the execution of the reaching movement with physiological noise in the neural and the musculoskeletal systems. If the noise results in a distribution of the arrival position with an amplitude less than $W/2$, aiming at the center of the target allows to always hit the selected target and thus trasmitting the

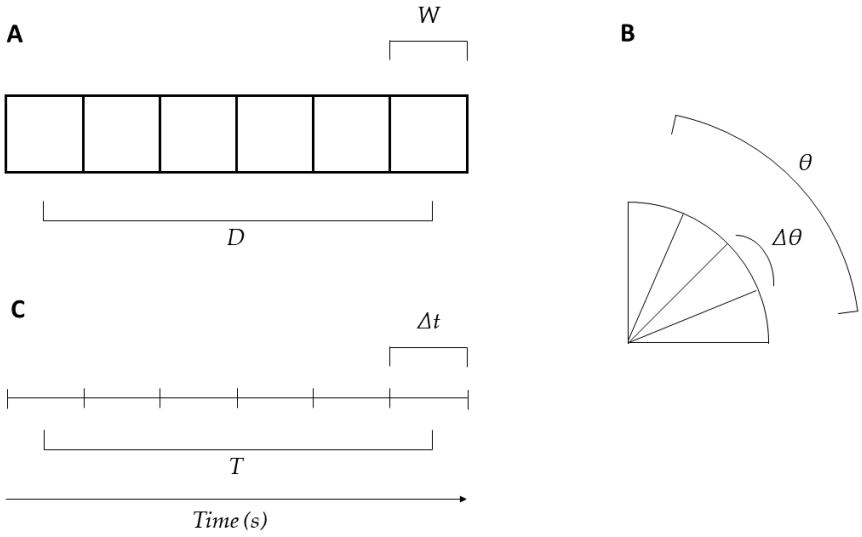

Figure 4.4: Schematization of target pattern for the three IDs used for performance quantification: (A) displacement ID, (B) rotational ID and (C) temporal ID.

message without error. Then, the ID quantifies the information that can be trasnsmitted in an aiming task with negligible error rate, equal to the source entropy for errorless transmission.

Apart from its theoretical framework, Fitts' law has been shown to be a robust empirical relation between movement time and the spatial parameters of a task as long as no temporal constraints are set, or if these constraints are relaxed in such a way that they do not influence too much the task itself [102–104].

Since in our task subjects were required to reach the spatial location (xyz coordinates) of the target and to align the cursor to the target orientation, we can define two distinct indices of difficulty for each one of the two components of the reaching movements (translation and rotation). For the 3D displacement of the cursor position, considering that the tolerance is always the same for the three axis, a displacement ID can be defined as:

$$ID_{xyz} = log_2\left(\frac{D}{W_{xyz}} + 1\right) = log_2\left(\frac{D}{2R} + 1\right),$$

where D is the target distance in % of MVF, and R is the target radius also in % of MVF. Recent research has shown a dependence of the movement time on the target angle for 2D and 3D tasks [105, 106]. According to our data, the dependence resembles

a linear combination of a sine term and a cosine term. Therefore, a better definition of the ID is:

$$ID_{xyz} = log_2\left(\frac{D}{2R} + 1\right) + c \cdot sin(\alpha) + d \cdot cos(\alpha),$$

where α is the direction angle of the target on the x-y plane. The two coefficient c and d were calculated by fitting movement times vs ID_{xyz} in the two EFC control. For the cursor rotation, a rotation ID can be defined as:

$$ID_\theta = log_2\left(\frac{D}{W_\theta} + 1\right) = log_2\left(\frac{D}{2\Delta\theta} + 1\right),$$

where θ is the rotation angle and $\Delta\theta$ is the rotation angle tolerance (Fig. 4.4B). The total *spatial* ID can then be defined as the sum of the displacement and rotation indices:

$$ID_S = ID_{xyz} + ID_\theta.$$

However, the application of this ID formulation to our experimental protocol raises three issues. First, Fitts' law has been formulated for an aiming task in which the participant is not required to hold the end-effector at the target location for a specific time interval, but rather to simply hit the target. However, when considering the ability of controlling an end-effector with myoelectic signal, it may be necessary to provide also a temporal command in addition to a spatial one. Being myoelectric control typically noisier than the natural limb control, it would be then useful to quantify also the target holding performance. Second, the Fitts' law does not consider the actual error rate in the reaching task, assuming that it is low enough to be neglected. This second issue has been addressed by estimating an effective target width for which the error rate is below a given small (but arbitrary) threshold [98, 107, 108]. However, individual ability in aiming at a target can be rigorously quantified using a communication model with transmission errors [96]. Third, to properly assess the individual ability to control the position and orientation of the cursor, we should have used targets of different size and different holding time requirements. Indeed, speed-accuracy trade-off functions derived by systematically varying the required accuracy have been used to assess individual skill in manual tasks [109, 110]. However, an additional factor in our experimental design would have required a large number of trials making the assessment too long to perform. We therefore opted for an approximate but faster assessment of the dependence of the individual cursor control ability on the specific

task parameters by simulating off-line the performance that would have been achieved with different parameters.

Concerning the first issue, we followed the model of a communication system to derive also a temporal ID. Making a parallel with the spatial case, in which we have n targets of width W in a length D, we can consider a time interval of duration T, which can be divided in n consecutive temporal targets of duration Δt. In this way, in addition to selecting a spatial target by reaching it, it is possible to select one of the temporal targets by holding at the spatial target until the specific time is elapsed. In addition to considering that "aiming is choosing" (Fig. 4.4A and B) [96], which means that an individual can choose one target from a set of many by aiming at it, we consider that "waiting is choosing" (Fig. 4.4C), which means that an individual can choose a "temporal target" from a set of many by waiting for a given time interval before moving. Following this reasoning, an expression for a temporal index of difficulty can be derived as:

$$ID_T = log_2\left(\frac{T}{\Delta t} + 1\right),$$

where T is the duration of the considered time interval, while Δt is the duration of the time sub-intervals, defining the required temporal accuracy.

Concerning the second issue, it is possible to calculate the effective size of the target that would satisfy the assumption of negligible error rate [107, 108]. Assuming the trial endpoint distribution to be normal, its entropy is equal to $log_2\sigma\sqrt{2\pi e}$. The quantity $\sqrt{2\pi e}$ is equal to about 4.133, which means $\sim \pm 2\sigma$, that is the 96% of the area of the distribution. Therefore, if success rate is equal to 96%, the effective width W_e of a target and its experimental width coincide. Otherwise, if the standard deviation of the endpoint distribution σ_e is known, the effective width can be calculated using the formula:

$$W_e = 4.133\sigma_e,$$

while if it is not known, the formula using the error rate ϵ can be applied:

$$W_e = \begin{cases} W\frac{2.066}{z(1-\epsilon/2)}, & \text{if } \epsilon > 0.0049\% \\ W \cdot 0.5089, & \text{otherwise} \end{cases}$$

where z is the standard score of a distribution with mean = 0 and SD = 1.

Nevertheless, this approach has been criticized because it is based on questionable

assumptions as the normal distribution of the endpoints and the coincidence that, with 4% of error rate, the information of a rectangular distribution of width W_e is equal to the one of a normal distribution [96].
Therefore, Gori and collaborators have proposed a new index of difficulty that takes into account the error rate [96]. It can be derived using a compound channel with two states (a good state and a bad state), as the Shannon-MacKenzie ID multiplied by the success rate $(1 - \epsilon)$:

$$ID(\epsilon) = (1 - \epsilon) \cdot log_2 \left(\frac{D}{W} + 1 \right).$$

In our case, we considered the reaching error rate ϵ_r (or the complementary success rate $1 - \epsilon_r$) related to the identification of the target in space, i.e., to the spatial ID, while the holding error rate ϵ_h (or the complementary success rate $1 - \epsilon_h$) to the identification of the time interval, i.e., to the temporal ID. Therefore, the corrected ID can be defined as:

$$ID(\epsilon_r, \epsilon_h) = (1 - \epsilon_r) \cdot ID_S + (1 - \epsilon_h) \cdot ID_T.$$

Concerning the third issue, in our experimental protocol we used only one target size (corresponding to a cursor translation accuracy of 4% MVF), one cursor rotation tolerance (corresponding to 4% of the MVCC). Moreover, the temporal accuracy required for the holding time (the Δt parameter) was not explicitly defined: partipants were required to keep cursor in position inside targets for a time $T = 1$ s. However, because we wanted to assess the individual ability in displacing and orienting the cursor and in holding the target regardless of specific task parameters, we used the data collected in one condition to simulate the performance that participants would have achieved in different conditions. Thus, we computed the reaching performance with targets of different sizes (6% to 3% of MVF and corresponding % of MVCC, with a step of 0.5%), and the performance for holding the target for the required time with differenent temporal tolerances (1 s $\pm$ 0.1 s to 1 s $\pm$ 0.9 s with a step of 0.1 s, and 1 s $\pm$ 0.999 s, this last being equivalent to just spatial reaching).
As a first step, we estimated the mean reaching movement time MT_R (defined as the time interval between the "target go" event and the first time the cursor entered the target) and the mean execution movement time MT_E (defined as the time interval between the "target go" event and the end of the holding phase) from simulations with different target size and holding time (for MT_E only) tolerances for each participant.

The simulation was performed by measuring if a target of a specific size would be hit by a participant with the real trajectories recorded during task execution, and how much time a participant kept the cursor inside the specified space region according to the real trajectories. Then, we linearly fitted reaching movement times vs reaching IDs (in the form: $MT_R = a_S \cdot ID_S + b$, where a_S and b are the fitted parameters) to verify that our data follow Fitts' law, and execution movement times versus total IDs (in the form: $MT_E = a_{S'} \cdot ID_S + a_T \cdot ID_T + b'$, where $a_{S'}$, a_T and b' are the fitted parameters) to verify that a linear relation still holds when the temporal ID is added. Finally, an additional measure of performance that can be obtained from the Fitts' law is the throughput, defined as the ratio between the ID and the movement time. The average movement times for each block and target were taken, and the mean across targets was computed. We then estimated the throughput considering only the reaching phase, because the holding phase has a fixed information rate. Whenever a target was not reached in a block, we set the throughput for that target to zero.

Statistical analysis. Statistical analysis was performed using MATLAB. Anderson-Darling test (function "adtest") was used to check the normality of the distribution of datasets from the simulation of the different extra DoF control laws. One-way ANOVA test (with multiple comparison with Tukey's honest significant difference criterion as post-hoc, functions "anova1" and "multcompare") between datasets composed by the same control methods from all the participants was performed to investigate differences between control methods. Similarly, Kruskal-Wallis one-way ANOVA, after Anderson-Darling test, was used to compare reaching and holding success rates, and the R^2 of reconstruction of the three force control blocks (one FC and two EFC blocks).
For the NSC blocks, the dependence of reaching and holding success on block and target was assessed by fitting a generalized linear mixed model (function "fitglme"), with the block and target as fixed effects and participant as random effect. Similarly, the dependence of angular deviation and holding time, on block and target was assessed by fitting a linear mixed model (function "fitlme"). Additionally, a generalized linear model (function "fitglm") and a linear model (function "fitlm") was fitted to the response variables for each participant separately.
Pearson correlation coefficient between force and extra DoF peak velocity times was calculated to assess the correlation between the two velocity peak times across blocks, and Kruskal-Wallis one-way ANOVA, after Anderson-Darling test, was used to find

eventual significant differences between the dataset distributions.

4.3 Results

4.3.1 Null space control validation

We performed a simulation on data collected during combined force and muscular null space activity generation [92] to select the variable to be used for the control of an extra DoF. We calculated the mean values for three candidate control variables, which differed for the null space components of the projection of the muscle patterns selected and for the mean muscle pattern used for subtraction. The mean values were calculated during four blocks in which participants generated only force (Force Control, Fig. 4.5) or force combined with increasing levels of co-contraction (Perturbation Blocks 1-3).

After verifying the normality of the distribution of the values of each control variable ($p > 0.05$, Anderson-Darling test), we performed a one-way ANOVA on the value of the control variable in each block with the method used to compute the control variable as factor. For pure force control, the first method, using the projection onto the null space principal components explaining 80% of NSM block data variance after subtracting the mean NSM block activation vector, presented significantly higher involuntary activation with respect to the other ones ($p < 0.001$ for both comparisons), making it unsuitable for our task. For combined force and co-contraction control with the lowest level of required co-contraction (Perturbation 1), there were no significant differences between the methods ($p = 0.33$). However, with higher levels of co-contraction (Perturbation 2 and 3) the second method had a higher level of the control variable with respect to the first ($p = 0.03$ and 0.02, respectively) but not with respect to the third ($p = 0.29$ and 0.19, respectively). Nonetheless, the one-way ANOVA performed on the activation differences between perturbation blocks and force control block, with control variable as factor, showed a significant higher activation range for the second method. According to these results, the second method, using the projection onto the principal components extracted during NSM block after subtracting the baseline mean null space activation vector, was selected as the best choice to control the extra DoF.

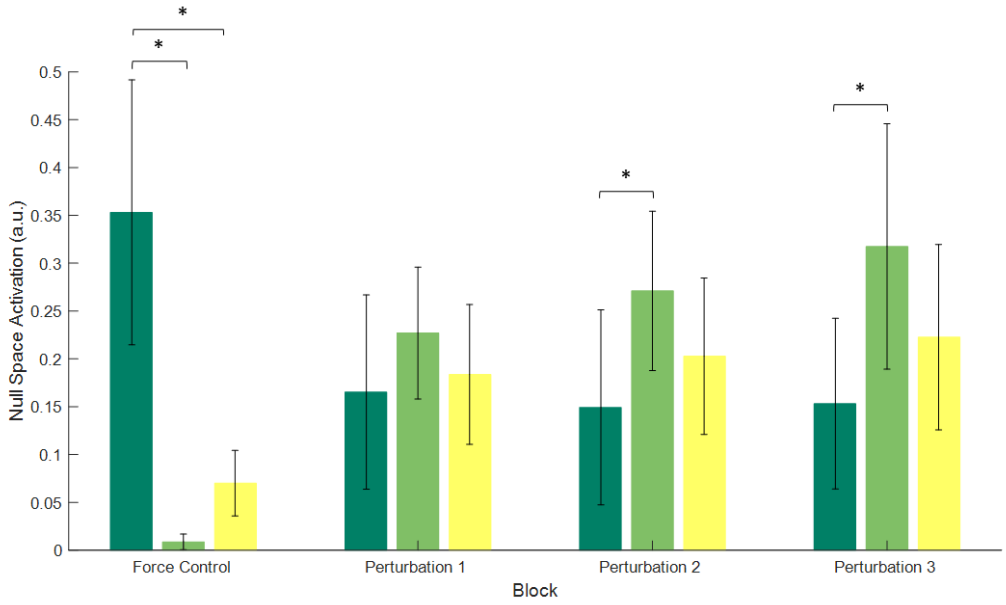

Figure 4.5: Bar plot with the mean simulated null space activations for each of three methods described in Section 4.2.6. The first control variable, in dark green, uses the norm of the projection of the null space activation vector onto the first principal components explaining 80% of data variation in the NSM block (after subtraction of the mean vector of null space activation in that block); the second, in light green, is based on the norm of the projection of the null space activation vector onto the first principal components that explain 80% of variance of NSM block (after subtraction of the mean vector of null space activation in baseline FC block, taken as a reference of residual, involuntary null space activation); finally, the third, in yellow, uses the norm of the projection of the null space activation vector onto the mean null space activation vector in baseline FC block. Error bars represent the standard deviation across participants.The second method clearly shows the lower involuntary activation during force control and the widest activation range.

4.3.2 Force control performance

After selecting the method to compute the null space control variable, we recruited eight participants to assess their ability to control simultaneously natural and extra DoF. We first assessed baseline performance in FC. During this block, participants displaced the cursor toward the targets along approximately straight paths, reached the target successfully in 92 ± 6 % (mean ± SD across participants) of the trials, and remained in the target for the required time in 63 ± 19 % of the trials (see Table 1 for individual data). Thus, while reaching the target was easily accomplished by our participants, holding was more challenging. Moreover, holding performance

varied considerably across participants, as indicated by its large standard deviation. Similar performances were observed during the initial EFC block, for which the success rates for reaching and holding were, respectively, 88 ± 25 % and 67 ± 31 %. No significant differences were found between FC and EFC blocks for both reaching and holding performance (p = 0.24 and 0.56, respectively, Kruskal-Wallis one-way ANOVA). Therefore, the shape (spherical or ellipsoidal) of cursor and targets did not affect force control performance.

The mean R^2 across participants of the three-dimensional force reconstruction during the FC block, was 0.76 ± 0.11 (see Table 4.1 for individual data). During the initial

ID	Reaching SR	Holding SR	Force R^2
1	0.92	0.59	0.85
2	0.88	0.42	0.52
3	0.96	0.51	0.74
4	0.96	0.78	0.75
5	0.89	0.46	0.79
6	0.97	0.72	0.84
7	0.83	0.56	0.70
8	0.99	0.98	0.89

Table 4.1: Individual performance, for each participant, and force reconstruction quality for the linear relation fit between forces and EMG activations.

EFC block, the mean horizontal (rather than three-dimensional, as targets were all planar in this block) force reconstruction R^2 was 0.78 ± 0.13, and no significant differences were found with respect to the initial FC (p = 0.46, Kruskal-Wallis one-way ANOVA). These results support the robustness of the EMG-to-force mapping, which was used for calculating the EMG null space and therefore the variable used to control the extra DoF.

4.3.3 Null space control performance

In NSC blocks, participants performed trials with eight ellipsoidal targets, positioned at a distance and with an orientation corresponding to 20% of MVF and 20% of MVCC respectively.

Differently from FC and EFC blocks, especially in the initial NSC blocks, cursor trajectories were more variable over repetitions because of the interference between the natural and extra DoFs and the lack of coordination among them. Although partici-

pants directed the cursor quite accurately toward the targets, they were less accurate with the cursor rotation (i.e., the extra DoF), which was controlled by null space activation, and the rotation angle often overshoot the target angle and oscillated around it. This is clearly visible in both panels of Fig. 4.6, where the trajectories of first blocks for the extra DoF often exceed the upper target threshold (dashed line).
Interference sometimes also led to an oscillation in the spatial position of the cursor, highlighting the difficulty in simultaneous control of the different DoFs, as it is visible in panel A of Fig. 4.6 With practice, however, all participants showed improvements in their control of the extra DoF. For example, for all three participants illustrated in Fig. 4.6B initially (Block 5, darkest lines) the first peak velocity of cursor rotation (vertical lines, top) occurred often much later than the peak velocity of the cursor translation (vertical lines, bottom), but it then occurred progressively earlier with practice (Blocks 8-16, lighter lines).
Mean success rate across participants in target reaching and holding increased during the 12 NSC blocks. Reaching success rate progressed from 72 $\pm$ 26 % to 93 $\pm$ 11 % in the last block. Holding success rate was initially low, 12 $\pm$ 12 % in the first block, and achieved a maximum value of 43 $\pm$ 31 % (Fig. 4.7A and B).
The mean movement time for reaching phase only across participants decreased among blocks, with a starting value of 2.79 $\pm$ 0.54 s and an ending value of 2.02 $\pm$ 0.54 s. Similar considerations can be done for the movement time including holding phase, with a value of 3.34 $\pm$ 0.25 s in the first block and a value of 2.78 $\pm$ 0.50 s in the last (close to the value of movement time for reaching in the first block). The mean holding time across participants increased, achieving the highest mean value of 0.70 $\pm$ 0.29 s, while the mean angular error decreased below the required target threshold of 7.2° (6.69 $\pm$ 2.18° for the last block, minimum mean value achieved) (Fig. 4.7C and D).
A generalized linear mixed model analysis, with block and target as fixed effects and participant as random effect, showed a significant dependence of both reaching and holding success rate on block ($p < 0.001$ for both variables, with a slope of 0.047 and 0.041, respectively), indicating a significant increase in average performance with practice. The effect of target was also significant for both reaching and holding ($p = 0.001$ and 0.041, respectively), which means performances were not equal across targets. In fact, both target 4, 5 and 8 showed lower mean reaching success rate with respect to target 1, taken as reference ($p = 0.006$, 0.002 and 0.004 respectively), while target 6

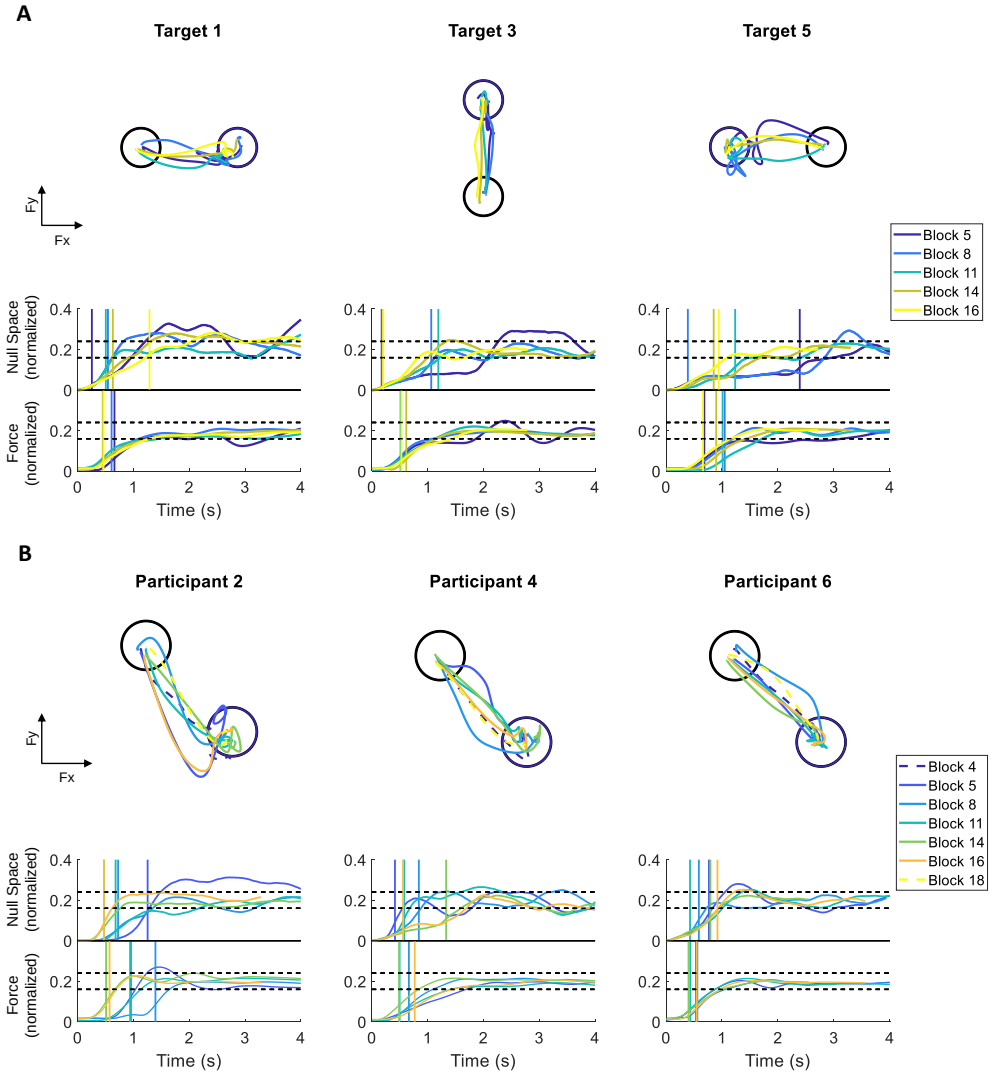

Figure 4.6: Examples of task performance during NSC blocks. (A) Example of cursor trajectories to different targets (1, 3 and 5) for participant 6: for each target (column) the plot on top shows the trajectory in Fx-Fy plane (being the target distance expressed in % of the MVF), the middle plot shows the evolution in time of the normalized null space control variable, and the plot on bottom the normalized force. To illustrate the temporal evolution of trajectories, the color changes with block number: trajectories became straighter over blocks. Vertical lines show the time of first velocity peak. (B) Example of trajectories in the x-y plane (top row) and time evolution of null space control variable (middle row) and force (bottom row) to one target (8), for participants 2, 4, and 6 (columns). Trajectories in the x-y plane during EFC are also shown for comparison (dashed lines, top row). The dashed black lines indicate target tolerance.

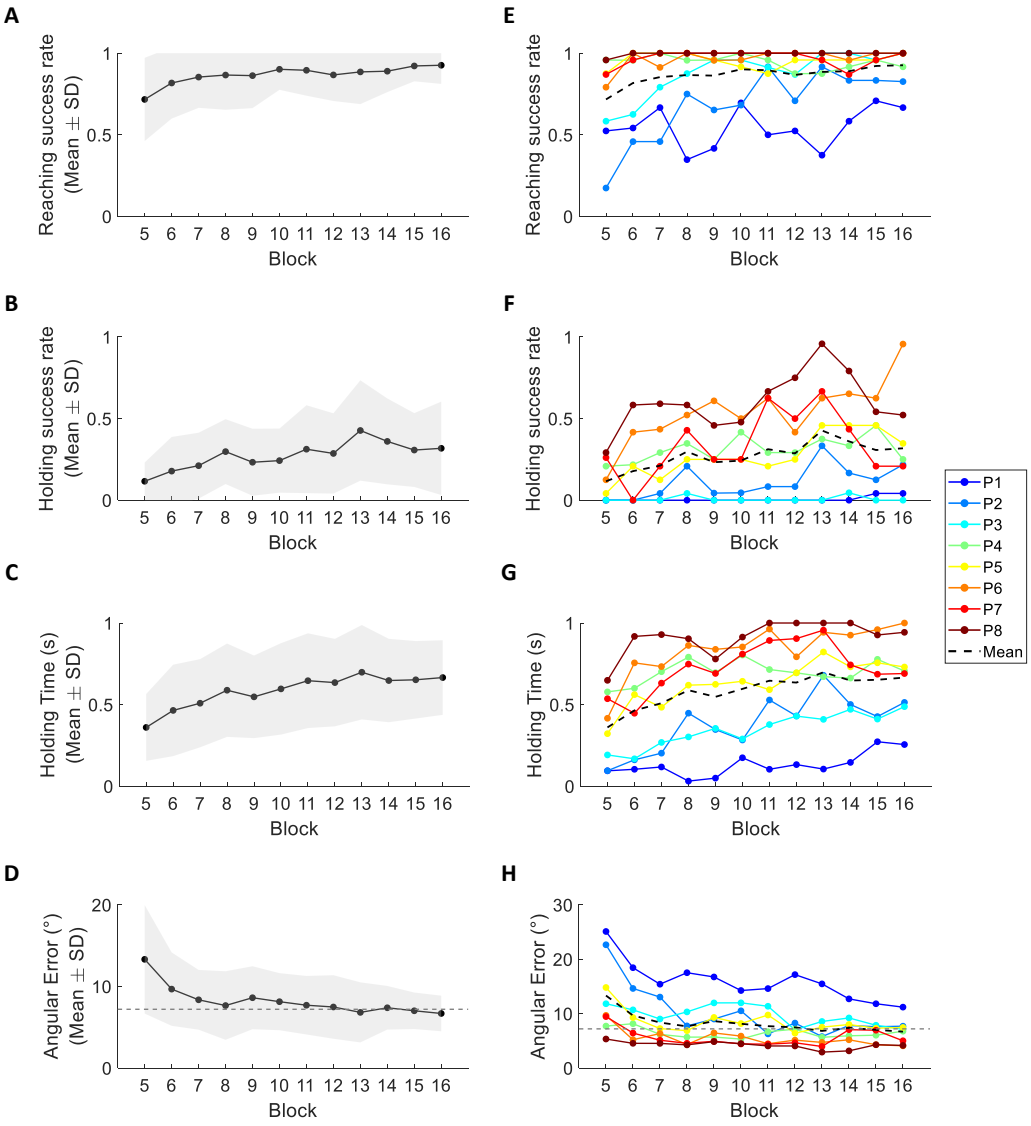

Figure 4.7: Simultaneous force and null space control performance. The mean values across participants (left column panels) show that reaching success rate (A), holding success rate (B) and holding time (C) increased with practice, while angular error (D) decreased. Right column panels show the curves for each participant separately and make visible the variability in performance among them. Shaded areas represent mean ± SD, and the gray dashed line in panels (D) and (H) represents target tolerance for angular error.

presented higher holding success rate ($p = 0.022$).

Remarkably, there was substantial inter-individual variability in performance, especially for target holding, as indicated by the large standard deviation (Fig. 4.7A, B, C and D). For this reason, we also analyzed the data of individual participants separately,

fitting them with a subject-specific generalized linear model with block and target as fixed effects. For reaching success rate, we found a significant effect of block only in participant 2, 3 and 6 (Table 4.2). This is because all the other participants, except participant 1, had high reaching success rate from the beginning of the experiment. Participant 1 was instead rather erratic, with a large variability in success rate from block to block, and always below 80%. For holding success rate, we found a significant effect of block for participants 2, 5, 6, 7 and 8 (Table 4.2). A significant target effect on reaching performance was found for participants 1, 2, 3 and 4 and on holding performance for participants 4, 5, 6, 7 and 8 (Table 4.3). These results indicate that with practice, participants improved their control skill, but learning capability was not the same for all participants, and it was not uniform across the different directions. As an example, participant 1 had lower reaching success rate for target 5 with respect to the reference target 1 ($p = 0.028$), but higher reaching success rate for targets 6 and 7 ($p = 0.027$ and 0.008, respectively), as well as participant 5 had higher holding success rates for the same targets ($p = 0.012$ and 0.040, respectively). Individual performances are plotted in Fig. 4.7E and F.

Concerning holding time and angular error, the linear mixed models, with block and target as fixed effects and subjects as random effect, showed a significant dependence on block ($p < 0.001$ for both variables, slope 0.009 and -0.12, respectively). Target effect was not significant for holding time ($p = 0.088$), while it was significant for angular error ($p < 0.001$). The linear model fitted separately to individual participants' data showed a significant block effect on holding time for all participants except participant 4, while for the angular error a significant block effect was found for all participants except participant 4 and 7 (Table 4.2). Both these participants had values close to their best values since the beginning of the experiment. Target effect on holding time was significant for all participants (while it was not the case when considering them together) and on angular error for all participants except participants 6 and 7 (Table 4.3). In sum, this analysis highlighted that, even when success rate does not increase significantly, learning can be anyway seen in continuous parameters such as holding time and angular error. Individual values are plotted in Fig. 4.7G and H.

We then investigated the force control and the null space control performances separately, i.e., the success rate for reaching and holding considering only either the position or the rotation of the cursor. The separate performances were better than the combined performance, which was provided as feedback to the participants during

ID	Reaching SR	Holding SR	Holding time	Angular error
1	0.26	0.17	< 0.001*	< 0.001*
2	< 0.001*	0.002*	< 0.001*	< 0.001*
3	< 0.001*	0.94	< 0.001*	< 0.001*
4	0.14	0.17	0.20	0.10
5	0.65	< 0.001*	< 0.001*	< 0.001*
6	0.005*	< 0.001*	< 0.001*	< 0.001*
7	0.61	0.02*	< 0.001*	0.09
8	0.33	0.003*	< 0.001*	< 0.001*

Table 4.2: p-values for the block effect of the generalized linear models and the linear models, for all subjects for success rate (reaching and holding), holding time and angular error. The asterisk indicates values of $p < 0.05$.

ID	Reaching SR	Holding SR	Holding time	Angular error
1	< 0.001*	1	0.048*	< 0.001*
2	< 0.001*	0.57	< 0.001*	< 0.001*
3	0.013*	1	0.015*	0.029*
4	0.029*	0.007*	< 0.001*	< 0.001*
5	0.29	< 0.001*	< 0.001*	< 0.001*
6	0.99	< 0.001*	0.001*	0.07
7	0.73	0.005*	0.004*	0.38
8	1	< 0.001*	< 0.001*	< 0.001*

Table 4.3: p-values for the target effect of the generalized linear models and the linear models, for all subjects for successful trials fraction (reaching and holding), holding time and angular error. The asterisk indicates values of $p < 0.05$.

the experiment, as the color of the target changed when both position and orientation of the cursor were within the target tolerance. All participants achieved a 100% reaching success rate in at least one block for both force control and null space control separately (maximum mean $\pm$ SD across participants: 100 $\pm$ 1 % and 99 $\pm$ 2 %, respectively). Holding success rate raised to 89 $\pm$ 12 % for force control, with 4 participants achieving 100%, and 60 $\pm$ 32 % for null space control. It was therefore the lack of coordination in displacing and rotating the cursor that significantly affected the global performance (Fig. 4.8).

A generalized linear mixed model analysis highlighted a significant dependence on block for both reaching and holding of both force and null space control performance ($p < 0.001$ for all cases, slope of 0.093, 0.051, 0.051 and 0.040 for force reaching, force holding, null space reaching and null space holding respectively). Target effect was

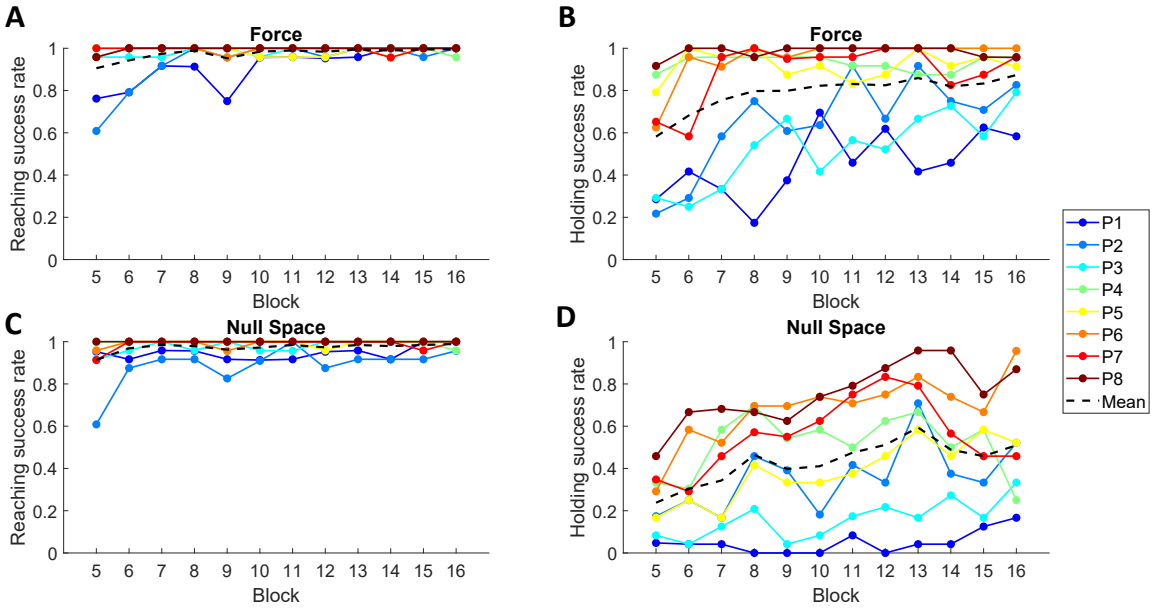

Figure 4.8: Separate force control and null space control performance. Reaching and holding success rates for force control (first row) and null space control (second row) are shown separately. The black dashed lines represent mean across participants.

significant only for null space reaching ($p < 0.001$), while it was not for force reaching ($p = 0.134$), force holding ($p = 0.149$) and null space holding ($p = 0.58$).

The analysis of the performances of each participant separately revealed different individual strategies, which were not evident when considering success rate for combined force and null space control. For example, participant 1 showed a significant block effect in all success rates except null space reaching, showing an improvement not visible with simultaneous control success rate. This participant, together with participant 2, was the only one with a significant improvement in force reaching, while in force holding participants 3, 6 and 7 also showed a significant improvement together with 1 and 2. In null space reaching only participants 2 and 3 had a significant block effect; nonetheless, all participants except participant 4 had significant block effect in null space holding. It is worth noting that participant 4 increased their performance in null space holding, but after nine blocks, performance started to decrease probably due to fatigue and/or reduced attention.

For the final EFC block, after the NFC blocks, mean success rates across participants for reaching and holding were respectively 95 ± 12 and 77 ± 24 %. No significant differences were found between initial and final EFC blocks, for both reaching and holding ($p = 0.19$ and 0.48, respectively, Kruskal-Wallis one-way ANOVA). This in-

dicates that practicing simultaneous force and null space control did not affect force control alone. The mean horizontal force reconstruction R^2 across participants during the final EFC block was 0.67 ± 0.23, and no significant differences were found with respect to the initial EFC block ($p = 0.48$, Kruskal-Wallis one-way ANOVA). This suggests that null space control did not affect standard force control patterns even after prolonged practice.

4.3.4 Peak velocity times and movement strategies

We analyzed peak velocities to better characterize the different strategies of individual participants. Each participant showed a specific timing of the peak velocity for cursor displacement and for cursor rotation. Some participants first rotated the cursor and then displaced it, others first displaced the cursor and then rotated it, and others performed both movements simultaneously. Furthermore, peak velocity times were not constant over blocks, and they decreased or increased depending on the participant and on the specific target. As can be seen in Fig. 4.9, the high SD values of the peak velocity times in individual blocks indicate a large variability across targets.

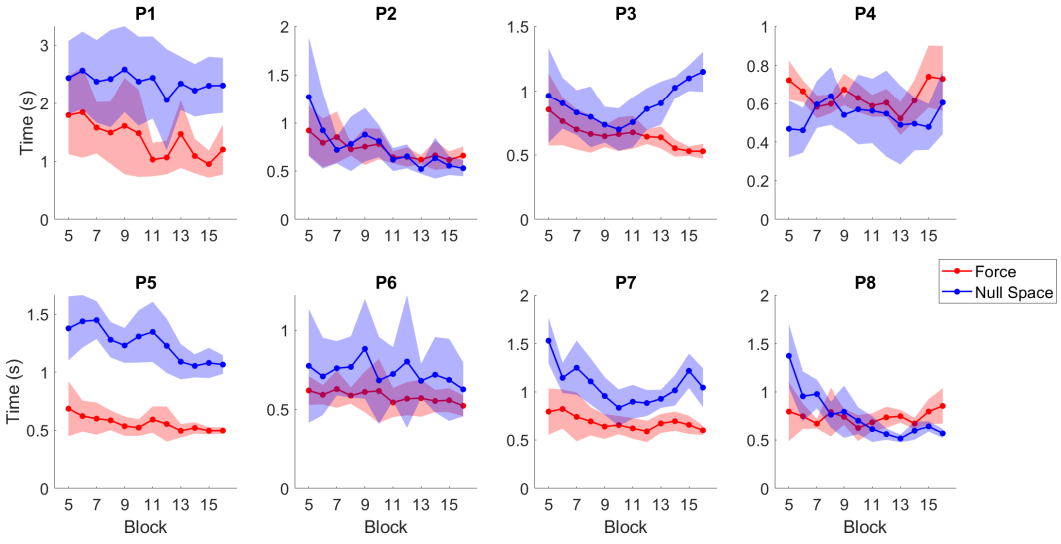

Figure 4.9: Individual movement strategies. Mean peak velocity times across targets, over null space control blocks, for both force and null space control variables. Shaded area represents standard deviation across targets.

Translation and rotation peak velocity times showed a strong positive correlation across blocks for participants 2 and 5 (Pearson correlation coefficient $r = 0.872$ and 0.827,

respectively) considering all targets directions together, with both mean times decreasing over time (blocks). Moderate positive correlation was found for participants 1 and 6 (r = 0.682 and 0.524, respectively), with both mean times also decreasing over time. Moderate negative correlation was instead found for participant 3 (r = -0.422), with both mean times decreasing up to block 10, after which the rotation peak time increased. Weak negative correlation was found for participant 4 (r = -0.233), while no significant correlation was found for participant 8 (r = 0.095), with a constant displacement peak velocity time and a decreasing rotation peak velocity time.
Kruskal-Wallis ANOVA was performed to compare translation and rotation peak velocity times of each participant. This revealed a significant difference between the translation and rotation peak velocity times for all participants ($p < 0.001$ for all except subject 4, for which $p = 0.002$) except 2 and 6 ($p = 0.817$ and 0.419 respectively), although subject 6 had a high variability in rotation peak velocity times across targets. It is also worth noting that, among the participants with significant differences between the two times, only participant 4 had significantly earlier rotation velocity peak than displacement velocity peak.

4.3.5 Individual null space control abilities

Because of the high variability among the participants in the performance metrics that we analyzed, such as success rate and holding time, which depend on task conditions such as target and time tolerances, we wondered if it was possible to generalize the assessment of individual ability in the simultaneous control of natural and extra DoF. To this aim, we used an information theory approach inspired by Fitts' law, with an ID comprising a spatial term for the reaching phase and a temporal term for the holding phase. We estimated the performance with different target sizes and holding time tolerance with a simulation.
For the reaching phase only, due to the variability in movement time for the different directions, the linear fit of the movement time itself as a function of the Shannon-MacKenzie ID resulted in a R^2 of 0.26 ± 0.17 (mean ± SD among participants). The linear fit was significant for seven participants ($p < 0.001$ for participant 2 to 8, while $p = 0.40$ for participant 1), which supports the validity of the Fitts' model for reaching. The plot of the corrected ID as a function of the target size (Fig. 4.10A) shows that the smallest target is not always the one that allows maximizing the transmitted information.

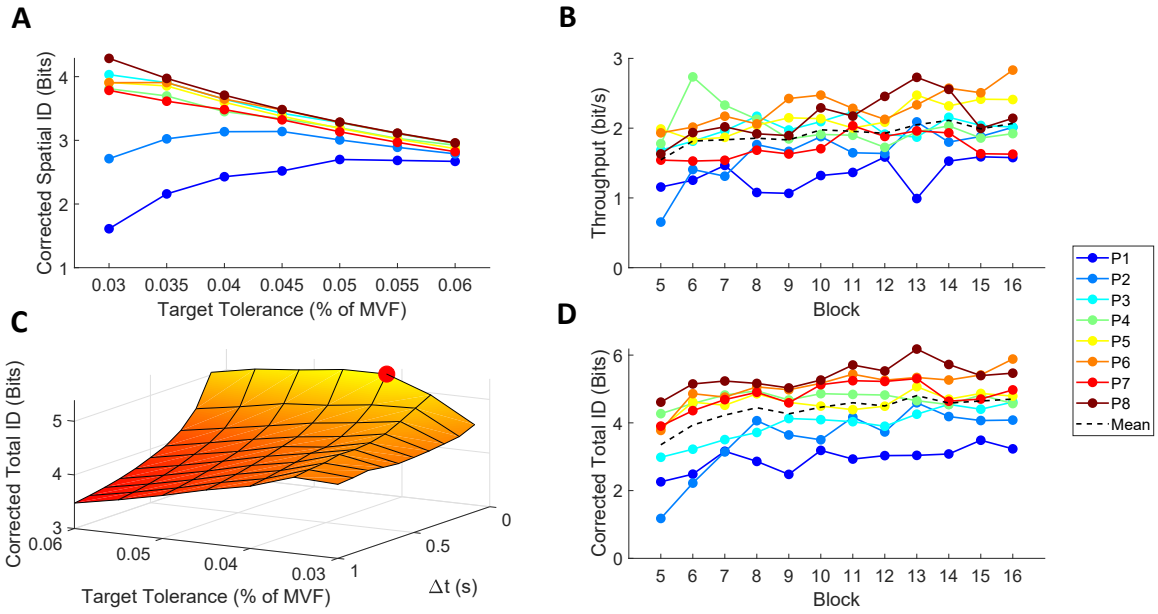

Figure 4.10: Assessment of individual control ability. (A) The corrected spatial ID (mean among the last three NSC blocks, estimated through a simulation) is shown as a function of target tolerance, showing the optimal target size for reaching of each participant. (B) Throughput as a function of block number. The dashed black line corresponds to the mean value among participants. (C) Example of corrected total ID (mean among the last three NSC blocks) as a function of target and time tolerances for participant 6. The red dot indicates the maximum value of transmitted information achieved by the participant among all the simulated conditions; the temporal evolution of its value is reported in orange curve of panel (D). It is worth noting that other maxima could be present outside the space covered by the simulation, and that the curve for $\Delta t = 0.999$ s (reaching condition) is equivalent to the one present in the panel (A). (D) Temporal evolution of the maximum information transmitted (among all the simulated conditions, i.e., the maximum of the surfaces such as that shown in panel (C)) for each block and participant. The dashed black line corresponds to the mean value among participants.

While simulated performances appear to be similar for what concerns the largest possible target, decreasing target size does not always lead to an increase in the transmitted information, because the increase in the total available information is overcome by a decrease in success rate. This means that a specific target size can maximize information transmitted through reaching, and it is strictly dependent on participants' ability. On average, the throughput, calculated as the ID divided by the movement time for reaching, increased during NSC blocks (Fig. 4.10B). This is expected, as the movement time for reaching also decreased among blocks. Such results mean that participants could move faster while keeping good accuracy.

When considering both the reaching and the holding phase, the linear fit of the simulated movement time as a function of combined ID resulted in a mean R^2 of 0.56 $\pm$ 0.18, and all fits were significant ($p < 0.001$ for all participants). This means that a linear relation still holds when the ID also includes a temporal term.
Introducing the additional temporal ID generally affects the ideal target size at which a participant can transmit the maximum information, as can be seen in the example of participant 8 illustrated in Fig. 4.10C. While for the reaching ID the best target size was 3.5% of MVF/MVCC, for holding the best target size was 4%, with a time tolerance of 0.1 s. Moreover, not all participants had their maximum information transmitted for the same time tolerance, indicating that also this quantity depends on participants' ability in holding the cursor in a fixed position.
Looking at the maximum information transmitted (considered as the maximum value of information among all the simulated conditions) (Fig. 4.10D), it is possible to see that it also increases with practice. This means that, not only participants could achieve a higher transmission rate (throughput increased), but they were also able to increase their spatial and temporal precision.

4.4 Discussion

The control of an extra limb or end-effector while simultaneously performing movements with the natural limbs requires using signals that do not interfere with limb motion [83, 111]. As a first step towards the ambitious goal of augmenting human motor capabilities, we tested whether simultaneous control of natural and extra DoFs through isometric force and intrinsic muscular null space signals is feasible. We developed a control interface in a virtual environment using isometric force generated at the hand to control the translation of an ellipsoidal cursor and, concurrently, muscle-to-force null space activations, i.e., patterns of muscular activations that do not generate force, to control the rotation of the cursor around one axis. We assessed how well 8 participants controlled the end-effector with such interface in a reaching task that required translating and rotating the cursor to match the position and orientation of 8 ellipsoidal targets, thus testing spatial control, and maintaining the cursor in the target for a 1 s, thus also testing temporal control. The results indicate that such an application of muscular null space is feasible, as after a moderate amount of practice average reaching performance was close to 100%. Furthermore, all the participants

showed improvements in different performance parameters with practice, such as an increase in reaching and holding success rate, a reduction of angular error, and an increase of holding time. However, we found remarkable inter-individual differences in task performance, learning capabilities, and strategies to coordinate natural and extra DoFs.

There are three kinds of null spaces that can be defined for the human motor system: kinematic, muscular, and neural [83]. Moreover, when considering null space signals to be used for controlling extra DoF during the performance of a task, we can define as task-extrinsic those null space signals generated by body parts, muscles, or neural circuits not directly involved in the task, and task-intrinsic those signals directly involved. Here we considered task-intrinsic muscular null space signals for extra DoFs control. Muscular null space may be a convenient choice for augmentation since it represents a trade-off between the low noise and non-invasiveness but low dimensionality of the kinematic null space and the high dimensionality but invasiveness of the neural one. A larger dimensionality of the null space allows for more flexibility in the selection of the dimensions to be used for control. Additionally, using intrinsic muscular task null space may avoid interfering with additional tasks. For example, using null space signal from arm muscles to control extra DoFs participating to the main task performed by the arms (e.g., an extra robotic limb positioning an object being manipulated by hands) may allow to perform secondary tasks such as standing or walking.

Our approach is novel because it is the first time that an intrinsic muscular null space signal extracted from multiple arm muscles is used to control an extra DoF. Many applications of extrinsic [9, 82, 112, 113] or intrinsic [114] kinematic null space, as well as extrinsic muscular null space [85, 86, 115] and neural null space [11, 116, 117] has been proposed in the past. However, the possibility of using intrinsic muscular null space for augmentation has received less attention. A recent study has shown that the muscle projection in the beta-band of spiking activity of motor neurons identified from high-density EMGs electrode from a single muscle could be suitable to control additional DoFs concurrently with natural limb motion [93], but possible interference with other muscles was not directly monitored. Another recent study [12] has demonstrated the possibility of controlling the vertical displacement of a cursor in a 2D environment through cocontraction of two antagonistic muscles (pectoralis major and posterior deltoid) while controlling the horizontal displacement through the reciprocal

activity of the two muscles. With respect to these recent studies, our interface allowed to directly test the feasibility of simultaneous control in a scenario closer to real-life, i.e., in a 3D virtual environment, of 3 natural DoFs (cursor translation) and an extra DoF (cursor rotation), for a total of 4 DoFs controlled simultaneously. Moreover, our task-intrinsic muscular null space signal was extracted from many muscles involved in the reaching/holding task. We could assess the interference between the different DoFs and the relative muscle activations, showing that participants could learn to reduce such interference with practice. In principle, our approach could also be extended to the control of multiple extra DoFs by selecting different components in the intrinsic muscular null space. However, further investigation is needed to assess how performance and learning rate depends on the number of extra DoFs.

Because of the high inter-individual variability among our participants, we developed an analysis framework based on information theory inspired by Fitts' law to assess individual control ability independently from the performance observed with specific task parameters. In fact, performance quantities such as success rates are strictly dependent on the task configuration and do not give direct knowledge on how much an individual is able to explore the task space (i.e., how much they are able to discern a point in the space from another). Evaluating performances in terms of transmitted information allows instead to generalize an individual's performance and extrapolate it from the specific context, also allowing to understand how many regions of the task space an individual can reach. Since its original formulation [94], Fitts' law has been widely employed to evaluate human performance during tracking [118], myoelectric control [119], prostheses control [120], and human-computer interaction (HCI) [98, 121, 122]. Fitts' law captures the speed-accuracy tradeoff typically observed in human aimed movements by relating movement duration to an ID defined according to target distance and size. Thus, since the ability to accurately control an end effector depends on the speed of movement, motor control ability should be assessed according to a speed-accuracy trade-off function rather than by accuracy alone [109]. However, the ID itself, corrected through the success rate of a participant, could be taken as a parameter for performance evaluation in terms of average transmitted information [96] related to spatial accuracy and exploration. In fact, while various formulation of Fitts' law have been developed to adapt to different tasks or to correct the index of difficulty to account for target misses [96, 108, 123], Fitts' law has always been considered in the spatial domain, with time taken into account only in the form of temporal constraints

influencing task execution [102, 103]. However, sometimes it could be necessary to evaluate the performance in temporal domain, such as to evaluate whether an individual is able to perform an action at the right time or for the required time lapse. To account for the effects of temporal targeting, i.e., a task in which spatial distance is minimal and for this reason movement time constant, a recent study applied Fitts' law to a temporal pointing task, in which the user has to decide exclusively when to perform an action (in this case, pressing a button when the cursor is inside targets) [124]. The authors stated that such a task is based on a two-stage process (plus another one relative to computer processing), with an internal time-keeping stage and a response-execution stage. Assuming a Gaussian response distribution for the endpoints, the error rate could be expressed as a function of an ID equal to the logarithm of a temporal target distance divided by a temporal target width. Similarly, to take into account the holding phase in our task, which can be considered a temporal task, we hypothesize that the total information transmitted performing the task is equal to the sum of two IDs, a spatial ID resembling the classical Fitts' index, and a temporal ID similar to the one proposed in [124]. As the Fitts' ID can be derived from an "aiming is choosing" rationale [96], we simply derived the temporal ID from a "waiting is choosing" rationale, which allows a generalization of the temporal ID to any compatible temporal task without relying on any assumption on the response function. We also corrected those ID multiplying them for the respective success rate (reaching or holding) [96]. Such ID therefore allows to consider not only reaching movements, but also holding movements, and could be hypothetically extended to more complex task composed by more reaching and holding phases to evaluate an invidual performance based on the average information transmitted for each phase. Through this framework, we found that, when considering only the reaching phase, the smallest target size is not always the one providing the highest information transmitted because the gain in source information associated with smaller targets may be overcome by the loss in transmission performance corresponding to a decrease in reaching success rate. When considering both reaching and holding phases, we found that spatial and temporal requirements affect each other, generally reducing a participants' optimal target size with respect to the reaching phase only, with the maximum information transmitted resulting for a specific, individual combination of spatial and temporal parameters. Such an approach could allow to hypothetically optimize an interface (not necessarily based on myoelectric control) depending on the user's capabilities, updating parame-

ters as they learn to control the device.

The prolonged exposition to the control of both prostheses and augmenting devices may have effects at the neural level. Amputation causes reorganization in the primary somatosensory cortex [125]. A recent study has showed that, in BCI control of independent DoFs, it is possible to dissociate neural gamma activity correlated to muscle activations [116]. Another study has shown that users of a third thumb controlled through a toe presented, after 5 days, a different representation of their hand in the sensorimotor cortex [126]. Considering the findings of such studies, we expect that even the intrinsic muscular null space control of an external device could bring some modifications in neural motor circuits. The exploitation of musculoskeletal redundance to control a device is actually a new motor skill that requires learning, as it has been shown by the success rate curves from our study, and it is something different from the natural modulation of limb impedance [92] and even from the tele-impedance, which is based on the use of muscular null space to control the impedance of robots, providing them with a task-related elastic profile in addition to position trajectories [90], while no actual additional DoF is controlled. We hypothesize that, in this context, training could make a user able to learn some sort of "muscular null space synergies" that could justify the increase in performance and therefore would bring modifications in cerebral or cerebellar cortices, but further investigation on inter-individual differences at a neural level is needed to confirm such a hypothesis.

Another important finding that has been illustrated in literature is that, as it is known for skill learning [77–79], feedback mechanisms integrated in an interface could help users improving their performance faster and to a higher level. It has been demonstrated that somatosensory feedback facilitates to learn controlling both prostheses [127] and augmenting devices [128]. For this reason, we think that integrating some form of feedback in a device based on intrinsic muscular null space control would be helpful and could also partially smooth out inter-individual variability.

In conclusion, we demonstrated the feasibility of a novel approach to control extra DoFs using muscular null space signals from a relatively high number of muscles directly involved in task being performed concurrently. Participants in our experiment were able to reach targets and their performances improved with practice. Such an approach could be applied to control more sophisticated assistive or augmentative robotic devices (as extra limbs) in everyday life situations, for both able-bodied and disable-bodied people. Such approach is substantially different from the myoelectric

control of exoskeletons, as they do not add additional DoFs [8, 129, 130]. We also developed a Fitts-like framework, with two indices of difficulty, which could be useful to quantify a participant's ability in reaching and holding a position independently from specific task parameters. Further work is needed to understand the neural origin and mechanisms underlying learning of null space control. These results can be taken as a starting point for the investigation of muscular null space control for augmentation, and our information theory approach can provide a novel tool to assess the ability of individual participants to control a device through noisy signals such as EMG, considering not only spatial precision, but also temporal precision.

5. Combined use of Magnetic Resonance-guided Focalized Ultrasound Surgery and functional near-infrared Spectroscopy for treatment and monitoring of neuro-motor disorders

5.1 Background

Investigating the changes in neural activities following the **learning of new motor skills** is fundamental to gain new knowledge on how the human motor system works. For this purpose, different techniques have been employed, such as functional magnetic resonance imaging (fMRI) or positron emission tomography (PET). However, these techniques can be used only to analyse the effects of learning at the end of the exposure, in a rest phase, or in case of tasks with limited movements, because they do not allow a high freedom of motion and are often not compatible with additional electronical instrumentation such as EMG. For all these reasons, new techniques are emerging to provide the possibility of analysing motor learning during motor complex task. One of these emerging techniques is **functional near-infrared spetroscopy** (**fNIRS**): it is based on the absorption process of optical light, generally in the ∼700-900 nm wavelength range, from chromophores such as oxy- and deoxy-haemoglobin (HbO and HbR, respectively), whose changes in concentration are strictly correlated to the blood-oxygen-level-dependent (BOLD) signal changes induced by neural activity. In fact, due to brain activations, arteriolar dilatation in the interested regions, with increased capillary filling, occurs in order to allow more oxygenated blood flow to satisfy brain's immediate metabolic needs [131].
With respect to the previous illustrated techniques, and in particular to fMRI, which is the most used technique in neurosciences, fNIRS offers several advantages such as higher temporal resolution, higher portability, lower costs, reduction of electrical noise, and, most importantly, the possibility for subjects to perform complex motor

tasks during data acquisition. For example, Ikegami and Taga [132] assessed brain activation changes during the learning of a multi-joint discrete motor task, i.e., the kendama task. In particular, participants had to toss a ball connected by a string to the kendama stick and catch it in the cup attached to the stick itself. In this work, they found significant positive correlations between the decrease in the magnitude of the event-related HbO responses and the decrease in the magnitude of the integrated upper limb muscle torques during learning. Hatakenaka and co-workers [15] assessed changes in cortical activations during a pursuit rotor task, in which participants had to keep the tip of a metal stylus rotating at constant speed on a disk. Through fNIRS measurements, they observed a shift in the task-related increase of HbO concentration from the presupplementary motor area to the supplementary motor area, underlying the role of the first one in early learning phase and of the second one in the late learning phase.

The assessment of activation changes during motor task is important not only to study learning in healthy people, but also to understand the mechanisms behind **neuropathological conditions**, such as essential tremor (ET), Parkinson's disease (PD), Alzheimer or stroke, and to see how such conditions can affect motor neural networks. Many investigations have been performed using fMRI during cognitive tasks, due to the limited freedom of movement allowed by such technique. This was the case of studies such as the one from Cerasa and collaborators [133], that measured the cerebral activation of ET patients during a Stroop task, in which they have to name the color of words in presence of a mismatch between the name color (the word) and the color of the font, or the work from Passamonti and collegues [134], in which ET patients executed a verbal working memory task. Eventually, simple motor tasks can also be employed. Haslinger and collegues [135] studied BOLD signal changes using fMRI on PD patients performing paced single joystick movements before and after levodopa therapy, finding an improvement in impaired motor iniziation in the supplementary motor area and a decrease in hyperactivation in lateral and primary motor cortices after the treatment. More recently, Buijink and co-workers [136] conducted a study in which thirty-one ET patients performed finger tapping sessions alternated with rest periods, while their cerebral and cerebellar activities were monitored through fMRI. They found that tremor is related to dysfunctions in the cerebellum, as a significant positive correlation between tremor severity and dentate nucleus activation, while reduction of activation in other cerebellar and cerebral cortical regions was found. Such

results are compatible with the ones found in other studies based on resting-state fMRI [137].

While there are standard pharmacological treatments for many neurological diseases, such as those based on pharmacological agents targeting dopaminergic neurotransmission [138], surgical approches are being studied as an alternative bringing several advantages in terms of efficacy and reduction of side effects. In this context, deep brain stimulation (DBS) [139, 140] has been often applied in the last decades for its adaptability, reversebility, and also for the possibility to perform bilateral interventions [141]. Nonetheless, DBS is an expensive technique that could introduce new challenges, such as intracranial hemorrhages and infections [142]. Alternative techniques have been developed to avoid such complications, such as **magnetic resonance-guided focused ultrasound surgery (MRgFUS)** [143]. This is an innovative, non-invasive surgical procedure for performing thalamotomies by combining magnetic resonance imaging to target the ablation spot and monitor the surgery progress, and focalised ultrasounds to ablate cerebral tissues. Such a technique has been already applied to treat, among the many, ET [144, 145] and obsessive-compulsive disorders [146, 147], and it is currently being tested for other neurological diseases such as PD [148, 149] and pathologies of different nature such as cancer [150–152].

In this chapter, a study is presented where fNIRS was used in order to investigate the changes of cortical activation patterns in subjects affected by bilateral Parkinson's disease, compared to healthy ones, before MRgFUS treatment, and at different intervals of time after the treatment, by execution of unimanual left and right finger-tapping tasks.

The results here presented can be helpful for brain rehabilitation, to examine the cortical activation during the assessment and to monitor treatment progress, especially for critical care patients for which frequent ambulatory assessments after brain injury are necessary, and for infant and children to which usual neuroimaging techniques cannot be applied.

ID	Neurological disorder	Treated hemisphere	Age	Sex
1	PD	R	76	m
2	PD	R	75	m
3	PD	R	79	f
4	PD	R	62	m
5	PD	R	67	f
C1	None	None	66	m
C2	None	None	68	f
C3	None	None	71	m

Table 5.1: Demographic data for Parkinson's disease patients and control subjects. In "Treated hemisphere", R = Right and L = Left.

5.2 Methods

5.2.1 Subjects

In this study, 5 patients from IRCCS Centro Neurolesi "Bonino-Pulejo" of Messina (Italy), affected by Parkinson's disease (age range 62-79, 2 female), participated in the experiment (demographic data are reported in Table 5.1).
Therapeutic improvements were evaluated through the Clinical Rating Scale for Tremor (CRST) A + B [153], the treated hand tremor subscore of the CRST, administered immediately before treatment, and at 1 week and 1 month post-treatment. This tremor subscore with a maximum of 32 points was calculated by summing the observed and the performance-based scores from parts A and B for the treated hand [154, 155].
All patients were treated on the right hemisphere. Furthermore, three subjects with no neurological diseases (mean ± SD age: 68.3 ± 2.5 years, age range: 66-71, 1 female) participated in the experiment as control subjects (subject identification code C1, C2 and C3; see Table 5.1).
The study protocol was approved by the Local Ethics Committee of IRCCS Centro Neurolesi "Bonino-Pulejo".

5.2.2 Experimental protocol

The experiment consisted in three sessions, the first one performed one day before the MRgFUS treatment (S0), the second one week after the MRgFUS treatment (S1), and the third one month after the MRgFUS treatment (S2). In all sessions, subjects performed two tasks, consisting in right and left finger tapping (RFT and LFT, respec-

tively). At the beginning of each finger tapping session, an interval of 10 s was spent to allow signal assessment. After that, an interval of 25 s of activation, alternated with an interval of 15 s of rest, was applied for six times. The total duration of each finger tapping task was 250 s (see Fig. 5.1).

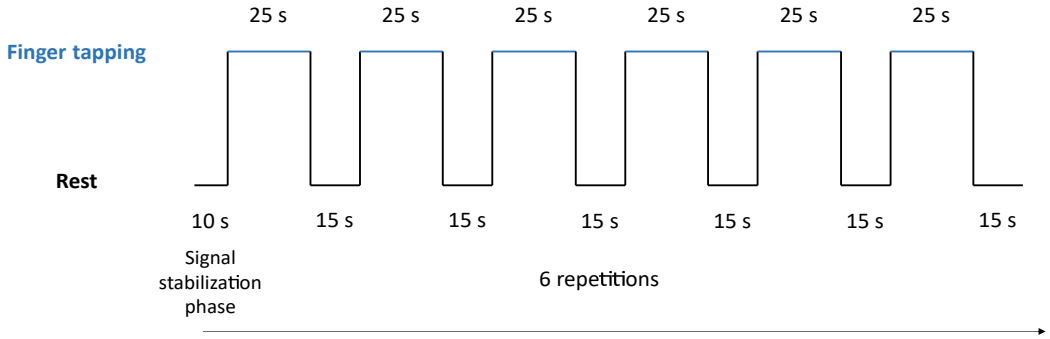

Figure 5.1: Experimental protocol for both LFT and RFT tasks. The total duration of each session was 250 s. The blue lines specify when finger tapping was executed.

Control subjects took part in a single session, and the collected data were used for comparison with those coming from all sessions of subjects with neurological disease. The analysis on the acquired data was performed using the NIRS-SPM (statistical parametric mapping) software (version 4, revision 1) [156–160], developed for MATLAB© R2009a (MathWorks Inc., Natick, MA).

5.2.3 Measurement model

According to the Modified Beer-Lambert Law (MBLL) [161], in the framework of a well-established model already successfully applied in literature [156–160], assuming that the involved chromophores are oxy- and deoxy-haemoglobin (HbO and HbR, respectively), the change in the optical density $\rho(\lambda, r, t)$ can be accounted by the formula:

$$\Delta\rho(\lambda, r, t) = -ln\left(\frac{I(\lambda, r, t)}{I_0(\lambda, r)}\right) = d(r)l(r)[a_{HbO}(\lambda)\Delta c_{HbO}(r, t) + a_{HbR}(\lambda)\Delta c_{HbR}(r, t)],$$

being λ the wavelength of the incident radiation, r the cerebral cortex position in (x,y,z) space and t the time. In the above equation, $I_0(\lambda, r)$ is the initial radiation intensity, $I(\lambda, r, t)$ the radiation intensity at time t, $a_{HbX}(\lambda)$ the extinction coefficient of the HbX chromophore (X = O or R), $\Delta c_{HbX}(r, t)$ the concentration change of the

HbX chromophore, $d(r)$ the differential path length factor (DPF), and $l(r)$ the source-detector distance (assuming the detector at position r).
Optical density measurements at two different wavelengths allow estimating HbO and HbR concentration changes. For two wavelengths λ_1 and λ_2, assuming $d(r)$ independent from λ, the following matrix formulation can be used:

$$\begin{bmatrix} \Delta\rho(\lambda_1, r, t) \\ \Delta\rho(\lambda_2, r, t) \end{bmatrix} = d(r)l(r) \begin{bmatrix} a_{HbO}(\lambda_1) & a_{HbR}(\lambda_1) \\ a_{HbO}(\lambda_2) & a_{HbR}(\lambda_2) \end{bmatrix} \begin{bmatrix} \Delta c_{HbO}(r, t) \\ \Delta c_{HbR}(r, t) \end{bmatrix} + \begin{bmatrix} w(\lambda_1, r, t) \\ w(\lambda_2, r, t) \end{bmatrix},$$

where $w(\lambda_i, r, t)$ is the additive noise relative to the i-th wavelength ($i = 1, 2$).
The signal $S_{HbX}(r, t)$ for the haemoglobins can be obtained by multiplying the inverse matrix of the extinction coefficients to the previous equation:

$$\begin{bmatrix} S_{HbO}(r, t) \\ S_{HbR}(r, t) \end{bmatrix} = d(r)l(r) \begin{bmatrix} \Delta c_{HbO}(r, t) \\ \Delta c_{HbR}(r, t) \end{bmatrix} + \begin{bmatrix} \epsilon_{HbO}(r, t) \\ \epsilon_{HbR}(r, t) \end{bmatrix},$$

where $\epsilon_{HbX}(r, t)$ is the additive zero mean Gaussian noises for the HbX chromophore. The DPF parameter $d(r)$ could be in principle obtained, in time-domain or frequency-domain systems, by calculating the temporal point spread function [162]. Furthermore, many other conditions, such as the aforementioned scalp depth and the conformation of the head, can negatively affect fNIRS measurements, with consequent scattering effects that are subject-dependent. For all the aforementioned reasons, analyzing fNIRS data using the magnitude of chromophore concentration changes can be difficult, and a generalized linear model is widely used in order to overcome these problems.

5.2.4 Data analysis

Clinical outcome assessment statistics. Kruskal-Wallis one-way ANOVA (MATLAB function "kruskalwallis") has been performed to find significant differences among clinical scores depending on the session. As a post-hoc comparison, Tukey's honest significance test (MATLAB function "multcompare") has been performed.

fNIRS data pre-processing. Before any further processing, fNIRS HbO and HbR data were low-pass filtered with the canonical hemodynamic response function (HRF) filter to remove high-frequency noise and temporal correlations (which means that the residual signal at the specific time is correlated with its temporal neighbors).

This was done according to the precoloring method, which has been shown to be more effective, with respect to the prewhitening method, in calculating activation maps [156, 157]. Finally, baseline correction was performed again, subtracting the new value of concentration change at initial time.

Generalized linear model (GLM) and wavelet minimum description length (wavelet-MDL) detrending. Generalized Linear Model (GLM) is nowadays a standard analysis method used for fMRI, as well as for fNIRS [156]. It describes a measured quantity in terms of a linear combination of N explanatory variables, plus an error term. In a matrix form, it can be written as:

$$\mathbf{S} = \mathbf{X}\boldsymbol{\beta} + \boldsymbol{\epsilon},$$

where $\mathbf{S}$ is the M-dimensional vector of the hemodynamic signal $S_{HbX}(r, t_i)$, $\boldsymbol{\epsilon}$ is the M-dimensional vector of noise $\epsilon_{HbX}(r, t_i)$, $\boldsymbol{\beta}$ is an L-dimensional vector of unknown strength responses, and $\mathbf{X}$ is the model design matrix, which serves as a predictor for the signal and must be specified first.
The signal can be approximated as the convolution of a stimulus function and a hemodynamic response function (HRF). For the model specification, the canonical HRF composed by two gamma functions was employed [156–160]. To take into account the global drift which affects fNIRS signals, we implemented the wavelet minimum description length (wavelet-MDL) algorithm described in [157]. In this case, the matrix formula for $\mathbf{S}$ becomes:

$$\mathbf{S} = \mathbf{X}\boldsymbol{\beta} + \boldsymbol{\theta} + \boldsymbol{\epsilon},$$

where $\boldsymbol{\theta}$ is the additional vector of global drift. A t-statistics coefficient can be calculated for this model, as described in [157], to test the null hypothesis of no significant activation for a specific channel with respect to a reference phase (in this work, the rest phase). In our case, this analysis was applied to both HbO and HbR signals, for each patient separately, using the procedure available on the NIRS-SPM software [156–160]. For the group analysis, the method of global alignment of interpolated maps of the patients present in the NIRS-SPM software was used. For the calculation of the p-value, expected Euler characteristics approach was used, with a p-value threshold of 0.05 [156, 157].

Evaluation of HbT task-related increments. To better understand the effects of MRgFUS on each hemisphere across the different sessions, we calculated the average difference in concentration changes for the total haemoglobin ($HbT = HbO + HbR$) between right and left hemispheres (laterality) of the task-related increments. Such an analysis was performed according to the following steps:

- the channel configuration of each subject was separated into left hemisphere (LH) and right hemisphere (RH) sub-groups;
- for each channel, the difference in mean HbT concentration changes between task and rest phases, normalized to the maximum absolute value during task phase, was calculated;
- for both LH and RH sub-groups, the mean values among the corresponding channels were estimated;
- for both LH and RH sub-groups, the mean values among subjects were calculated;
- for LFT, mean LH sub-group values were subtracted to mean RH sub-group values.

Furthermore, Pearson correlation coefficient between HbT task-related increments and clinical scores was calculated (MATLAB function "corrcoef").

5.3 Results

5.3.1 Clinical outcomes

A significant clinical improvement in patients' conditions, across the three experimental sessions, has been found through Kruskal-Wallis one-way ANOVA analysis ($p < 0.001$). Post-hoc comparison showed a significant difference only between S0 and S2 ($p < 0.001$). The plot of the patients' clinical scores as a function of the session can be found in Fig. 5.2.

5.3.2 fNIRS analysis

Using the GLM described before, data collected from each participant were analysed separately. Due to the different initial neurophysiological conditions and to the dif-

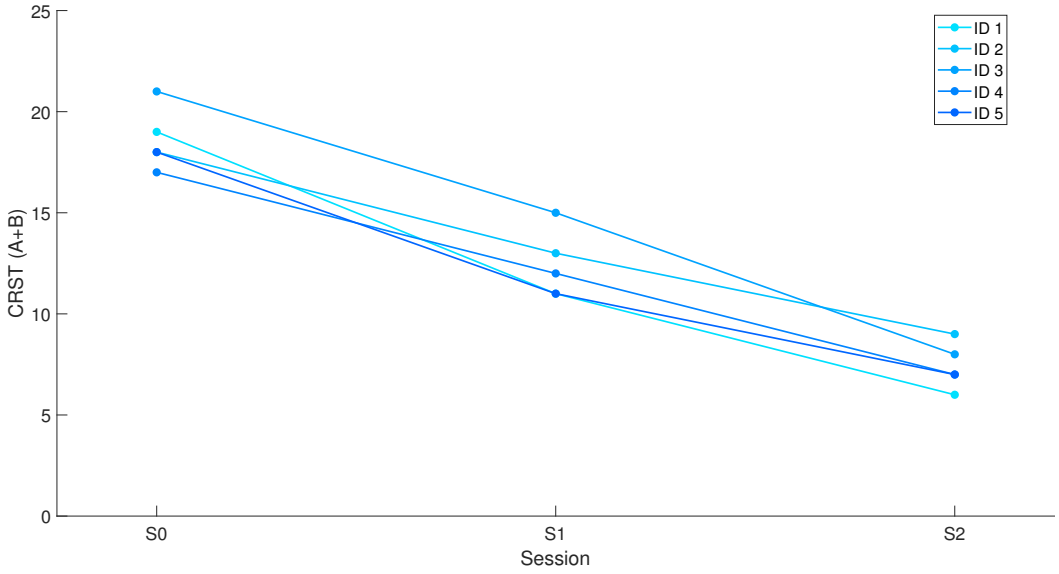

Figure 5.2: Examples of HbO (blue line) and HbR (red line) concentration changes during session S0, taken from subjects ID 2 and ID 3, during the execution of LFT (on the left) and RFT (on the right), as obtained from channel N = 21 for LFT and N = 15 for RFT.

ferent efficacy of MRgFUS treatment on each patient, a moderate inter-individual variability among the activation maps of different patients was found for both HbO and HbR during LFT and RFT tasks, as it can be seen from their concentration changes over time reported in Fig. 5.3, for ID 2 and ID 3 patients, obtained from channel N = 21 (in the right hemisphere) for LFT and N = 15 (in the left hemisphere) for RFT, as example.

Moreover, other variables such as physiological baseline properties, task performance, attention and/or motivation could have contributed to this variability [163].

For what concerns the temporal evolution of the density change curves, phase differences among all sessions were generally observed for both HbO and HbR, during both LFT and RFT tasks. Worth of note, a similar trend was observed for sessions S2 and S0, consisting in a more oscillating signal with respect to that revealed for session S1, as can be seen in the examples shown in Fig. 5.4. Interindividual differences were present in all three sessions, and were accounted through the analysis at group level.

HbO group-averaged activation maps are shown in Fig. 5.5.

In the case of session S0, group analysis presented significant enhancements in the left hemisphere during LFT task. As far as session S1 is concerned, a significant increase for HbO concentration was found in the left hemisphere during RFT task. Finally,

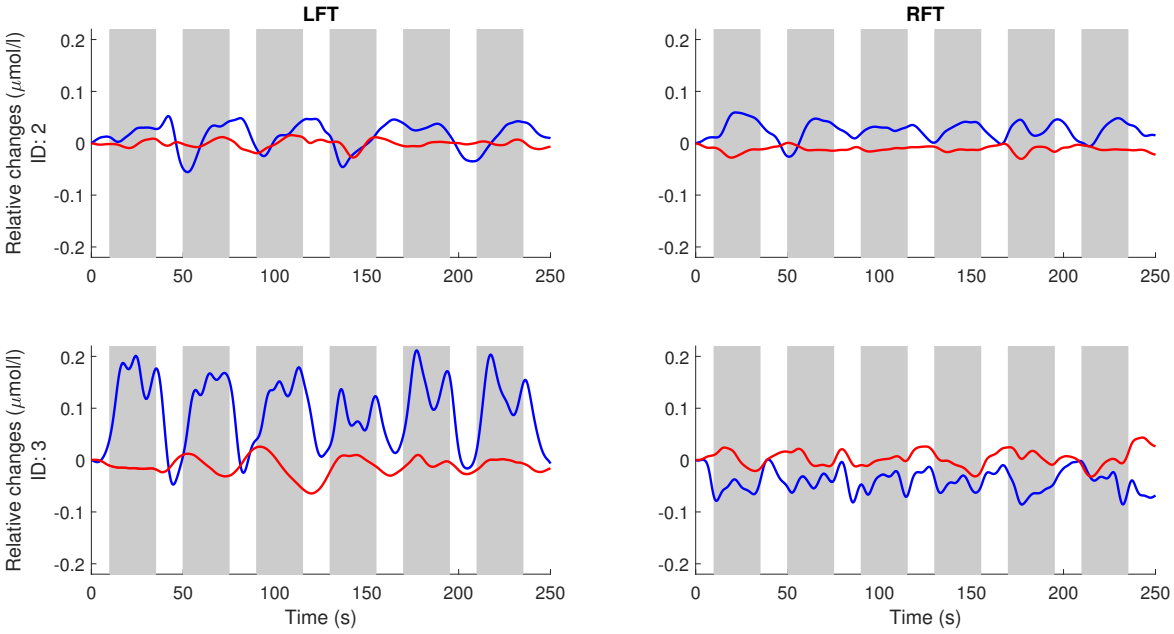

Figure 5.3: Examples of HbO (blue line) and HbR (red line) concentration changes during session S0, taken from subjects ID 2 and ID 3, during the execution of LFT (on the left) and RFT (on the right), as obtained from channel N = 21 for LFT and N = 15 for RFT.

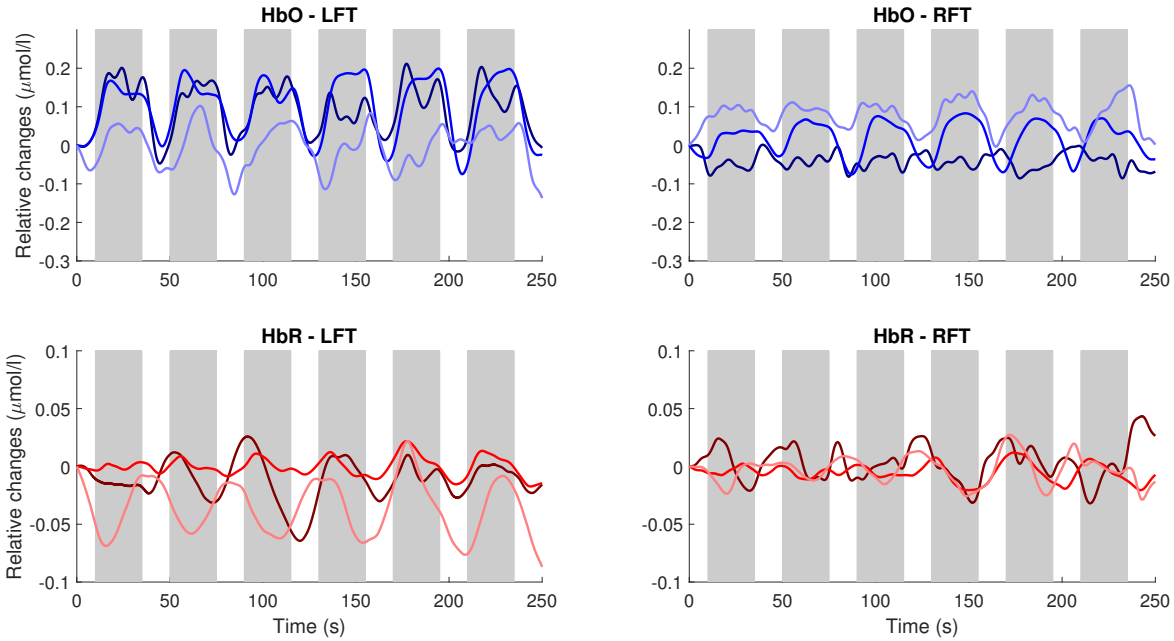

Figure 5.4: Examples of HbO (blue line) and HbR (red line) changes during session S0, S1 and S2, taken from subjects ID 3, during the execution of LFT (on the left) and RFT (on the right), as obtained from channel N = 21 for LFT and N = 15 for RFT. S0, S1 and S2 are indicated by progressively lighter colors.

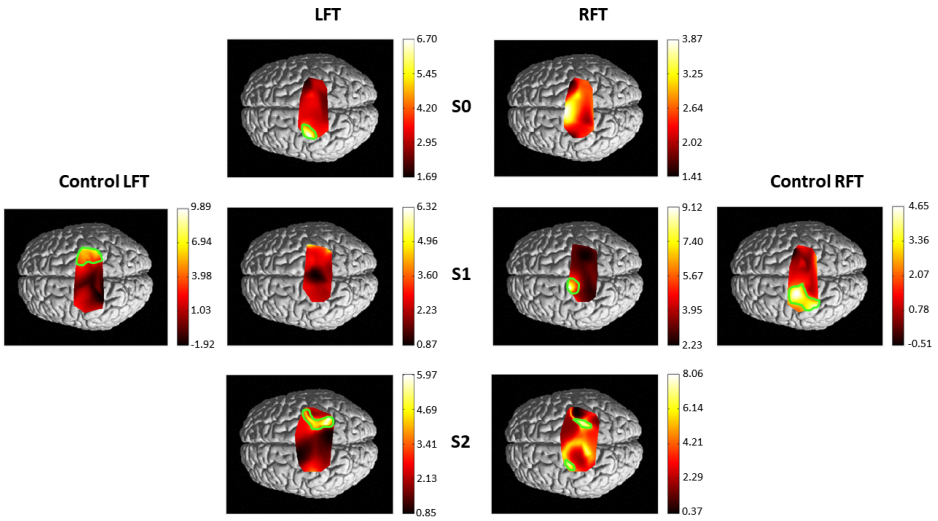

Figure 5.5: Group-average activation maps of HbO, during the three sessions (S0, S1, S2) of both LFT and RFT tasks. For comparison, the control group-average activation maps of HbO during LFT and RFT are shown on the respective sides. The regions with significant activations are enclosed in a green line. See text for details.

for session S2, significant changes in HbO concentration were found in the right hemisphere for LFT, and in both hemispheres for RFT.

Fig. 5.6 reports the group-averaged activation maps of HbR.

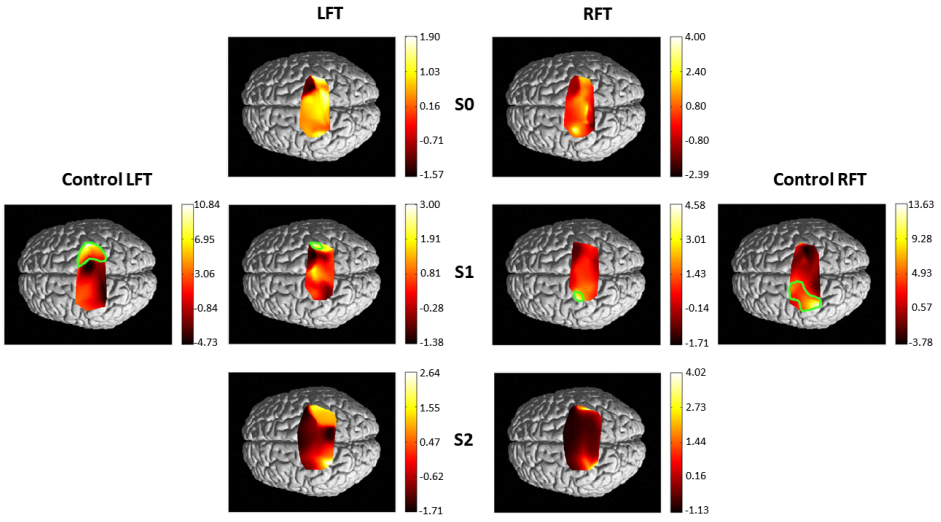

Figure 5.6: Group-average activation maps of HbR, during the three sessions (S0, S1, S2) of both LFT and RFT tasks. For comparison, the control group-average activation maps of HbR during LFT and RFT are shown on the respective sides. The regions with significant activations are enclosed in a green line. See text for details.

In the case of session S0, no significant changes are detected in HbR concentrations, for

both LFT and RFT. For what concerns session S1, a significant decrease for HbR concentration is revealed in the right hemisphere during LFT, and in the left hemisphere during RFT. Finally, during session S2, no significant changes in HbR concentration were observed.
To verify the efficacy of the MRgFUS treatment, we also report the time course of the HbT task-related increment laterality (Figure 5.7), obtained as described in Materials and Methods section. Only the LFT case is reported, being patients treated on the right hemisphere.

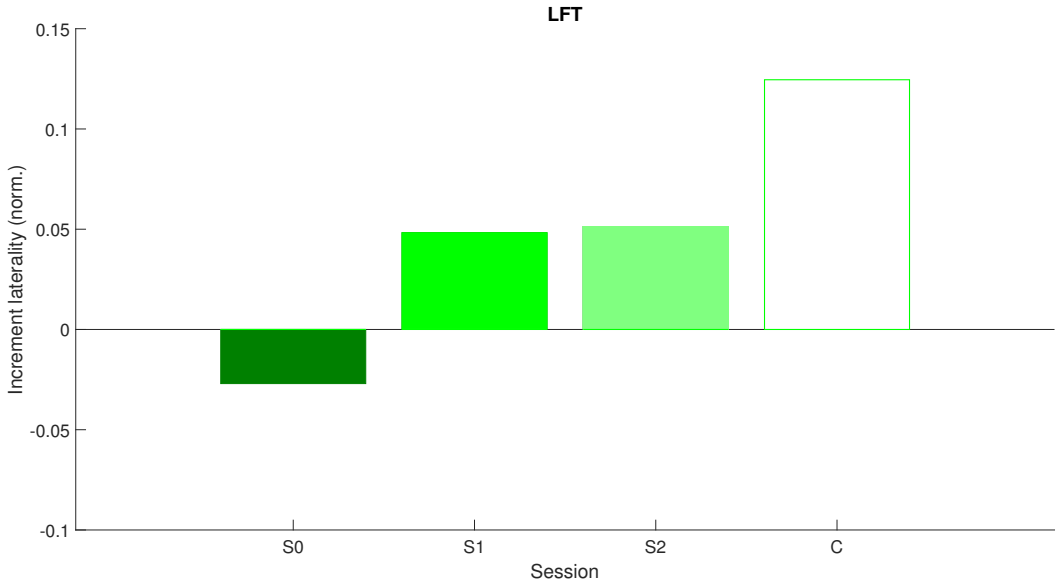

Figure 5.7: Average HbT task-related increment laterality, obtained as described in paragraph 2.6. The "C" column represents control group average.

Task-related increment laterality during LFT is observed to increase passing from S0 session, in which a higher change in HbT is present in the left hemisphere, to S1 session, where a higher change in HbT can be seen in the right hemisphere. Therefore, an evolution trend towards the control situation is observed, with a strong negative correlation (P = -0.91) with the clinical scores previously reported.

5.4 Discussion

The results of the analysis on the recruited PD patients evidenced the efficacy of MRgFUS treatment with respect to pre-treatment phase, at least in the observed follow-up time. An improvement in the patients' status can be observed immediately after the treatment, followed by a slight worsening one month later, and this scenario appears in

agreement with the reported results in literature about the effects of unilateral thalamotomy with MRgFUS in patients with tremor other than essential tremor [148, 149]. Therefore, such results highlight the validity of fNIRS as a monitoring tool of neural activations in PD patients. This could be important when traditional techniques, such as fMRI, cannot be used, and when it is necessary to observe cortical activations during specific, complex motor tasks.

In conclusion, we found that, after MRgFUS treatment, significant changes in HbO and HbR concentrations, resembling those in control group activation patterns, were predominantly observed in the S1 session, whereas in the case of S2 session, probably due to the neurodegenerative factor of the PD, conditions more similar to the pre-MRgFUS situation (S0 session) appeared. Nonetheless, they seemed to be improved, with respect to the pre-treatment phase, even one month later. Furthermore, the observed changes turned out to be principally related to LFT task, being the treatment performed on the right hemisphere.

These results, although preliminary and based on a low number of patients, which could not guarantee a generalization of the proposed approach, gave nevertheless evidence of the potentiality of fNIRS as a neuroimaging technique for monitoring the remodeling of neural connectivities, promoted by MRgFUS, in association with symptomatic improvements. In principle, this combined procedure could be employed within the clinical assessment of the human motor function, especially in patient populations and clinical settings where traditional neuroimaging methods are not suitable.

6. Conclusions and future perspectives

This thesis presented two related aims, both particularly important for the comprehension of the motor control and learning problems. The first aim was to investigate the exploration of muscular null space to learn new motor patterns, i.e., new muscle synergies, and to investigate the capability of modulating muscular null space to control an additional DoF concurrently with natural DoFs for augmenting purposes. The second aim was to validate the use of fNIRS to assess the changes in neural activations of patients affected by neurological disorders while performing a motor task before and after a MRgFUS treatment.

The results of the first study presented in this thesis showed that with enough practice it is possible to compensate perturbations that require new null space patterns, with participants exposed to such perturbations being able to reach performance comparable to that of participants exposed to compatible perturbations.

The second study showed the feasibility of the simultaneous control of natural DoFs, expressed by the isometric force used to move a cursor in a virtual environment, and of additional DoFs, expressed by the muscular null space activation used to rotate the same cursor along a specified axis.

Finally, the third study presented here demonstrated the usability of fNIRS as a monitoring tool of cerebral activity during a motor task in patients affected by Parkinson's disease, showing changes in haemoglobin concentrations after the MRgFUS treatment.

This work could lead to many future applications. As the exploration of null space underlies the learning of new motor skills, adding new ways of interacting with the environment, it is possible to think that the reverse process could occur in people affected by neuropathologies, who might generate activaties in the null space as a consequence of their conditions. Then, neurorehabilition processes based on synergy perturbations applied through myoelectric control and virtual reality could be used to develop specific treatments helping patients to discover new functional muscle patterns outside of the null space. These treatments would be based on the patient's musculoskeletal properties, easy to use and portable, or even for domestic use. Moreover, it

may be possible to develop new augmenting devices based on muscular null space, to help workers performing difficult tasks without the help of other individuals, such as lifting multiple weights or manipulating simultaneously numerous tools in building a structure, or surgeons performing surgeries with greater autonomy, without the risk of misunderstandings, being all under their control. As mentioned before, many prostheses and exoskeletons based on myoelectric control exist, and muscular null space could also provide a new way to enhance such devices, maybe combined with other forms of null space, such as kinematic and neural null spaces. Finally, the neural mechanisms underlying both the learning of new motor synergies through exploration of null space and the direct modulation of all forms of null spaces could be unveiled using fNIRS, allowing to better adapt the aforementioned protocols and devices to an individual, who could be healthy or unhealthy. Such technique has the significant advantage, with respect to other imaging techniques currently used in neuroscience, of being highly portable and adaptable to different situations, allowing a direct evaluation "in the field", i.e., while performing complex real-life motor skills, surely more effective than measurements made in specific, ideal context such as in laboratory with simpler tasks and less realistic conditions.

Special thanks

I thank my supervisor prof. V. Venuti and co-supervisors prof. G. Acri and prof. A. d'Avella for the support in this work.
I also thank the research group of the laboratory of prof. A. d'Avella (D. Borzelli, P. De Pasquale, D. Berger and M. Russo) for making possible my participation in the first two studies presented here, and the group of the Centro Neurolesi "Bonino-Pulejo" for the help with the third study presented in this thesis.
And finally, I thank my family, my friends and my colleagues for being next to me in this important moment of my life.

Sergio Gurgone

Bibliography

[1] N. A. Bernstein. *The co-ordination and regulation of movements*. 1st English ed. Oxford, New York: Pergamon Press, 1967. 196 pp.

[2] M. C. Tresch and E. Bizzi. "Responses to spinal microstimulation in the chronically spinalized rat and their relationship to spinal systems activated by low threshold cutaneous stimulation". In: *Experimental Brain Research* 129.3 (Nov. 1, 1999), pp. 401–416. ISSN: 1432-1106. DOI: 10.1007/s002210050908. URL: https://doi.org/10.1007/s002210050908.

[3] E. Bizzi and V. C. Cheung. "The neural origin of muscle synergies". In: *Frontiers in Computational Neuroscience* 7 (2013). Publisher: Frontiers. ISSN: 1662-5188. DOI: 10.3389/fncom.2013.00051. URL: https://www.frontiersin.org/articles/10.3389/fncom.2013.00051/full.

[4] D. D. Lee and H. S. Seung. "Learning the parts of objects by non-negative matrix factorization". In: *Nature* 401.6755 (Oct. 1999). Bandiera_abtest: a Cg_type: Nature Research Journals Number: 6755 Primary_atype: Research Publisher: Nature Publishing Group, pp. 788–791. ISSN: 1476-4687. DOI: 10.1038/44565. URL: https://www.nature.com/articles/44565.

[5] E. Bizzi, F. A. Mussa-Ivaldi, and S. Giszter. "Computations Underlying the Execution of Movement: A Biological Perspective". In: *Science* 253.5017 (July 19, 1991). Publisher: American Association for the Advancement of Science, pp. 287–291. DOI: 10.1126/science.1857964. URL: https://www.science.org/doi/abs/10.1126/science.1857964.

[6] M. A. Lemay and W. M. Grill. "Modularity of Motor Output Evoked By Intraspinal Microstimulation in Cats". In: *Journal of Neurophysiology* 91.1 (Jan. 1, 2004). Publisher: American Physiological Society, pp. 502–514. ISSN: 0022-3077. DOI: 10.1152/jn.00235.2003. URL: https://journals.physiology.org/doi/full/10.1152/jn.00235.2003.

[7] D. J. Berger, R. Gentner, T. Edmunds, D. K. Pai, and A. d'Avella. "Differences in Adaptation Rates after Virtual Surgeries Provide Direct Evidence for Modularity". In: *Journal of Neuroscience* 33.30 (July 24, 2013). Publisher: Society for Neuroscience Section: Articles, pp. 12384–12394. ISSN: 0270-6474, 1529-2401. DOI: 10.1523/JNEUROSCI.0122-13.2013. URL: https://www.jneurosci.org/content/33/30/12384.

[8] C. Fleischer and G. Hommel. "A Human–Exoskeleton Interface Utilizing Electromyography". In: *IEEE Transactions on Robotics* 24.4 (Aug. 2008). Conference Name: IEEE Transactions on Robotics, pp. 872–882. ISSN: 1941-0468. DOI: 10.1109/TRO.2008.926860.

[9] P. Kieliba, D. Clode, R. O. Maimon-Mor, and T. R. Makin. "Neurocognitive consequences of hand augmentation". In: *bioRxiv* (June 16, 2020). Publisher: Cold Spring Harbor Laboratory Section: New Results, p. 2020.06.16.151944. DOI: 10.1101/2020.06.16.151944. URL: https://www.biorxiv.org/content/10.1101/2020.06.16.151944v1.

[10] D. Prattichizzo, M. Malvezzi, I. Hussain, and G. Salvietti. "The Sixth-Finger: A modular extra-finger to enhance human hand capabilities". In: *The 23rd IEEE International Symposium on Robot and Human Interactive Communication*. The 23rd IEEE International Symposium on Robot and Human Interactive Communication. ISSN: 1944-9437. Aug. 2014, pp. 993–998. DOI: 10.1109/ROMAN.2014.6926382.

[11] C. I. Penaloza and S. Nishio. "BMI control of a third arm for multitasking". In: *Science Robotics* 3.20 (July 25, 2018). Publisher: Science Robotics Section: Research Article, pp. 1–6. ISSN: 2470-9476. DOI: 10.1126/scirobotics.aat1228. URL: https://robotics.sciencemag.org/content/3/20/eaat1228.

[12] A. Takagi, H. Kambara, and Y. Koike. "Independent control of cocontraction and reciprocal activity during goal-directed reaching in muscle space". In: *Scientific Reports* 10.1 (Dec. 18, 2020). Number: 1 Publisher: Nature Publishing Group, p. 22333. ISSN: 2045-2322. DOI: 10.1038/s41598-020-79526-1. URL: https://www.nature.com/articles/s41598-020-79526-1.

[13] D. L. Kent, D. R. Haynor, W. T. Longstreth, and E. B. Larson. "The Clinical Efficacy of Magnetic Resonance Imaging in Neuroimaging". In: *Annals of Internal Medicine* 120.10 (May 15, 1994). Publisher: American College of Physicians,

pp. 856–871. ISSN: 0003-4819. DOI: 10.7326/0003-4819-120-10-199405150-00007. URL: https://www.acpjournals.org/doi/abs/10.7326/0003-4819-120-10-199405150-00007.

[14] D. R. Leff, F. Orihuela-Espina, C. E. Elwell, T. Athanasiou, D. T. Delpy, A. W. Darzi, and G.-Z. Yang. "Assessment of the cerebral cortex during motor task behaviours in adults: A systematic review of functional near infrared spectroscopy (fNIRS) studies". In: *NeuroImage* 54.4 (Feb. 14, 2011), pp. 2922–2936. ISSN: 1053-8119. DOI: 10.1016/j.neuroimage.2010.10.058. URL: https://www.sciencedirect.com/science/article/pii/S1053811910013510.

[15] M. Hatakenaka, I. Miyai, M. Mihara, S. Sakoda, and K. Kubota. "Frontal regions involved in learning of motor skill—A functional NIRS study". In: *NeuroImage* 34.1 (Jan. 2007), pp. 109–116. ISSN: 10538119. DOI: 10.1016/j.neuroimage.2006.08.014. URL: https://linkinghub.elsevier.com/retrieve/pii/S1053811906008718.

[16] D. S. Childress. *Historical Aspects of Powered Limb Prostheses | O&P Virtual Library*. 1985. URL: http://www.oandplibrary.org/cpo/1985_01_002.asp.

[17] R. Reiter. "A new electrical arts hand". In: *Grenzgebiete Der Medizin* 1.4 (Sept. 1948), pp. 133–135.

[18] C. K. Battye, A. Nightingale, and J. Whillis. "The use of myo-electric currents in the operation of prostheses". In: *The Journal of Bone and Joint Surgery. British volume* 37-B.3 (Aug. 1, 1955). Publisher: The British Editorial Society of Bone & Joint Surgery, pp. 506–510. ISSN: 0301-620X. DOI: 10.1302/0301-620X.37B3.506. URL: https://online.boneandjoint.org.uk/doi/abs/10.1302/0301-620X.37B3.506.

[19] S. Morita, K. Shibata, X. Z. Zheng, and K. Ito. "Prosthetic hand control based on torque estimation from EMG signals". In: *Proceedings. 2000 IEEE/RSJ International Conference on Intelligent Robots and Systems (IROS 2000) (Cat. No.00CH37113)*. Proceedings. 2000 IEEE/RSJ International Conference on Intelligent Robots and Systems (IROS 2000) (Cat. No.00CH37113). Vol. 1. Oct. 2000, 389–394 vol.1. DOI: 10.1109/IROS.2000.894636.

[20] R. D. Alley and H. H. Sears. “Powered Upper Limb Prosthetics in Adults”. In: *Powered Upper Limb Prostheses: Control, Implementation and Clinical Application*. Ed. by A. Muzumdar. Berlin, Heidelberg: Springer, 2004, pp. 117–145. ISBN: 978-3-642-18812-1. DOI: 10.1007/978-3-642-18812-1_7. URL: https://doi.org/10.1007/978-3-642-18812-1_7.

[21] S.-H. Park and S.-P. Lee. “EMG pattern recognition based on artificial intelligence techniques”. In: *IEEE Transactions on Rehabilitation Engineering* 6.4 (Dec. 1998). Conference Name: IEEE Transactions on Rehabilitation Engineering, pp. 400–405. ISSN: 1558-0024. DOI: 10.1109/86.736154.

[22] K. Englehart and B. Hudgins. “A robust, real-time control scheme for multifunction myoelectric control”. In: *IEEE Transactions on Biomedical Engineering* 50.7 (July 2003). Conference Name: IEEE Transactions on Biomedical Engineering, pp. 848–854. ISSN: 1558-2531. DOI: 10.1109/TBME.2003.813539.

[23] S. Muceli, N. Jiang, and D. Farina. “Multichannel surface EMG based estimation of bilateral hand kinematics during movements at multiple degrees of freedom”. In: *2010 Annual International Conference of the IEEE Engineering in Medicine and Biology*. 2010 Annual International Conference of the IEEE Engineering in Medicine and Biology. ISSN: 1558-4615. Aug. 2010, pp. 6066–6069. DOI: 10.1109/IEMBS.2010.5627622.

[24] A. J. Young, L. H. Smith, E. J. Rouse, and L. J. Hargrove. “Classification of Simultaneous Movements Using Surface EMG Pattern Recognition”. In: *IEEE Transactions on Biomedical Engineering* 60.5 (May 2013), pp. 1250–1258. ISSN: 1558-2531. DOI: 10.1109/TBME.2012.2232293.

[25] M. Vukobratovic, B. Borovac, D. Surla, and D. Stokic. *Biped Locomotion: Dynamics, Stability, Control and Application*. Google-Books-ID: nWnvCAAAQBAJ. Springer Science & Business Media, Dec. 6, 2012. 366 pp. ISBN: 978-3-642-83006-8.

[26] H. Kazerooni and R. Steger. “The Berkeley Lower Extremity Exoskeleton”. In: *Journal of Dynamic Systems, Measurement, and Control* 128.1 (Sept. 17, 2005), pp. 14–25. ISSN: 0022-0434. DOI: 10.1115/1.2168164. URL: https://doi.org/10.1115/1.2168164.

[27] G. Colombo, M. Joerg, R. Schreier, and V. Dietz. "Treadmill training of paraplegic patients using a robotic orthosis". In: *Journal of rehabilitation research and development* 37.6 (2000). Publisher: REHIBILITATION RESEARCH & DEVELOPMENT SERVICE, pp. 693–700.

[28] E. Ambrosini, S. Ferrante, T. Schauer, C. Klauer, M. Gaffuri, G. Ferrigno, and A. Pedrocchi. "A myocontrolled neuroprosthesis integrated with a passive exoskeleton to support upper limb activities". In: *Journal of Electromyography and Kinesiology* 24.2 (Apr. 1, 2014), pp. 307–317. ISSN: 1050-6411. DOI: 10.1016/j.jelekin.2014.01.006. URL: http://www.sciencedirect.com/science/article/pii/S1050641114000273.

[29] J. Stein, K. Narendran, J. McBean, K. Krebs, and R. Hughes. "Electromyography-Controlled Exoskeletal Upper-Limb–Powered Orthosis for Exercise Training After Stroke". In: *American Journal of Physical Medicine & Rehabilitation* 86.4 (Apr. 2007), pp. 255–261. ISSN: 0894-9115. DOI: 10.1097/PHM.0b013e3180383cc5. URL: https://journals.lww.com/ajpmr/Abstract/2007/04000/Electromyography_Controlled_Exoskeletal.2.aspx.

[30] K. Nazarpour, A. Barnard, and A. Jackson. "Flexible Cortical Control of Task-Specific Muscle Synergies". In: *Journal of Neuroscience* 32.36 (Sept. 5, 2012). Publisher: Society for Neuroscience Section: Articles, pp. 12349–12360. ISSN: 0270-6474, 1529-2401. DOI: 10.1523/JNEUROSCI.5481-11.2012. URL: https://www.jneurosci.org/content/32/36/12349.

[31] A. d. Rugy, G. E. Loeb, and T. J. Carroll. "Muscle Coordination Is Habitual Rather than Optimal". In: *Journal of Neuroscience* 32.21 (May 23, 2012). Publisher: Society for Neuroscience Section: Articles, pp. 7384–7391. ISSN: 0270-6474, 1529-2401. DOI: 10.1523/JNEUROSCI.5792-11.2012. URL: https://www.jneurosci.org/content/32/21/7384.

[32] I. Vujaklija, V. Shalchyan, E. N. Kamavuako, N. Jiang, H. R. Marateb, and D. Farina. "Online mapping of EMG signals into kinematics by autoencoding". In: *Journal of NeuroEngineering and Rehabilitation* 15.1 (Mar. 13, 2018), p. 21. ISSN: 1743-0003. DOI: 10.1186/s12984-018-0363-1. URL: https://doi.org/10.1186/s12984-018-0363-1.

[33] N. Lotti and V. Sanguineti. "EMG-Driven Force Fields: Toward a Myoprocessor for 'Virtual Biomechanics'". In: *Converging Clinical and Engineering Research on Neurorehabilitation III*. Ed. by L. Masia, S. Micera, M. Akay, and J. L. Pons. Biosystems & Biorobotics. Cham: Springer International Publishing, 2019, pp. 1161–1165. ISBN: 978-3-030-01845-0. DOI: 10.1007/978-3-030-01845-0_232.

[34] H. J. Hermens, B. Freriks, R. Merletti, D. Stegeman, J. Blok, G. Rau, C. Disselhorst-Klug, and G. Hägg. "European Recommendations for Surface ElectroMyoGraphy". In: (2000), p. 4.

[35] F. F. Jöbsis. "Noninvasive, Infrared Monitoring of Cerebral and Myocardial Oxygen Sufficiency and Circulatory Parameters". In: *Science* 198.4323 (Dec. 23, 1977). Publisher: American Association for the Advancement of Science, pp. 1264–1267. DOI: 10.1126/science.929199. URL: https://www.science.org/doi/abs/10.1126/science.929199.

[36] M. Ferrari, I. Giannini, G. Sideri, and E. Zanette. "Continuous Non Invasive Monitoring of Human Brain by Near Infrared Spectroscopy". In: *Oxygen Transport to Tissue VII*. Ed. by F. Kreuzer, S. M. Cain, Z. Turek, and T. K. Goldstick. Advances in Experimental Medicine and Biology. Boston, MA: Springer US, 1985, pp. 873–882. ISBN: 978-1-4684-3291-6. DOI: 10.1007/978-1-4684-3291-6_88. URL: https://doi.org/10.1007/978-1-4684-3291-6_88.

[37] J. S. Wyatt, D. T. Delpy, M. Cope, S. Wray, and E. O. R. Reynolds. "QUANTIFICATION OF CEREBRAL OXYGENATION AND HAEMODYNAMICS IN SICK NEWBORN INFANTS BY NEAR INFRARED SPECTROPHOTOMETRY". In: *The Lancet*. Originally published as Volume 2, Issue 8515 328.8515 (Nov. 8, 1986), pp. 1063–1066. ISSN: 0140-6736. DOI: 10.1016/S0140-6736(86)90467-8. URL: https://www.sciencedirect.com/science/article/pii/S0140673686904678.

[38] M. Ferrari and V. Quaresima. "A brief review on the history of human functional near-infrared spectroscopy (fNIRS) development and fields of application". In: *NeuroImage* 63.2 (Nov. 1, 2012), pp. 921–935. ISSN: 1053-8119. DOI: 10.1016/j.neuroimage.2012.03.049. URL: https://www.sciencedirect.com/science/article/pii/S1053811912003308.

[39] Y. Hoshi and M. Tamura. "Detection of dynamic changes in cerebral oxygenation coupled to neuronal function during mental work in man". In: *Neuroscience Letters* 150.1 (Feb. 5, 1993), pp. 5–8. ISSN: 0304-3940. DOI: 10.1016/0304-3940(93)90094-2. URL: https://www.sciencedirect.com/science/article/pii/0304394093900942.

[40] F. Okada, Y. Tokumitsu, Y. Hoshi, and M. Tamura. "Gender- and handedness-related differences of forebrain oxygenation and hemodynamics". In: *Brain Research* 601.1 (Jan. 22, 1993), pp. 337–342. ISSN: 0006-8993. DOI: 10.1016/0006-8993(93)91733-9. URL: https://www.sciencedirect.com/science/article/pii/0006899393917339.

[41] Y. Hoshi and M. Tamura. "Dynamic multichannel near-infrared optical imaging of human brain activity". In: *Journal of Applied Physiology* 75.4 (Oct. 1, 1993). Publisher: American Physiological Society, pp. 1842–1846. ISSN: 8750-7587. DOI: 10.1152/jappl.1993.75.4.1842. URL: https://journals.physiology.org/doi/abs/10.1152/jappl.1993.75.4.1842.

[42] F. Okada, Y. Tokumitsu, Y. Hoshi, and M. Tamura. "Impaired interhemispheric integration in brain oxygenation and hemodynamics in schizophrenia". In: *European Archives of Psychiatry and Clinical Neuroscience* 244.1 (June 1, 1994), pp. 17–25. ISSN: 1433-8491. DOI: 10.1007/BF02279807. URL: https://doi.org/10.1007/BF02279807.

[43] A. Maki, Y. Yamashita, Y. Ito, E. Watanabe, Y. Mayanagi, and H. Koizumi. "Spatial and temporal analysis of human motor activity using noninvasive NIR topography". In: *Medical Physics* 22.12 (1995). _eprint: https://onlinelibrary.wiley.com/doi/ pp. 1997–2005. ISSN: 2473-4209. DOI: 10.1118/1.597496. URL: https://onlinelibrary.wiley.com/doi/abs/10.1118/1.597496.

[44] H. Ito, I. Kanno, and H. Fukuda. "Human cerebral circulation: positron emission tomography studies". In: *Annals of Nuclear Medicine* 19.2 (Apr. 1, 2005), pp. 65–74. ISSN: 1864-6433. DOI: 10.1007/BF03027383. URL: https://doi.org/10.1007/BF03027383.

[45] D. M. Wolpert. "Computational approaches to motor control". In: *Trends in Cognitive Sciences* 1.6 (Sept. 1, 1997), pp. 209–216. ISSN: 1364-6613. DOI: 10.1016/S1364-6613(97)01070-X. URL: https://www.sciencedirect.com/science/article/pii/S136466139701070X.

[46] F. M. M. O. Campos and J. M. F. Calado. "Approaches to human arm movement control—A review". In: *Annual Reviews in Control* 33.1 (Apr. 1, 2009), pp. 69–77. ISSN: 1367-5788. DOI: 10.1016/j.arcontrol.2009.03.001. URL: https://www.sciencedirect.com/science/article/pii/S1367578809000091.

[47] T. Flash and N. Hogan. "The coordination of arm movements: an experimentally confirmed mathematical model". In: *Journal of Neuroscience* 5.7 (July 1, 1985). Publisher: Society for Neuroscience Section: Articles, pp. 1688–1703. ISSN: 0270-6474, 1529-2401. DOI: 10.1523/JNEUROSCI.05-07-01688.1985. URL: https://www.jneurosci.org/content/5/7/1688.

[48] E. Todorov and M. I. Jordan. "Smoothness Maximization Along a Predefined Path Accurately Predicts the Speed Profiles of Complex Arm Movements". In: *Journal of Neurophysiology* 80.2 (Aug. 1, 1998). Publisher: American Physiological Society, pp. 696–714. ISSN: 0022-3077. DOI: 10.1152/jn.1998.80.2.696. URL: https://journals.physiology.org/doi/full/10.1152/jn.1998.80.2.696.

[49] Y. Uno, M. Kawato, and R. Suzuki. "Formation and control of optimal trajectory in human multijoint arm movement". In: *Biological Cybernetics* 61.2 (June 1, 1989), pp. 89–101. ISSN: 1432-0770. DOI: 10.1007/BF00204593. URL: https://doi.org/10.1007/BF00204593.

[50] C. M. Harris and D. M. Wolpert. "Signal-dependent noise determines motor planning". In: *Nature* 394.6695 (Aug. 1998). Number: 6695 Publisher: Nature Publishing Group, pp. 780–784. ISSN: 1476-4687. DOI: 10.1038/29528. URL: https://www.nature.com/articles/29528.

[51] E. Todorov and M. I. Jordan. "Optimal feedback control as a theory of motor coordination". In: *Nature Neuroscience* 5.11 (Nov. 2002). Number: 11 Publisher: Nature Publishing Group, pp. 1226–1235. ISSN: 1546-1726. DOI: 10.1038/nn963. URL: https://www.nature.com/articles/nn963.

[52] A. Ebied, E. Kinney-Lang, L. Spyrou, and J. Escudero. "Evaluation of matrix factorisation approaches for muscle synergy extraction". In: *Medical Engineering & Physics* 57 (July 1, 2018), pp. 51–60. ISSN: 1350-4533. DOI: 10.1016/j.medengphy.2018.04.003. URL: https://www.sciencedirect.com/science/article/pii/S1350453318300572.

[53] M. C. Tresch, V. C. K. Cheung, and A. d'Avella. "Matrix Factorization Algorithms for the Identification of Muscle Synergies: Evaluation on Simulated and Experimental Data Sets". In: *Journal of Neurophysiology* 95.4 (Apr. 1, 2006). Publisher: American Physiological Society, pp. 2199–2212. ISSN: 0022-3077. DOI: 10.1152/jn.00222.2005. URL: https://journals.physiology.org/doi/full/10.1152/jn.00222.2005.

[54] A. d'Avella and F. Lacquaniti. "Control of reaching movements by muscle synergy combinations". In: *Frontiers in Computational Neuroscience* 7 (2013), p. 42. ISSN: 1662-5188. DOI: 10.3389/fncom.2013.00042. URL: https://www.frontiersin.org/article/10.3389/fncom.2013.00042.

[55] J. E. Jackson. *A User's Guide to Principal Components*. Google-Books-ID: f9s6g6cmUTUC. John Wiley & Sons, Jan. 21, 2005. 597 pp. ISBN: 978-0-471-72532-9.

[56] A. Hyvärinen and E. Oja. "Independent component analysis: algorithms and applications". In: *Neural Networks* 13.4 (June 1, 2000), pp. 411–430. ISSN: 0893-6080. DOI: 10.1016/S0893-6080(00)00026-5. URL: https://www.sciencedirect.com/science/article/pii/S0893608000000265.

[57] A. T. Basilevsky. *Statistical Factor Analysis and Related Methods: Theory and Applications*. Google-Books-ID: uvZkWmRTZhUC. John Wiley & Sons, Sept. 25, 2009. 771 pp. ISBN: 978-0-470-31773-0.

[58] A. d'Avella, P. Saltiel, and E. Bizzi. "Combinations of muscle synergies in the construction of a natural motor behavior". In: *Nature Neuroscience* 6.3 (Mar. 2003). Bandiera_abtest: a Cg_type: Nature Research Journals Number: 3 Primary_atype: Research Publisher: Nature Publishing Group, pp. 300–308. ISSN: 1546-1726. DOI: 10.1038/nn1010. URL: https://www.nature.com/articles/nn1010.

[59] G. Torres-Oviedo and L. H. Ting. "Muscle Synergies Characterizing Human Postural Responses". In: *Journal of Neurophysiology* 98.4 (Oct. 1, 2007). Publisher: American Physiological Society, pp. 2144–2156. ISSN: 0022-3077. DOI: 10.1152/jn.01360.2006. URL: https://journals.physiology.org/doi/full/10.1152/jn.01360.2006.

[60] G. Torres-Oviedo and L. H. Ting. "Subject-Specific Muscle Synergies in Human Balance Control Are Consistent Across Different Biomechanical Contexts". In: *Journal of Neurophysiology* 103.6 (June 1, 2010). Publisher: American Physiological Society, pp. 3084–3098. ISSN: 0022-3077. DOI: 10.1152/jn.00960.2009. URL: https://journals.physiology.org/doi/full/10.1152/jn.00960.2009.

[61] Y. P. Ivanenko, R. E. Poppele, and F. Lacquaniti. "Five basic muscle activation patterns account for muscle activity during human locomotion". In: *The Journal of Physiology* 556.1 (2004). _eprint: https://onlinelibrary.wiley.com/doi/pdf/10.1113/jphysio pp. 267–282. ISSN: 1469-7793. DOI: 10.1113/jphysiol.2003.057174. URL: https://onlinelibrary.wiley.com/doi/abs/10.1113/jphysiol.2003.057174.

[62] N. Dominici, Y. P. Ivanenko, G. Cappellini, A. d'Avella, V. Mondì, M. Cicchese, A. Fabiano, T. Silei, A. Di Paolo, C. Giannini, R. E. Poppele, and F. Lacquaniti. "Locomotor Primitives in Newborn Babies and Their Development". In: *Science* 334.6058 (Nov. 18, 2011). Publisher: American Association for the Advancement of Science, pp. 997–999. DOI: 10.1126/science.1210617. URL: https://www.science.org/doi/abs/10.1126/science.1210617.

[63] A. d'Avella, A. Portone, L. Fernandez, and F. Lacquaniti. "Control of Fast-Reaching Movements by Muscle Synergy Combinations". In: *Journal of Neuroscience* 26.30 (July 26, 2006). Publisher: Society for Neuroscience Section: Articles, pp. 7791–7810. ISSN: 0270-6474, 1529-2401. DOI: 10.1523/JNEUROSCI.0830-06.2006. URL: https://www.jneurosci.org/content/26/30/7791.

[64] M. C. Tresch and A. Jarc. "The case for and against muscle synergies". In: *Current Opinion in Neurobiology*. Motor systems • Neurology of behaviour 19.6 (Dec. 1, 2009), pp. 601–607. ISSN: 0959-4388. DOI: 10.1016/j.conb.2009.09.002. URL: https://www.sciencedirect.com/science/article/pii/S095943880900124X.

[65] J. J. Kutch and F. J. Valero-Cuevas. "Challenges and New Approaches to Proving the Existence of Muscle Synergies of Neural Origin". In: *PLOS Computational Biology* 8.5 (May 3, 2012). Publisher: Public Library of Science, e1002434. ISSN: 1553-7358. DOI: 10.1371/journal.pcbi.1002434. URL: https://

journals.plos.org/ploscompbiol/article?id=10.1371/journal.pcbi.1002434.

[66] D. Borzelli, S. Gurgone, P. De Pasquale, D. J. Berger, and A. d'Avella. "Consistency of Myoelectric Control Across Multiple Sessions". In: *Converging Clinical and Engineering Research on Neurorehabilitation III*. Ed. by L. Masia, S. Micera, M. Akay, and J. L. Pons. Biosystems & Biorobotics. Cham: Springer International Publishing, 2019, pp. 1166–1170. ISBN: 978-3-030-01845-0. DOI: 10.1007/978-3-030-01845-0_233.

[67] T. Zachry, G. Wulf, J. Mercer, and N. Bezodis. "Increased movement accuracy and reduced EMG activity as the result of adopting an external focus of attention". In: *Brain Research Bulletin* 67.4 (Oct. 30, 2005), pp. 304–309. ISSN: 0361-9230. DOI: 10.1016/j.brainresbull.2005.06.035. URL: https://www.sciencedirect.com/science/article/pii/S0361923005002765.

[68] D. Borzelli, D. Berger, D. Pai, and A. d'Avella. "Effort minimization and synergistic muscle recruitment for three-dimensional force generation". In: *Frontiers in Computational Neuroscience* 7 (2013), p. 186. ISSN: 1662-5188. DOI: 10.3389/fncom.2013.00186. URL: https://www.frontiersin.org/article/10.3389/fncom.2013.00186.

[69] R. Shadmehr and T. Brashers-Krug. "Functional Stages in the Formation of Human Long-Term Motor Memory". In: *Journal of Neuroscience* 17.1 (1997), pp. 409–419. ISSN: 0270-6474. DOI: 10.1523/JNEUROSCI.17-01-00409.1997. eprint: https://www.jneurosci.org/content/17/1/409.full.pdf. URL: https://www.jneurosci.org/content/17/1/409.

[70] M. Fu, X. Yu, J. Lu, and Y. Zuo. "Repetitive motor learning induces coordinated formation of clustered dendritic spines in vivo". In: *Nature* 483.7387 (Mar. 2012). Bandiera_abtest: a Cg_type: Nature Research Journals Number: 7387 Primary_atype: Research Publisher: Nature Publishing Group Subject_term: Learning and memory;Motor cortex;Spine regulation and structure Subject_term_id: learning-and-memory;motor-cortex;spine-regulation-and-structure, pp. 92–95. ISSN: 1476-4687. DOI: 10.1038/nature10844. URL: https://www.nature.com/articles/nature10844.

[71] E. R. Oby, M. D. Golub, J. A. Hennig, A. D. Degenhart, E. C. Tyler-Kabara, B. M. Yu, S. M. Chase, and A. P. Batista. "New neural activity patterns emerge with long-term learning". In: *Proceedings of the National Academy of Sciences* 116.30 (July 23, 2019), pp. 15210–15215.

[72] R. Shadmehr and J. W. Krakauer. "A computational neuroanatomy for motor control". In: *Experimental Brain Research* 185.3 (Mar. 2008), pp. 359–381. ISSN: 1432-1106. DOI: 10.1007/s00221-008-1280-5.

[73] J. A. Taylor, N. M. Klemfuss, and R. B. Ivry. "An explicit strategy prevails when the cerebellum fails to compute movement errors". In: *Cerebellum (London, England)* 9.4 (Dec. 2010), pp. 580–586. ISSN: 1473-4230. DOI: 10.1007/s12311-010-0201-x.

[74] J. M. Galea, A. Vazquez, N. Pasricha, J.-J. O. de Xivry, and P. Celnik. "Dissociating the roles of the cerebellum and motor cortex during adaptive learning: the motor cortex retains what the cerebellum learns". In: *Cerebral Cortex (New York, N.Y.: 1991)* 21.8 (Aug. 2011), pp. 1761–1770. ISSN: 1460-2199. DOI: 10.1093/cercor/bhq246.

[75] T. A. Martin, J. G. Keating, H. P. Goodkin, A. J. Bastian, and W. T. Thach. "Throwing while looking through prisms. II. Specificity and storage of multiple gaze-throw calibrations". In: *Brain: A Journal of Neurology* 119 (Pt 4) (Aug. 1996), pp. 1199–1211. ISSN: 0006-8950. DOI: 10.1093/brain/119.4.1199.

[76] W. J. Kargo and D. A. Nitz. "Early skill learning is expressed through selection and tuning of cortically represented muscle synergies". In: *The Journal of Neuroscience: The Official Journal of the Society for Neuroscience* 23.35 (Dec. 3, 2003), pp. 11255–11269. ISSN: 1529-2401.

[77] D. Morris, H. Tan, F. Barbagli, T. Chang, and K. Salisbury. "Haptic Feedback Enhances Force Skill Learning". In: *Second Joint EuroHaptics Conference and Symposium on Haptic Interfaces for Virtual Environment and Teleoperator Systems (WHC'07)*. Second Joint EuroHaptics Conference and Symposium on Haptic Interfaces for Virtual Environment and Teleoperator Systems (WHC'07). Mar. 2007, pp. 21–26. DOI: 10.1109/WHC.2007.65.

[78] D. Wolpert, R. Miall, and M. Kawato. “Internal models in the cerebellum”. In: *Trends in Cognitive Sciences* 2.9 (1998), pp. 338–347. DOI: 10.1016/S1364-6613(98)01221-2.

[79] G. Wulf, C. H. Shea, and S. Matschiner. “Frequent Feedback Enhances Complex Motor Skill Learning”. In: *Journal of Motor Behavior* 30.2 (June 1, 1998). Publisher: Routledge _eprint: https://doi.org/10.1080/00222899809601335, pp. 180–192. ISSN: 0022-2895. DOI: 10.1080/00222899809601335. URL: https://doi.org/10.1080/00222899809601335.

[80] D. Ao, R. Song, and J. Gao. “Movement Performance of Human–Robot Cooperation Control Based on EMG-Driven Hill-Type and Proportional Models for an Ankle Power-Assist Exoskeleton Robot”. In: *IEEE Transactions on Neural Systems and Rehabilitation Engineering* 25.8 (Aug. 2017). Conference Name: IEEE Transactions on Neural Systems and Rehabilitation Engineering, pp. 1125–1134. ISSN: 1558-0210. DOI: 10.1109/TNSRE.2016.2583464.

[81] V. Krasin, V. Gandhi, Z. Yang, and M. Karamanoglu. “EMG based elbow joint powered exoskeleton for biceps brachii strength augmentation”. In: *2015 International Joint Conference on Neural Networks (IJCNN)*. 2015 International Joint Conference on Neural Networks (IJCNN). ISSN: 2161-4407. July 2015, pp. 1–6. DOI: 10.1109/IJCNN.2015.7280643.

[82] E. Abdi, E. Burdet, M. Bouri, S. Himidan, and H. Bleuler. “In a demanding task, three-handed manipulation is preferred to two-handed manipulation”. In: *Scientific Reports* 6.1 (Feb. 2016), p. 21758. ISSN: 2045-2322. DOI: 10.1038/srep21758. URL: http://www.nature.com/articles/srep21758.

[83] G. Dominijanni, S. Shokur, G. Salvietti, S. Buehler, E. Palmerini, S. Rossi, F. De Vignemont, A. d’Avella, T. R. Makin, D. Prattichizzo, and S. Micera. “The neural resource allocation problem when enhancing human bodies with extra robotic limbs”. In: *Nature Machine Intelligence* 3.10 (Oct. 2021). Bandiera_abtest: a Cg_type: Nature Research Journals Number: 10 Primary_atype: Reviews Publisher: Nature Publishing Group Subject_term: Biomedical engineering;Brain–machine interface Subject_term_id: biomedical-engineering;brain-machine-interface, pp. 850–860. ISSN: 2522-5839. DOI: 10.1038/s42256-021-00398-9. URL: https://www.nature.com/articles/s42256-021-00398-9.

[84] T. L. Baldi, N. D'Aurizio, C. Gaudeni, S. Gurgone, D. Borzelli, A. D'Avella, and D. Prattichizzo. "Exploiting Implicit Kinematic Kernel for Controlling a Wearable Robotic Extra-finger". In: *arXiv:2012.03600 [cs]* (Dec. 7, 2020). arXiv: 2012.03600. URL: http://arxiv.org/abs/2012.03600.

[85] G. Salvietti, I. Hussain, D. Cioncoloni, S. Taddei, S. Rossi, and D. Prattichizzo. "Compensating Hand Function in Chronic Stroke Patients Through the Robotic Sixth Finger". In: *IEEE Transactions on Neural Systems and Rehabilitation Engineering* 25.2 (Feb. 2017). Conference Name: IEEE Transactions on Neural Systems and Rehabilitation Engineering, pp. 142–150. ISSN: 1558-0210. DOI: 10.1109/TNSRE.2016.2529684.

[86] F. Parietti and H. H. Asada. "Independent, voluntary control of extra robotic limbs". In: *2017 IEEE International Conference on Robotics and Automation (ICRA)*. 2017 IEEE International Conference on Robotics and Automation (ICRA). Singapore, Singapore: IEEE, May 2017, pp. 5954–5961. ISBN: 978-1-5090-4633-1. DOI: 10.1109/ICRA.2017.7989702. URL: http://ieeexplore.ieee.org/document/7989702/.

[87] E. Burdet, R. Osu, D. W. Franklin, T. E. Milner, and M. Kawato. "The central nervous system stabilizes unstable dynamics by learning optimal impedance". In: *Nature* 414.6862 (Nov. 2001). Number: 6862 Publisher: Nature Publishing Group, pp. 446–449. ISSN: 1476-4687. DOI: 10.1038/35106566. URL: https://www.nature.com/articles/35106566.

[88] T. E. Milner. "Adaptation to destabilizing dynamics by means of muscle cocontraction". In: *Experimental Brain Research* 143.4 (Apr. 1, 2002), pp. 406–416. ISSN: 1432-1106. DOI: 10.1007/s00221-002-1001-4. URL: https://doi.org/10.1007/s00221-002-1001-4.

[89] L. P. J. Selen, D. W. Franklin, and D. M. Wolpert. "Impedance Control Reduces Instability That Arises from Motor Noise". In: *Journal of Neuroscience* 29.40 (Oct. 7, 2009). Publisher: Society for Neuroscience Section: Articles, pp. 12606–12616. ISSN: 0270-6474, 1529-2401. DOI: 10.1523/JNEUROSCI.2826-09.2009. URL: https://www.jneurosci.org/content/29/40/12606.

[90] A. Ajoudani, N. G. Tsagarakis, and A. Bicchi. "Tele-impedance: Towards transferring human impedance regulation skills to robots". In: *2012 IEEE International Conference on Robotics and Automation*. 2012 IEEE International Con-

ference on Robotics and Automation. ISSN: 1050-4729. May 2012, pp. 382–388. DOI: 10.1109/ICRA.2012.6224904.

[91] M. Laghi, A. Ajoudani, M. G. Catalano, and A. Bicchi. "Unifying bilateral teleoperation and tele-impedance for enhanced user experience". In: *The International Journal of Robotics Research* 39.4 (Mar. 1, 2020). Publisher: SAGE Publications Ltd STM, pp. 514–539. ISSN: 0278-3649. DOI: 10.1177/0278364919891773. URL: https://doi.org/10.1177/0278364919891773.

[92] D. Borzelli, B. Cesqui, D. J. Berger, E. Burdet, and A. d'Avella. "Muscle patterns underlying voluntary modulation of co-contraction". In: *PLOS ONE* 13.10 (Oct. 19, 2018). Publisher: Public Library of Science, e0205911. ISSN: 1932-6203. DOI: 10.1371/journal.pone.0205911. URL: https://journals.plos.org/plosone/article?id=10.1371/journal.pone.0205911.

[93] M Bräcklein, J Ibáñez, D. Y. Barsakcioglu, and D Farina. "Towards human motor augmentation by voluntary decoupling beta activity in the neural drive to muscle and force production". In: *Journal of Neural Engineering* 18.1 (Feb. 1, 2021), p. 016001. ISSN: 1741-2560, 1741-2552. DOI: 10.1088/1741-2552/abcdbf. URL: https://iopscience.iop.org/article/10.1088/1741-2552/abcdbf.

[94] P. M. Fitts. "The information capacity of the human motor system in controlling the amplitude of movement". In: *Journal of Experimental Psychology* 47.6 (1954). Place: US Publisher: American Psychological Association, pp. 381–391. ISSN: 0022-1015(Print). DOI: 10.1037/h0055392.

[95] A. Newell. *Unified Theories of Cognition*. Google-Books-ID: 1lbY14DmV2cC. Harvard University Press, 1994. 580 pp. ISBN: 978-0-674-92101-6.

[96] J. Gori, O. Rioul, and Y. Guiard. "Speed-Accuracy Tradeoff: A Formal Information-Theoretic Transmission Scheme (FITTS)". In: *ACM Transactions on Computer-Human Interaction* 25.5 (Sept. 24, 2018), 27:1–27:33. ISSN: 1073-0516. DOI: 10.1145/3231595. URL: https://doi.org/10.1145/3231595.

[97] E. N. Kamavuako, E. J. Scheme, and K. B. Englehart. "On the usability of intramuscular EMG for prosthetic control: A Fitts' Law approach". In: *Journal of Electromyography and Kinesiology* 24.5 (Oct. 2014), pp. 770–777. ISSN:

10506411. DOI: 10.1016/j.jelekin.2014.06.009. URL: https://linkinghub.elsevier.com/retrieve/pii/S1050641114001370.

[98] R. W. Soukoreff and I. S. MacKenzie. "Towards a standard for pointing device evaluation, perspectives on 27 years of Fitts' law research in HCI". In: *International Journal of Human-Computer Studies* 61.6 (Dec. 2004), pp. 751–789. ISSN: 10715819. DOI: 10.1016/j.ijhcs.2004.09.001. URL: https://linkinghub.elsevier.com/retrieve/pii/S1071581904001016.

[99] R. W. Soukoreff and I. S. MacKenzie. "An informatic rationale for the speed-accuracy trade-off". In: *2009 IEEE International Conference on Systems, Man and Cybernetics*. 2009 IEEE International Conference on Systems, Man and Cybernetics - SMC. San Antonio, TX, USA: IEEE, Oct. 2009, pp. 2890–2896. ISBN: 978-1-4244-2793-2. DOI: 10.1109/ICSMC.2009.5346580. URL: http://ieeexplore.ieee.org/document/5346580/.

[100] I. S. MacKenzie and W. Buxton. "Extending Fitts' law to two-dimensional tasks". In: *Proceedings of the SIGCHI Conference on Human Factors in Computing Systems*. CHI '92. Monterey, California, USA: Association for Computing Machinery, June 1, 1992, pp. 219–226. ISBN: 978-0-89791-513-7. DOI: 10.1145/142750.142794. URL: https://doi.org/10.1145/142750.142794.

[101] D. E. Meyer, J. E. Keith-Smith, S. Kornblum, R. A. Abrams, and C. E. Wright. "Speed-accuracy tradeoffs in aimed movements: Toward a theory of rapid voluntary action". In: *Attention and performance 13: Motor representation and control*. Hillsdale, NJ, US: Lawrence Erlbaum Associates, Inc, 1990, pp. 173–226. ISBN: 978-0-8058-0565-9.

[102] L. G. Carlton. "The Effects of Temporal-Precision and Time-Minimization Constraints on the Spatial and Temporal Accuracy of Aimed Hand Movements". In: *Journal of Motor Behavior* 26.1 (Mar. 1, 1994). Publisher: Routledge _eprint: https://doi.org/10.1080/00222895.1994.9941660, pp. 43–50. ISSN: 0022-2895. DOI: 10.1080/00222895.1994.9941660. URL: https://doi.org/10.1080/00222895.1994.9941660.

[103] H. N. Zelaznik, S. Mone, G. P. McCabe, and C. Thaman. "Role of temporal and spatial precision in determining the nature of the speed-accuracy trade-off in aimed-hand movements". In: *Journal of Experimental Psychology: Human Perception and Performance* 14.2 (1988). Place: US Publisher: American Psycho-

logical Association, pp. 221–230. ISSN: 1939-1277(Electronic),0096-1523(Print). DOI: 10.1037/0096-1523.14.2.221.

[104] X. Zhou, X. Cao, and X. Ren. "Speed-Accuracy Tradeoff in Trajectory-Based Tasks with Temporal Constraint". In: *Human-Computer Interaction – INTERACT 2009*. Ed. by T. Gross, J. Gulliksen, P. Kotzé, L. Oestreicher, P. Palanque, R. O. Prates, and M. Winckler. Lecture Notes in Computer Science. Berlin, Heidelberg: Springer, 2009, pp. 906–919. ISBN: 978-3-642-03655-2. DOI: 10.1007/978-3-642-03655-2_99.

[105] A. Murata and H. Iwase. "Extending Fitts' law to a three-dimensional pointing task". In: *Human Movement Science* 20.6 (Dec. 1, 2001), pp. 791–805. ISSN: 0167-9457. DOI: 10.1016/S0167-9457(01)00058-6. URL: https://www.sciencedirect.com/science/article/pii/S0167945701000586.

[106] Y. Cha and R. Myung. "Extended Fitts' law for 3D pointing tasks using 3D target arrangements". In: *International Journal of Industrial Ergonomics* 43.4 (July 1, 2013), pp. 350–355. ISSN: 0169-8141. DOI: 10.1016/j.ergon.2013.05.005. URL: https://www.sciencedirect.com/science/article/pii/S0169814113000723.

[107] A. T. Welford. "The measurement of sensory-motor performance: Survey and reappraisal of twelve years' progress". In: *Ergonomics* 3.3 (July 1960), pp. 189–230. ISSN: 0014-0139, 1366-5847. DOI: 10.1080/00140136008930484. URL: http://www.tandfonline.com/doi/abs/10.1080/00140136008930484.

[108] A. Welford. *Fundamentals of skill*. Fundamentals of skill. New York, NY, US: Methuen, 1968.

[109] J. Reis, H. M. Schambra, L. G. Cohen, E. R. Buch, B. Fritsch, E. Zarahn, P. A. Celnik, and J. W. Krakauer. "Noninvasive cortical stimulation enhances motor skill acquisition over multiple days through an effect on consolidation". In: *Proceedings of the National Academy of Sciences* 106.5 (Feb. 3, 2009). Publisher: National Academy of Sciences Section: Biological Sciences, pp. 1590–1595. ISSN: 0027-8424, 1091-6490. DOI: 10.1073/pnas.0805413106. URL: https://www.pnas.org/content/106/5/1590.

[110] L. Shmuelof, J. W. Krakauer, and P. Mazzoni. "How is a motor skill learned? Change and invariance at the levels of task success and trajectory control". In: *Journal of Neurophysiology* 108.2 (July 15, 2012), pp. 578–594. ISSN: 0022-3077, 1522-1598. DOI: 10.1152/jn.00856.2011. URL: https://www.physiology.org/doi/10.1152/jn.00856.2011.

[111] T. R. Makin, F. de Vignemont, and A. A. Faisal. "Neurocognitive barriers to the embodiment of technology". In: *Nature Biomedical Engineering* 1.1 (Jan. 10, 2017). Number: 1 Publisher: Nature Publishing Group, pp. 1–3. ISSN: 2157-846X. DOI: 10.1038/s41551-016-0014. URL: https://www.nature.com/articles/s41551-016-0014.

[112] A. Noccaro, J. Eden, G. Di Pino, D. Formica, and E. Burdet. "Human performance in three-hands tasks". In: *Scientific Reports* 11.1 (May 4, 2021). Number: 1 Publisher: Nature Publishing Group, p. 9511. ISSN: 2045-2322. DOI: 10.1038/s41598-021-88862-9. URL: https://www.nature.com/articles/s41598-021-88862-9.

[113] M. Y. Saraiji, T. Sasaki, K. Kunze, K. Minamizawa, and M. Inami. "MetaArms: Body Remapping Using Feet-Controlled Artificial Arms". In: *The 31st Annual ACM Symposium on User Interface Software and Technology - UIST '18*. The 31st Annual ACM Symposium. Berlin, Germany: ACM Press, 2018, pp. 65–74. ISBN: 978-1-4503-5948-1. DOI: 10.1145/3242587.3242665. URL: http://dl.acm.org/citation.cfm?doid=3242587.3242665.

[114] J. Guggenheim, R. Hoffman, H. Song, and H. H. Asada. "Leveraging the Human Operator in the Design and Control of Supernumerary Robotic Limbs". In: *IEEE Robotics and Automation Letters* 5.2 (Apr. 2020). Conference Name: IEEE Robotics and Automation Letters, pp. 2177–2184. ISSN: 2377-3766. DOI: 10.1109/LRA.2020.2970948.

[115] J. W. Guggenheim, F. Parietti, T. Flash, and H. H. Asada. "Laying the Groundwork for Intra-Robotic-Natural Limb Coordination: Is Fully Manual Control Viable?" In: *ACM Transactions on Human-Robot Interaction* 9.3 (May 31, 2020), 18:1–18:12. DOI: 10.1145/3377329. URL: https://doi.org/10.1145/3377329.

[116] L. Bashford, J. Wu, D. Sarma, K. Collins, R. P. N. Rao, J. G. Ojemann, and C. Mehring. "Concurrent control of a brain–computer interface and natural overt movements". In: *Journal of Neural Engineering* 15.6 (Oct. 2018). Publisher: IOP Publishing, p. 066021. ISSN: 1741-2552. DOI: 10.1088/1741-2552/aadf3d. URL: https://doi.org/10.1088/1741-2552/aadf3d.

[117] I. Milovanovic, R. Robinson, E. E. Fetz, and C. T. Moritz. "Simultaneous and independent control of a brain-computer interface and contralateral limb movement". In: *Brain-Computer Interfaces* 2.4 (Oct. 2, 2015). Publisher: Taylor & Francis _eprint: https://doi.org/10.1080/2326263X.2015.1080961, pp. 174–185. ISSN: 2326-263X. DOI: 10.1080/2326263X.2015.1080961. URL: https://doi.org/10.1080/2326263X.2015.1080961.

[118] E. R. Hoffmann. "Capture of moving targets: a modification of Fitts' Law". In: *Ergonomics* 34.2 (Feb. 1, 1991), pp. 211–220. ISSN: 0014-0139. DOI: 10.1080/00140139108967307. URL: https://doi.org/10.1080/00140139108967307.

[119] C. N. Borish, M. Bertucco, and T. D. Sanger. "Effect of target distance on controllability for myocontrol". In: *International Journal of Human-Computer Studies* 140 (Aug. 1, 2020), p. 102432. ISSN: 1071-5819. DOI: 10.1016/j.ijhcs.2020.102432. URL: http://www.sciencedirect.com/science/article/pii/S1071581920300355.

[120] V. Mendez, F. Iberite, S. Shokur, and S. Micera. "Current Solutions and Future Trends for Robotic Prosthetic Hands". In: *Annual Review of Control, Robotics, and Autonomous Systems* 4.1 (May 3, 2021), pp. 595–627. ISSN: 2573-5144, 2573-5144. DOI: 10.1146/annurev-control-071020-104336. URL: https://www.annualreviews.org/doi/10.1146/annurev-control-071020-104336.

[121] I. S. MacKenzie. "Fitts' Law as a Research and Design Tool in Human-Computer Interaction". In: *Human–Computer Interaction* 7.1 (Mar. 1992), pp. 91–139. ISSN: 0737-0024, 1532-7051. DOI: 10.1207/s15327051hci0701_3. URL: http://www.tandfonline.com/doi/abs/10.1207/s15327051hci0701_3.

[122] S. K. Card, W. K. English, and B. J. Burr. "Evaluation of Mouse, Rate-Controlled Isometric Joystick, Step Keys, and Text Keys for Text Selection on a CRT". In: *Ergonomics* 21.8 (Aug. 1978), pp. 601–613. ISSN: 0014-0139, 1366-

5847. DOI: 10.1080/00140137808931762. URL: https://www.tandfonline.com/doi/full/10.1080/00140137808931762.

[123] E. Crossman. "The speed and accuracy of simple hand movements". In: *The nature and acquisition of industrial skills* (1957). Publisher: Report to the MRC and DSIR Joint Committee on Individual Efficiency in Industry.

[124] B. Lee and A. Oulasvirta. "Modelling Error Rates in Temporal Pointing". In: *Proceedings of the 2016 CHI Conference on Human Factors in Computing Systems*. CHI '16. San Jose, California, USA: Association for Computing Machinery, May 7, 2016, pp. 1857–1868. ISBN: 978-1-4503-3362-7. DOI: 10.1145/2858036.2858143. URL: https://doi.org/10.1145/2858036.2858143.

[125] T. R. Makin and H. Flor. "Brain (re)organisation following amputation: Implications for phantom limb pain". In: *NeuroImage* 218 (Sept. 1, 2020), p. 116943. ISSN: 1053-8119. DOI: 10.1016/j.neuroimage.2020.116943. URL: https://www.sciencedirect.com/science/article/pii/S1053811920304298.

[126] P. Kieliba, D. Clode, R. O. Maimon-Mor, and T. R. Makin. "Robotic hand augmentation drives changes in neural body representation". In: *Science Robotics* 6.54 (May 19, 2021). Publisher: Science Robotics Section: Research Article. ISSN: 2470-9476. DOI: 10.1126/scirobotics.abd7935. URL: https://robotics.sciencemag.org/content/6/54/eabd7935.

[127] C. Stepp, Q. An, and Y. Matsuoka. "Repeated training with augmentative vibrotactile feedback increases object manipulation performance". In: *PLoS ONE* 7.2 (2012). DOI: 10.1371/journal.pone.0032743.

[128] E. Amoruso, L. Dowdall, M. T. Kollamkulam, O. Ukaegbu, P. Kieliba, T. Ng, H. Dempsey-Jones, D. Clode, and T. R. Makin. "Somatosensory signals from the controllers of an extra robotic finger support motor learning". In: *bioRxiv* (May 18, 2021). Publisher: Cold Spring Harbor Laboratory Section: New Results, p. 2021.05.18.444661. DOI: 10.1101/2021.05.18.444661. URL: https://www.biorxiv.org/content/10.1101/2021.05.18.444661v1.

[129] A. Dollar and H. Herr. "Lower extremity exoskeletons and active orthoses: Challenges and state-of-the-art". In: *IEEE Transactions on Robotics* 24.1 (2008), pp. 144–158. DOI: 10.1109/TRO.2008.915453.

[130] R. M. Singh and S. Chatterji. “Trends and Challenges in EMG Based Control Scheme of Exoskeleton Robots - A Review”. In: *International Journal of Scientific and Engineering Research* 3.8 (2012), pp. 1–8.

[131] P. T. Fox and M. E. Raichle. “Focal physiological uncoupling of cerebral blood flow and oxidative metabolism during somatosensory stimulation in human subjects”. In: *Proceedings of the National Academy of Sciences* 83.4 (Feb. 1, 1986). Publisher: National Academy of Sciences Section: Research Article, pp. 1140–1144. ISSN: 0027-8424, 1091-6490. DOI: 10.1073/pnas.83.4.1140. URL: https://www.pnas.org/content/83/4/1140.

[132] T. Ikegami and G. Taga. “Decrease in cortical activation during learning of a multi-joint discrete motor task”. In: *Experimental Brain Research* 191.2 (Nov. 2008), pp. 221–236. ISSN: 0014-4819, 1432-1106. DOI: 10.1007/s00221-008-1518-2. URL: http://link.springer.com/10.1007/s00221-008-1518-2.

[133] A. Cerasa, L. Passamonti, F. Novellino, M. Salsone, M. Gioia, M. Morelli, S. Paglionico, L. Giofrè, G. Arabia, and A. Quattrone. “Fronto-parietal overactivation in patients with essential tremor during Stroop task”. In: *NeuroReport* 21.2 (2010), pp. 148–151. DOI: 10.1097/WNR.0b013e328335b42c.

[134] L. Passamonti, F. Novellino, A. Cerasa, C. Chiriaco, F. Rocca, M. Matina, F. Fera, and A. Quattrone. “Altered cortical-cerebellar circuits during verbal working memory in essential tremor”. In: *Brain* 134.8 (2011), pp. 2274–2286. DOI: 10.1093/brain/awr164.

[135] B. Haslinger, P. Erhard, N. Kämpfe, H. Boecker, E. Rummeny, M. Schwaiger, B. Conrad, and A. Ceballos-Baumann. “Event-related functional magnetic resonance imaging in Parkinson’s disease before and after levodopa”. In: *Brain* 124.3 (2001), pp. 558–570. DOI: 10.1093/brain/124.3.558.

[136] A. W. G. Buijink, M. Broersma, A. M. M. van der Stouwe, G. A. van Wingen, P. F. C. Groot, J. D. Speelman, N. M. Maurits, and A. F. van Rootselaar. “Rhythmic finger tapping reveals cerebellar dysfunction in essential tremor”. In: *Parkinsonism & Related Disorders* 21.4 (Apr. 1, 2015), pp. 383–388. ISSN: 1353-8020. DOI: 10.1016/j.parkreldis.2015.02.003. URL: https://www.sciencedirect.com/science/article/pii/S1353802015000565.

[137] S. F. Bucher, K. C. Seelos, R. C. Dodel, M. Reiser, and W. H. Oertel. "Activation mapping in essential tremor with functional magnetic resonance imaging". In: *Annals of Neurology* 41.1 (1997). _eprint: https://onlinelibrary.wiley.com/doi/pdf/10.100 pp. 32–40. ISSN: 1531-8249. DOI: 10.1002/ana.410410108. URL: https://onlinelibrary.wiley.com/doi/abs/10.1002/ana.410410108.

[138] J.-M. Beaulieu and R. R. Gainetdinov. "The Physiology, Signaling, and Pharmacology of Dopamine Receptors". In: *Pharmacological Reviews* 63.1 (Mar. 1, 2011). Ed. by D. R. Sibley. Publisher: American Society for Pharmacology and Experimental Therapeutics Section: Review Article, pp. 182–217. ISSN: 0031-6997, 1521-0081. DOI: 10.1124/pr.110.002642. URL: https://pharmrev.aspetjournals.org/content/63/1/182.

[139] B. Ford. "Deep Brain Stimulation". In: *Encyclopedia of Movement Disorders*. Ed. by K. Kompoliti and L. V. Metman. Oxford: Academic Press, Jan. 1, 2010, pp. 277–282. ISBN: 978-0-12-374105-9. DOI: 10.1016/B978-0-12-374105-9.00453-6. URL: https://www.sciencedirect.com/science/article/pii/B9780123741059004536.

[140] M. I. Hariz and G.-M. Hariz. "Chapter 6 - Therapeutic stimulation versus ablation". In: *Handbook of Clinical Neurology*. Ed. by A. M. Lozano and M. Hallett. Vol. 116. Brain Stimulation. Elsevier, Jan. 1, 2013, pp. 63–71. DOI: 10.1016/B978-0-444-53497-2.00006-1. URL: https://www.sciencedirect.com/science/article/pii/B9780444534972000061.

[141] F. M. Weaver, K. Follett, M. Stern, K. Hur, C. Harris, W. J. Marks, J. Rothlind, O. Sagher, D. Reda, C. S. Moy, R. Pahwa, K. Burchiel, P. Hogarth, E. C. Lai, J. E. Duda, K. Holloway, A. Samii, S. Horn, J. Bronstein, G. Stoner, J. Heemskerk, G. D. Huang, and f. t. CSP 468 Study Group. "Bilateral Deep Brain Stimulation vs Best Medical Therapy for Patients With Advanced Parkinson Disease: A Randomized Controlled Trial". In: *JAMA* 301.1 (Jan. 7, 2009), pp. 63–73. ISSN: 0098-7484. DOI: 10.1001/jama.2008.929. URL: https://doi.org/10.1001/jama.2008.929.

[142] J. M. Bronstein, M. Tagliati, R. L. Alterman, A. M. Lozano, J. Volkmann, A. Stefani, F. B. Horak, M. S. Okun, K. D. Foote, P. Krack, R. Pahwa, J. M. Henderson, M. I. Hariz, R. A. Bakay, A. Rezai, W. J. Marks Jr, E. Moro, J. L. Vitek, F. M. Weaver, R. E. Gross, and M. R. DeLong. "Deep Brain Stimula-

tion for Parkinson Disease: An Expert Consensus and Review of Key Issues". In: *Archives of Neurology* 68.2 (Feb. 1, 2011), pp. 165–165. ISSN: 0003-9942. DOI: 10.1001/archneurol.2010.260. URL: https://doi.org/10.1001/archneurol.2010.260.

[143] D. Weintraub and W. J. Elias. "The emerging role of transcranial magnetic resonance imaging–guided focused ultrasound in functional neurosurgery". In: *Movement Disorders* 32.1 (2017). _eprint: https://movementdisorders.onlinelibrary.wiley.com pp. 20–27. ISSN: 1531-8257. DOI: 10.1002/mds.26599. URL: https://movementdisorders.onlinelibrary.wiley.com/doi/abs/10.1002/mds.26599.

[144] W. Chang, H. Jung, E. Kweon, E. Zadicario, I. Rachmilevitch, and J. Chang. "Unilateral magnetic resonance guided focused ultrasound thalamotomy for essential tremor: Practices and clinicoradiological outcomes". In: *Journal of Neurology, Neurosurgery and Psychiatry* 86.3 (2015), pp. 257–264. DOI: 10.1136/jnnp-2014-307642.

[145] J. Chang, C. Park, N. Lipsman, M. Schwartz, P. Ghanouni, J. Henderson, R. Gwinn, J. Witt, T. Tierney, G. Cosgrove, B. Shah, K. Abe, T. Taira, A. Lozano, H. Eisenberg, P. Fishman, and W. Elias. "A prospective trial of magnetic resonance–guided focused ultrasound thalamotomy for essential tremor: Results at the 2-year follow-up". In: *Annals of Neurology* 83.1 (2018), pp. 107–114. DOI: 10.1002/ana.25126.

[146] H. Jung, S. Kim, D. Roh, J. Chang, W. Chang, E. Kweon, C.-H. Kim, and J. Chang. "Bilateral thermal capsulotomy with MR-guided focused ultrasound for patients with treatment-refractory obsessive-compulsive disorder: A proof-of-concept study". In: *Molecular Psychiatry* 20.10 (2015), pp. 1205–1211. DOI: 10.1038/mp.2014.154.

[147] H. Jung, W. Chang, I. Rachmilevitch, T. Tlusty, E. Zadicario, and J. Chang. "Different magnetic resonance imaging patterns after transcranial magnetic resonance-guided focused ultrasound of the ventral intermediate nucleus of the thalamus and anterior limb of the internal capsule in patients with essential tremor or obsessive-compulsive disorder". In: *Journal of Neurosurgery* 122.1 (2015), pp. 162–168. DOI: 10.3171/2014.8.JNS132603.

[148] A. Fasano, M. Llinas, R. Munhoz, E. Hlasny, W. Kucharczyk, and A. Lozano. "MRI-guided focused ultrasound thalamotomy in non-ET tremor syndromes". In: *Neurology* 89.8 (2017), pp. 771–775. DOI: 10.1212/WNL.0000000000004268.

[149] N. Jung, C. Park, M. Kim, P. Lee, Y. Sohn, and J. Chang. "The efficacy and limits of magnetic resonance–guided focused ultrasound pallidotomy for Parkinson's disease: A Phase I clinical trial". In: *Journal of Neurosurgery* 1306.6 (2019), pp. 1853–1861. DOI: 10.3171/2018.2.JNS172514.

[150] H. Furusawa, K. Namba, S. Thomsen, F. Akiyama, A. Bendet, C. Tanaka, Y. Yasuda, and H. Nakahara. "Magnetic Resonance–Guided Focused Ultrasound Surgery of Breast Cancer: Reliability and Effectiveness". In: *Journal of the American College of Surgeons* 203.1 (July 1, 2006), pp. 54–63. ISSN: 1072-7515. DOI: 10.1016/j.jamcollsurg.2006.04.002. URL: https://www.sciencedirect.com/science/article/pii/S1072751506003851.

[151] R. Catane, A. Beck, Y. Inbar, T. Rabin, N. Shabshin, S. Hengst, R. M. Pfeffer, A. Hanannel, O. Dogadkin, B. Liberman, and D. Kopelman. "MR-guided focused ultrasound surgery (MRgFUS) for the palliation of pain in patients with bone metastases—preliminary clinical experience". In: *Annals of Oncology* 18.1 (Jan. 1, 2007), pp. 163–167. ISSN: 0923-7534. DOI: 10.1093/annonc/mdl335. URL: https://www.sciencedirect.com/science/article/pii/S0923753419375672.

[152] L. Lamsam, E. Johnson, I. Connolly, M. Wintermark, and M. Gephart. "A review of potential applications of MR-guided focused ultrasound for targeting brain tumor therapy". In: *Neurosurgical Focus* 44.2 (2018). DOI: 10.3171/2017.11.FOCUS17620.

[153] M. A. Stacy, R. J. Elble, W. G. Ondo, S.-C. Wu, J. Hulihan, and T. S. Group. "Assessment of interrater and intrarater reliability of the Fahn–Tolosa–Marin Tremor Rating Scale in essential tremor". In: *Movement Disorders* 22.6 (2007). _eprint: https://onlinelibrary.wiley.com/doi/pdf/10.1002/mds.21412, pp. 833–838. ISSN: 1531-8257. DOI: 10.1002/mds.21412. URL: https://onlinelibrary.wiley.com/doi/abs/10.1002/mds.21412.

[154] W. J. Elias, N. Lipsman, W. G. Ondo, P. Ghanouni, Y. G. Kim, W. Lee, M. Schwartz, K. Hynynen, A. M. Lozano, B. B. Shah, D. Huss, R. F. Dallapiazza, R. Gwinn, J. Witt, S. Ro, H. M. Eisenberg, P. S. Fishman, D. Gandhi, C. H.

Halpern, R. Chuang, K. Butts Pauly, T. S. Tierney, M. T. Hayes, G. R. Cosgrove, T. Yamaguchi, K. Abe, T. Taira, and J. W. Chang. "A Randomized Trial of Focused Ultrasound Thalamotomy for Essential Tremor". In: *New England Journal of Medicine* 375.8 (Aug. 25, 2016). Publisher: Massachusetts Medical Society _eprint: https://doi.org/10.1056/NEJMoa1600159, pp. 730–739. ISSN: 0028-4793. DOI: 10.1056/NEJMoa1600159. URL: https://doi.org/10.1056/NEJMoa1600159.

[155] M. Wintermark, J. Druzgal, D. S. Huss, M. A. Khaled, S. Monteith, P. Raghavan, T. Huerta, L. C. Schweickert, B. Burkholder, J. J. Loomba, E. Zadicario, Y. Qiao, B. Shah, J. Snell, M. Eames, R. Frysinger, N. Kassell, and W. J. Elias. "Imaging Findings in MR Imaging–Guided Focused Ultrasound Treatment for Patients with Essential Tremor". In: *American Journal of Neuroradiology* 35.5 (May 1, 2014). Publisher: American Journal of Neuroradiology Section: Brain, pp. 891–896. ISSN: 0195-6108, 1936-959X. DOI: 10.3174/ajnr.A3808. URL: http://www.ajnr.org/content/35/5/891.

[156] J. C. Ye, S. Tak, K. E. Jang, J. Jung, and J. Jang. "NIRS-SPM: Statistical parametric mapping for near-infrared spectroscopy". In: *NeuroImage* 44.2 (Jan. 15, 2009), pp. 428–447. ISSN: 1053-8119. DOI: 10.1016/j.neuroimage.2008.08.036. URL: https://www.sciencedirect.com/science/article/pii/S1053811908009695.

[157] K. E. Jang, S. Tak, J. Jung, J. Jang, Y. Jeong, and J. C. Ye. "Wavelet minimum description length detrending for near-infrared spectroscopy". In: *Journal of Biomedical Optics* 14.3 (2009), p. 034004. ISSN: 10833668. DOI: 10.1117/1.3127204. URL: http://biomedicaloptics.spiedigitallibrary.org/article.aspx?doi=10.1117/1.3127204.

[158] H. Li, S. Tak, and J. C. Ye. "Lipschitz-Killing curvature based expected Euler characteristics for p-value correction in fNIRS". In: *Journal of Neuroscience Methods* 204.1 (Feb. 15, 2012), pp. 61–67. ISSN: 0165-0270. DOI: 10.1016/j.jneumeth.2011.10.016. URL: https://www.sciencedirect.com/science/article/pii/S0165027011006169.

[159] S. Tak, J. Jang, K. Lee, and J. C. Ye. "Quantification of CMRO2without hypercapnia using simultaneous near-infrared spectroscopy and fMRI measurements". In: *Physics in Medicine and Biology* 55.11 (May 2010). Publisher: IOP Pub-

lishing, pp. 3249–3269. ISSN: 0031-9155. DOI: 10.1088/0031-9155/55/11/017. URL: https://doi.org/10.1088/0031-9155/55/11/017.

[160] S. Tak, S. J. Yoon, J. Jang, K. Yoo, Y. Jeong, and J. C. Ye. "Quantitative analysis of hemodynamic and metabolic changes in subcortical vascular dementia using simultaneous near-infrared spectroscopy and fMRI measurements". In: *NeuroImage* 55.1 (Mar. 1, 2011), pp. 176–184. ISSN: 1053-8119. DOI: 10.1016/j.neuroimage.2010.11.046. URL: https://www.sciencedirect.com/science/article/pii/S1053811910015247.

[161] M. Cope and D. T. Delpy. "System for long-term measurement of cerebral blood and tissue oxygenation on newborn infants by near infra-red transillumination". In: *Medical and Biological Engineering and Computing* 26.3 (May 1, 1988), pp. 289–294. ISSN: 1741-0444. DOI: 10.1007/BF02447083. URL: https://doi.org/10.1007/BF02447083.

[162] H. Zhao, Y. Tanikawa, F. Gao, Y. Onodera, A. Sassaroli, K. Tanaka, and Y. Yamada. "Maps of optical differential pathlength factor of human adult forehead, somatosensory motor and occipital regions at multi-wavelengths in NIR". In: *Physics in Medicine and Biology* 47.12 (June 2002). Publisher: IOP Publishing, pp. 2075–2093. ISSN: 0031-9155. DOI: 10.1088/0031-9155/47/12/306. URL: https://doi.org/10.1088/0031-9155/47/12/306.

[163] L. Holper, M. Biallas, and M. Wolf. "Task complexity relates to activation of cortical motor areas during uni- and bimanual performance: A functional NIRS study". In: *NeuroImage* 46.4 (July 2009), pp. 1105–1113. ISSN: 10538119. DOI: 10.1016/j.neuroimage.2009.03.027. URL: https://linkinghub.elsevier.com/retrieve/pii/S1053811909002705.